Stony Brook University

OFFICIAL COPY

The official electronic file of this thesis or dissertation is maintained by the University Libraries on behalf of The Graduate School at Stony Brook University.

© All Rights Reserved by Author.

Mechanisms Controlling Variability in Long Island Sound

A Dissertation Presented

by

Younjoo Lee

to

The Graduate School

in Partial fulfillment of the

Requirements

for the Degree of

Doctor of Philosophy

in

Marine and Atmospheric Science

Stony Brook University

December 2009

Stony Brook University

The Graduate School

Younjoo Lee

We, the dissertation committee for the above candidate for the

Doctor of Philosophy degree, hereby recommend

acceptance of this dissertation.

Kamazima M. M. Lwiza – Dissertation Advisor
Associate Professor, School of Marine and Atmospheric Sciences

Dong-Ping Wang – Chairperson of Defense
Professor, School of Marine and Atmospheric Sciences

Charles N. Flagg
Research Professor, School of Marine and Atmospheric Sciences

Robert E. Wilson
Associate Professor, School of Marine and Atmospheric Sciences

Minghua Zhang
Professor, School of Marine and Atmospheric Sciences

Arnoldo Valle-Levinson
Professor, Physical Oceanography
Department of Civil and Coastal Engineering, University of Florida

This dissertation is accepted by the Graduate School

Lawrence Martin
Dean of the Graduate School

Abstract of the Dissertation

Mechanisms Controlling Variability in Long Island Sound

by

Younjoo Lee

Doctor of Philosophy

in

Marine and Atmospheric Science

Stony Brook University

2009

The variability of temperature, salinity, and bottom dissolved oxygen (DO) in Long Island Sound (LIS) is examined using observations. During summer, stratification is intensified under weak wind and bottom DO starts to decrease, in general. For the westernmost and shallow stations, bottom DO is correlated with stratification, while the relationship between oxygen depletion and stratification is not significant at deep stations. The bottom DO continues to decrease until reaching its minimum when bottom temperature is around 19-20 ºC. Then, the recovery of minimum DO in early fall is fast, but not necessarily associated with increased wind mixing. Hypoxia is weakly correlated to summer wind, total nitrogen, spring chlorophyll *a*, and river discharge. When all variables are combined, the coefficient of determinant (r^2) is 0.92. The weakest variable is the total nitrogen, because when it is excluded the coefficient only drops to 0.84. The results suggest spring bloom may be an important source of organic carbon and biological uptake plays a more crucial role in seasonal evolution of bottom DO than previously thought. There is a strong seasonal variation in temperature, and its interannual variability is characterized by a higher variance during winter than summer. Salinity shows seasonal cycles, but there is a long-term change. Empirical orthogonal function analysis indicates the first modes of principle components contain quasi-biennial periodicities. In addition, the salinity anomaly shows an additional signal at a decadal time-scale. The seasonal variations are primarily associated with heat flux and freshwater,

but forcings other than local processes control the interannual variability, most probably through horizontal exchange. The significant correlation between the salinity and the Gulf Stream suggests the long-term variability of the salinity in LIS is possibly connected to shelf-slope water. This is also supported by findings in the Chesapeake Bay. Using wavelet methods, bottom salinity reveals significant powers centered at the periods of 2 and 7.5 years. This demonstrates the interannual variability is forced by freshwater, and the quasi-decadal variability is associated with shelf-slope water condition. The numerical model is used to examine the role of horizontal advection in seasonal heat budget. It is found the net surface heat flux dominates the fall/winter heat balance, acting to cool the water column throughout the sound. In contrast, the horizontal advection plays a significant role during spring/summer due to the heat loss over the shallow areas and the heat gain along the deep channel.

To
my parents, wife, and daughter

Table of Contents

List of Figures ……..……..…….……..……..…..…. viii

List of Tables …….……..……..… xiii

Acknowledgments ……..…….…….. xiv

Chapter 1: Introduction ……..…… 1
1.1 Background …….….. 1
1.2 Thesis Organization ……..… 3
References …….……..… 5

Chapter 2: Characteristics of Bottom Dissolved Oxygen in Long Island Sound, New York ……...…….……..... 6
Abstract ……..…… 6
2.1 Introduction ……... 7
2.2 Study Area …..…….…….…….…….…….... 10
2.3 Data and Methods ……..……..……... 11
2.3.1 LIS data …….....…… 11
2.3.2 Wind and freshwater discharge ……...……..… 14
2.3.3 Cluster analysis ……. 14
2.4 Results …….… 15
2.5 Discussions ……..…….……...…..…..… 30
2.6 Summary …….…… 36

Chapter 3: Interannual Variability of Temperature and Salinity in Shallow Water Long Island Sound, New York …….…….……...…….……38
Abstract ……..38
3.1 Introduction ……..38
3.2 Study Area ……..……...…….…….……... 41
3.3 Data and Methods…….……..…..… 42
3.3.1 LIS water column data …….....… 42
2.3.2 Climate data and surface heat flux …….……...…… 44
3.3.3 Effective degrees of freedom …….……..……. 45
3.4 Results ……..……..……. 45
3.4.1 Temperature …….……..……..……. 45
3.4.2 Salinity …….……. 51
3.5 Discussions ……..……...…..…… 57
3.6 Summary …….…… 61

Chapter 4: Factors driving bottom salinity variability in the Chesapeake Bay 63
Abstract …….…….…….……..63
4.1 Introduction ……..……63

4.2 Study Area……. 65
4.3 Data and Methods …… 67
4.3.1 Salinity anomaly …… 67
4.3.2 Freshwater influx …… 69
4.3.3 The Gulf Stream index …… 71
4.3.4 Wavelet …… 71
4.4 Results …… 75
4.5 Discussions …… 84
4.6 Summary …… 87

Chapter 5: Numerical Simulation of Exchange Transport and Heat Budget in Long Island Sound ……88
Abstract ……88
5.1 Introduction ……88
5.2 Study Area…… 93
5.3 The Regional Ocean Model …… 93
5.3.1 Model configuration ……95
5.3.2 Temperature and salinity climatology ……96
5.3.3 Surface forcing ……96
5.4 Results ……98
5.4.1 Model-data comparison ……98
5.4.2 Exchange transport ……110
5.4.3 Heat budget ……111
5.5 Discussions ……117
5.6 Summary ……120

References …… 121

List of Figures

Chapter 1

Figure 2-1. Bathymetry of Long Island Sound (SS, Stratford Shoal; CA, Cable and Anchor Reef; MS, Mattituck Sill; SB, Smithtown Bay) ……..…….…. 8
Figure 2-2. The Connecticut Department of Environmental Protection water quality sampling stations (+) in Long Island Sound (square markers indicate the positions of major stations) ……..….. 13
Figure 2-3. Time series of bottom dissolved oxygen (mg/l) at stations A4 (the Narrows), 09 (the Western Basin), H2 (the Central Basin), and J2 (the Eastern Basin) from 1995 to 2004. The dotted-line indicates the threshold of hypoxic condition (3 mg/l of dissolved oxygen) …….……... 16
Figure 2-4. A bi-plot of principle components and empirical orthogonal function vectors of bottom dissolved oxygen (DO) in summer, spring chlorophyll a (CHLA), spring total nitrogen (TN), summer bottom temperature (BT), summer wind speed (WIND), summer density stratification (DS), and spring river discharge (RIVER) at major stations from 1995 to 2004. Stations in the Narrows are represented by N, C is for the Central Basin, W is for the Western Basin, and E is for the Eastern Basin. There is a good separation between the Narrows stations, the Eastern stations, and the rest of the sound ……..…... 18
Figure 2-5. Time series of surface total nitrogen (dashed line) and surface chlorophyll a (solid line) for station D3 in the Narrows of Long Island Sound from 1995 to 2004 …….….….…. 19
Figure 2-6. A 4×3 self-organizing map (SOM) array of the bottom dissolved oxygen for June-September. The unit of patterns is indicated in the upper-left corner of each map. The relative frequency of units is shown in the lower-right corner of each map as a percentage (%). The bottom dissolved oxygen concentration is contoured every 0.5 mg/l from 2.0 to 8.0 mg/l ……...…….. 21
Figure 2-7. Monthly relative frequency map of the 4×3 self-organizing map (SOM) array of the bottom dissolved oxygen from June to September. The coordinates of the each frequency map correspond to SOM unit (top panel) where numbers indicate the unit of patterns in the SOM array (see Figure 6). The percentage in a monthly frequency map accounts for the relative occurrence of each pattern in a given month. For example, unit 1 and 3 are only patterns observed in August and no other units of patterns have occurred ……..…..……. 23
Figure 2-8. The relationship between the bottom dissolved oxygen (mg/l) with bottom temperature (°C) at stations B3, 15, H6, and K2. The solid line indicates the mean solubility and dotted lines are the maximum and minimum solubility depending on salinity ……..……..…. 25
Figure 2-9. The relationship between the density stratification (DS) calculated as a difference between surface and bottom values (kg/m3), and the saturation of bottom dissolved oxygen as a percentage (%) for June-August. The name of station is indicated in the upper-left and the correlation coefficient (r) is shown

in the upper-right or the lower-left. A solid line indicates the linear relationship when the slope is significantly different from zero (p<0.05) …. 28
Figure 2-10. The relationship between the maximum hypoxic volume as a percentage (%) and (a) mean spring (February-May) total chlorophyll a for the whole sound (ton), (b) mean summer (July-August) wind speed (m/s), (c) maximum spring (February-May) discharge into Long Island Sound (m3/s), and (d) mean spring (February-May) total nitrogen (mg/l), from 1995 to 2004. The solid lines indicate the least-squares fit from linear regression and the coefficient of determination (r2) is shown in the upper-right …….…….....…… 29
Figure 2-11. Multiple linear regression showing the relationship between the maximum hypoxic volume as a percentage (%) and the combined effect of four variables from the Figure 10, i.e., (i) mean spring total chlorophyll a for the whole sound (CHLA), (ii) mean summer wind speed (WIND), (iii) maximum spring discharge into Long Island Sound (RIVER), and (iv) mean spring total nitrogen (TN). The solid line represents the least-squares best fit from linear regression with the coefficient of determination (r2) shown in the upper-right …….……..…….. 31

Chapter 3

Figure 3-1. Long Island Sound ('+' represents CTDEP sampling stations. Square markers indicate the names of stations where the water column data were selected for this study) …….……...……... 43
Figure 3-2. Central LIS - Station I2: (a) depth-averaged temperature (b) February temperature anomaly, and (c) September temperature anomaly …..……. 46
Figure 3-3. Depth-averaged temperature anomalies at (a) station F3, (b) station I2, and (c) station M3 …….…..... 47
Figure 3-4. Depth-averaged temperature anomaly (a) spatial pattern of the first EOF mode and (b) time coefficient ……..…….. 49
Figure 3-5. (a) Net surface heat flux (dashed) and the time rate change of temperature (solid), (b) same as (a), but units of both data are given in ^{o}C/month, and (c) surface heat flux anomaly (dashed) and the time rate change of temperature anomaly (solid) based on (b) in Long Island Sound ……..... 50
Figure 3-6. (a) Connecticut River discharge, depth-averaged salinity at (b) station F3 and (c) station M3, and depth-averaged salinity anomaly at (d) station F3 and (e) station M3 …….……..…….…….... 52
Figure 3-7. Depth-averaged salinity anomaly (a) spatial pattern of the first EOF mode and (b) time coefficient …….…….…….…….. 55

Chapter 4

Figure 4-1. The Chesapeake Bay (Square markers indicate the locations of the Environmental Protection Agency water quality monitoring stations selected for this study …….…….…….……... 66

Figure 4-2. The monthly time series of (a) the bottom salinity anomaly (the principle component of combined EOF modes 1 to 7), (b) the Susquehanna River discharge, and (c) the Gulf Stream index. The principle component is constructed by combining the first seven modes in empirical orthogonal function analysis, and hereafter it is referred as the bottom salinity anomaly ……..……..……..…….... 78
Figure 4-3. The monthly time series of the Gulf Stream (GS) index (dotted line) and mean surface salinity (solid line) across the continental shelf and Slope Sea (between 50 km and 250 km from Ambrose Light, New York) from the NOAA National Marine Fisheries Service ecosystem monitoring program on the Oleander. The data have been low-pass filtered with a 12-month moving average ……..……..…… 70
Figure 4-4. Linear regression analysis (a) between the bottom salinity at station CB5.2 and the Susquehanna River discharge and (b) between the bottom salinity and the Gulf Stream index. The analysis is based on annual mean data, and the correlation coefficient (r) is displayed with p-values ……..... 76
Figure 4-5. The power spectra for (a) the bottom salinity anomaly, (b) the Susquehanna River discharge anomaly, and (c) the Gulf Stream index during 1985-2004 …….…….. 76
Figure 4-6. Left column: The wavelet power spectra of (a) the bottom salinity anomaly, (c) the Susquehanna River discharge anomaly, and (e) the Gulf Stream index. A thick black contour designates the 5% significant level against red noise. The dashed line indicates the cone of influence, and the color bar represents the variance for each panel. Right column: the global wavelet power spectra for (b) the bottom salinity anomaly, (d) the Susquehanna River discharge anomaly, and (f) the Gulf Stream index …….……..……. 78
Figure 4-7. The wavelet coherence and phase (a) between the bottom salinity anomaly and the Susquehanna River discharge anomaly, and (b) between the bottom salinity anomaly and the Gulf Stream index. Contours are wavelet squared coherences 0.5, 0.7, 0.8, and 0.9. The 5% significance level from a Monte Carlo simulation (300 of surrogate data sets) is shown as a thick contour and the dashed line indicates the cone of influence. The vectors indicate the relative phase relationship between the first and the second time series (with in-phase pointing right, anti-phase pointing left, and the second time series leading the first by 90º pointing straight down ……..…..... 80
Figure 4-8. The relationship (a) between the bottom salinity anomaly and the Gulf Stream index (band-pass filtered at 8-10 year band), and (b) between the bottom salinity anomaly and the Susquehanna River discharge (band-pass filtered 10-14 year band). The correlation coefficient (r) are also indicated in each panel …… 82
Figure 4-9. The wavelet coherence and phase (a) between the Susquehanna River discharge anomaly and the Southern Oscillation Index, and (b) between the Susquehanna River discharge anomaly and the North Atlantic Oscillation. Contours are wavelet squared coherences 0.5, 0.7, 0.8, and 0.9. The 5% significance level from a Monte Carlo simulation (300 of surrogate data sets) is shown as a thick contour and the dashed line indicates the cone of influence.

The vectors indicate the relative phase relationship between the first and the second time series (with in-phase pointing right, anti-phase pointing left, and the second time series leading the first by 90º pointing straight down …..... 83

Chapter 5

Figure 5-1. Long Island Sound and its bathymetry (SS, Stratford Shoal; CA, Cable and Anchor Reef; MS, Mattituck Sill; SB, Smithtown Bay) ……..... 92
Figure 5-2. Model grid (240×400×16) (sub-sampled every 5 grid points) …….. 94
Figure 5-3. (a) Observational buoys and C-MAN stations around the Mid-Atlantic Bight including Long Island Sound. (b) Connecticut Department of Environmental Protection water quality monitoring stations are indicated as squares (17 major stations) with station names. ADCP mooring sites by Codiga and Rear (2004) are marked as triangles. Solid lines indicate ferry-based ADCP observations (BP, Bridgeport-Port Jefferson ferry service; CS, Cross Sound ferry service between Orient Point, NY, and New London, CT) …….….. 97
Figure 5-4. (a) amplitude and (b) phase of M2 tidal elevation in Long Island Sound … 99
Figure 5-5. Vertical structure of M2 tidal ellipse parameters at the North(N), West(W), Central(C), East(E), and South(S) sites during fall/winter 2001 (Codiga and Rear, 2004) outside Block Island Sound. Model results are shown in dashed lines and observations in solid ones ……..……..……. 102
Figure 5-6. M2 amplitude and phase during summer. The ferry-based observations (7/19/03 to 8/13/03) between Port Jefferson, NY and Bridgeport, CT, (Hao, 2008) are displayed in the left column. The results from model simulation during summer are shown in the right column ….……..…….…… 103
Figure 5-7. Comparison of M2 tidal ellipse parameters between ferry ADCP observation at eastern Long Island Sound (see also Codiga and Aurine, 2007) and model simulation in 2005 …….…….…….…… 104
Figure 5-8. Left column: residual currents (m/s) from ferry ADCP observations at eastern Long Island Sound in 2005 (see also Codiga and Aurine, 2007). Right column: residual currents of along-estuary and cross-estuary components from model simulation of 2005 …….…….. 106
Figure 5-9. Scatter diagrams of observed versus modeled temperature at (a) surface and (b) bottom at sampling stations in the Connecticut Department of Environmental Protection monitoring program. Histograms of errors at (c) surface and (d) bottom between observation and model are also shown … 107
Figure 5-10. Means and standard deviations of exchanged (solid) and net volume transport (dashed) in Long Island Sound …….… 108
Figure 5-11. Monthly exchanged transport at each section shown in Figure 5-10. Positive values indicates inward (in-to-estuary) and negative values are outward (out-of-estuary) transport ……. 109
Figure 5-12. Winter seasonal average (January-March) of the three terms in the depth-integrated heat budget: (a) storage ($\partial T / \partial t$), (b) horizontal advection ($\boldsymbol{u} \cdot \nabla T$), and (c) net surface heat flux (Q_{net}) …….. 113

Figure 5-13. Spring seasonal average (April-June) of the three terms in the depth-integrated heat budget: (a) storage ($\partial T / \partial t$), (b) horizontal advection ($\boldsymbol{u} \cdot \nabla T$), and (c) net surface heat flux (Q_{net})…….…. 114

Figure 5-14. Summer seasonal average (July-September) of the three terms in the depth-integrated heat budget: (a) storage ($\partial T / \partial t$), (b) horizontal advection ($\boldsymbol{u} \cdot \nabla T$), and (c) net surface heat flux (Q_{net})…….. 115

Figure 5-15. Fall seasonal average (October-December) of the three terms in the depth-integrated heat budget: (a) storage ($\partial T / \partial t$), (b) horizontal advection ($\boldsymbol{u} \cdot \nabla T$), and (c) net surface heat flux (Q_{net})…….. 116

List of Tables

Chapter 2

Table 2-1. Self-Organizing Map (SOM) parameters ……..…….…..... 20
Table 2-2. Correlation coefficients between bottom temperature (BT) and bottom dissolved oxygen (BDO), and mean temperature for the summer season (June-August) ……..…..... 26

Chapter 3

Table 3-1. Relationship between anomaly of monthly Connecticut River discharge and depth-averaged salinity anomaly from 1991 to 2002 ……..…..…… 54

Chapter 5

Table 5-1. Tidal current ellipse parameters for observations (Moody et al., 1984) and model results …….…….…….…. 100
Table 5-2. Sound-wide averaged seasonal surface heat fluxes (W/m^2) …….…… 112

Acknowledgements

I am heartily thankful to my supervisor, Dr. Kamazima M.M. Lwiza, for his encouragement, guidance and support during my research and study at Stony Brook University. His perpetual energy and enthusiasm in science has inspired and motivated me to continue the graduate study.

I was delighted to interact with Dr. Dong-Ping Wang, Dr. Robert E. Wilson, and Dr. Minghua Zhanng by attending his classes and having them as my committee members. Dr. Charles N. Flagg and Dr. Arnoldo Valle-Levinson deserve a special thank as my committee members whose comments and suggestions improved this work tremendously. I would also like to thank Dr. Enrique Curchitser for his valuable comment.

Last but not least, I would like to thank all people who have helped me during my doctoral study in the School of Marine and Atmospheric Sciences.

Chapter 1
General Introduction

1.1 Background and Motivation

An estuary is classically defined as a semi-enclosed coastal body of water which has a free connection with the open sea and within which sea water is measurably diluted with fresh water derived from land drainage (Cameron and Pritchard, 1963). Its circulation is traditionally described as a two-layered system since freshwater flows at the surface towards the ocean while denser saline water flows inward along the bottom. Due to the interaction between influences from the open sea and rivers, estuaries are recognized as the highly productive and biologically diverse areas which provide various habitats for a large number of organisms. Estuaries are also economically important to local communities because they contribute to regional economy from fishing, boating, and tourism.

However, estuaries have been under threats from anthropogenic activities such as pollution, eutrophication, overfishing, and development. For instance, toxic chemicals are found to be accumulated in many species of aquatic life (bioaccumulation), and some of them are harmful to ecosystem and human health such as mercury and PCBs. Excessive amounts of nutrients from fertilizers and waste materials are discharged into estuaries causing eutrophication which often deplete dissolved oxygen in the water column. This phenomenon has been frequently observed in many estuaries around the U.S. coast. Hypoxia, the depletion of dissolved oxygen below 2 or 3 mg/l (Diaz and Rosenberg, 1995; Ritter and Montagna, 1999), can result in reducing water quality, stressing marine life, and destroying benthic environment. Overfishing is also linked to an overall degradation of an ecosystem by exploiting our sustainable marine resources. Increased human populations and associated activities in coastal regions have already caused the habitat destruction of estuarine species because of commercial development, agriculture, construction, and dredging.

In addition, climate change due to global warming has been affecting various processes in every region of the world. Some signs of this change are already evident and will probably be exacerbated, i.e., frequent hurricanes, severe droughts and floods, and rapid sea level rise. Climate model projections indicate that global temperature will probably rise a further 2~4 ºC during the twenty first century (IPCC, 2007). As a scientist, we are concerned about how this change will have impacts on ecosystems on which our life is directly or indirectly dependent. There have been increasing efforts to understand how climate variability regulates marine ecosystem structures. It is has been found that, for example, a warming trend may be responsible for reduced primary production which plays a vital role in carbon cycling. Behrenfeld et al. (2008) demonstrated that global primary production is reduced because of increased thermal stratification which can suppress the nutrient supply from deep water. Oviatt (2004) also showed that during warm winters, winter-spring bloom is suppressed and zooplankton abundance increases, while nutrient levels remain high. From an estuary to open sea, the mechanistic links explaining the reduction of primary production are found to be different, but previous studies underscore the importance of temperature variability as an ecological regulator.

As global warming is expected to continue, there have been various attempts to examine the temperature variability in North Atlantic (e.g., Alexander et al., 2001; Czaja and Frankignoul, 2002; Dong and Kelly, 2004; Halliwell, 1997; Kushnir, 1994; Verbrugge and Reverdin, 2003). However, our knowledge on how estuaries respond to climate variability is still at a rudimentary level. Although previous studies have evidenced the warming trend (Nixon et al., 2004) and its impact on ecosystem (Oviatt, 2004; Stchowicz et al., 2002) in coastal waters, few studies have focused on the interannual variability of physical properties in Long Island Sound (LIS). Stachowicz et al. (2002) reported that the interannual variation in water temperature changes the biotic community structure and facilitates non-indigenous species invasions into the eastern LIS. Also, the temperature rise leads to the intensification of the stratification of the water column which consequently causes an increase in the duration of hypoxia as well as extending it to the western LIS (Kaputa and Olsen, 2000; O'Shea, 2000).

Furthermore, the die-off of the American lobsters (*Homarus americanus*) was observed in LIS, which was most severe in the fall seasons of 1998 to 1999 (CTDEP,

2000). This devastating ecological impact in LIS has been a key fisheries issue in the local community. There are several ongoing researches investigating the cause of mortality of American lobsters, but these studies are mainly focusing on pathological or physiological processes. There is no question that the physical properties of the water column play an important role and affects the ecosystem structures in LIS since the temperature in LIS has been associated with a global warming trend. However, it is little understood how physical properties has been varied temporally and spatially and how they interact with local and non-local forcing throughout the sound. Since LIS currently confronts various environmental concerns and issues as following:

i) The influences from anthropogenic activities from New York metropolitan areas.
ii) The frequent occurrence of severe hypoxia.
iii) The alteration of ecosystem structure such as lobster collapse and invasion of foreign species.
iv) The decline of commercial fishing and harvesting.
v) The increase of water temperature and the decrease of primary production along with climate change.

it is importance to investigate the sound as a whole and integrate the knowledge discovered from each process. Therefore, we can address current and future environmental issues in connection with climate variability, i.e., temperature warming, ecological regime shifts, carbon cycling, and hypoxic condition.

1.2. Objectives and Approach

The main goal of this research is (1) to examine the characteristics of variability in dissolved oxygen (DO), temperature, and salinity, (2) to attempt to associate different time scale with possible forcing mechanisms, and (3) to quantify the volume transport and estimate the heat budget throughout LIS. Investigating such processes requires a

modeling approach where hydrographic surveys are constrained. Specific research objectives are (1) to examine the primary factors controlling DO and hypoxic volume on seasonal to interannual time scales (2) to describe the characteristic of temperature and salinity in LIS, with emphasis on the effect of external forcing on interannual variability, (3) to determine the long-term variability of salinity in the Chesapeake Bay associated with adjacent ocean, (4) to estimate the volume transport and heat budget using a numerical simulation, and (5) to discuss the outcome of this thesis research and give guidance for management decisions in coastal ocean.

Meeting these objectives has required advanced techniques to analyze various data sets and to run a hydrodynamic ocean model. This has been achieved using long-term data sets from Connecticut Department of Environment Protection (CTDEP) and Chesapeake Bay Program (CBP) and running the Regional Ocean Modeling System (ROMS) in a parallel supercomputing system. The specific objectives of this research are addressed using several approaches. First the variability of DO is describes throughout the sound, and the spatial and temporal patterns of DO are determined using principle component analysis (PCA) and self-organizing map (SOM). The variability of DO is also examined with possible forcing variables. Then the hypoxic volume is estimated using optimal interpolation and projected using a statistical modeling approach (Chapter 2).

The interannual variability of temperature and salinity in LIS is explored using empirical orthogonal function (EOF) analysis. The temperature tendency and salinity anomaly are compared with local forcing, i.e., net surface heat flux and freshwater discharge. In order to determine the role of horizontal advection, the interannual variability of salinity is compared to the Gulf Stream (GS) index (Chapter 3). In addition, the long-term variability of salinity in the Chesapeake Bay is evaluated and its relationship with local and external forcings is determined using wavelet methods. The influence of El Niño Southern Oscillation (ENSO) and North Atlantic Oscillation (NAO) is also considered (Chapter 4).

Finally the heat budget due to horizontal advection is addressed by using a numerical model throughout the sound. ROMS is used to simulate estuarine flow and temperature fields around the LIS regions for a one-year (2005) period. The model results are compared with observations, i.e., tides, temperature, and currents. Then, it is

examined how much of water is transported in and out of the sound. Also, the role of horizontal advection in heat budget is also investigated by separating the depth-integrated heat budget into its three contributions, i.e., heat storage, net surface heat flux, and horizontal advection (Chapter 5).

Chapter 2

Characteristics of Bottom Dissolved Oxygen in Long Island Sound, New York

Abstract

The variability of bottom dissolved oxygen (DO) in Long Island Sound, New York, is examined using water quality monitoring data collected by the Connecticut Department of Environmental Protection from 1995 to 2004. Self-Organizing Map analysis indicates that hypoxia always occurs in the Narrows during summer and less frequently in the Western and the Central basins. The primary factor controlling the bottom DO changes spatially and temporally. For non-summer seasons, the levels of bottom DO are strongly associated with water temperature, which means DO availability is primarily driven by solubility. During summer, stratification intensifies under weak wind conditions and bottom DO starts to decrease and deviate from the saturation level except for stations in the Eastern Basin. For the westernmost and shallow (<15 m) stations, bottom DO is correlated with the density stratification (represented by difference between surface and bottom density). In contrast, at deep stations (>20 m), the relationship between oxygen depletion and stratification is not significant. For stations located west of the Central Basin, bottom DO continues to decrease during summer until it reaches its minimum when bottom temperature is around 19~20 °C. In most cases the recovery to saturation levels at the beginning of fall is fast, but not necessarily associated with increased wind mixing. Therefore, we propose that the DO recovery may be a manifestation of either the reduced microbial activity combined with the depletion of organic matter or horizontal exchange. Hypoxic volume is weakly correlated to the summer wind speed, spring total nitrogen, spring chlorophyll *a*, and maximum river discharge. When all variables are combined in a multiple regression, the coefficient of determination (r^2) is 0.92. Surprisingly, the weakest variable is the total nitrogen, because when it is excluded the coefficient r^2 only drops to 0.84. Spring bloom seems to be an

important source of organic carbon pool and biological uptake of oxygen plays a more crucial role in the seasonal evolution of bottom DO than previously thought. Our results indicate that the reassessment phase of Long Island Sound Total Maximum Daily Load policy on nitrogen loading will most likely fail, because it ignores the contributions of the spring organic carbon pool and river discharge. Also, it is questionable whether the goal of 58.5% anthropogenic nitrogen load reduction is enough.

2.1 Introduction

Dynamics of dissolved oxygen (DO) involves complex interactions between physical and biogeochemical processes, i.e., (1) vertical and horizontal mixing, (2) air–water exchange, (3) nutrient loadings and speciation, (4) photosynthesis, (5) sediment and water column oxygen demand, and (6) chemical oxygen demand. These processes can vary semi-independently from one another. It is therefore important to understand how temporal variations in nutrient loadings, phytoplankton blooms, bacterial production and grazing, temperature, and stratification of the water column manifest themselves in bottom water DO depletion. The variability of DO in water column generally results from the interplay between physical transport and biological consumption of oxygen. Thus, bottom DO gets depleted when rates of consumption exceed rates of supply. Hypoxia, the depletion of DO below 2 or 3 mg/l (Diaz and Rosenberg, 1995; Ritter and Montagna, 1999), is a seasonal phenomenon that occurs in shallow water in most temperate coastal regions (e.g., Hearn and Robson, 2001; Buzzelli et al., 2002; Hagy et al, 2004). The occurrence of hypoxia in shallow waters appears to be increasing, and it has been argued that hypoxia is most likely accelerated by human activities (Diaz and Rosenberg, 1995). Diaz and Rosenberg also noted that no other environmental variable of such ecological importance to estuarine marine ecosystems as DO has changed so drastically and in such a short period of time. Since hypoxia causes numerous economical and ecological losses, i.e., habitat degradation, alteration of food web dynamics, and regime shifts in ecosystem (e.g., Rabalais et al., 2002; Breitburg et al., 2003; Kemp et al., 2005), it is regarded as one of the major global issues in water quality management.

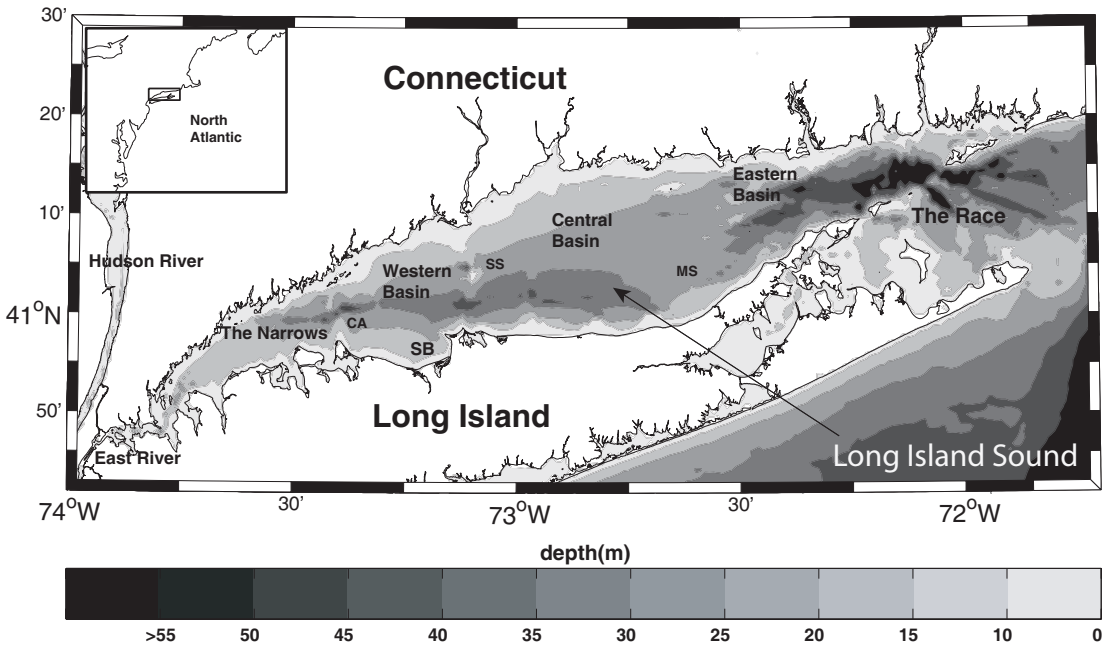

Figure 2-1. Bathymetry of Long Island Sound (SS, Stratford Shoal; CA, Cable and Anchor Reef; MS, Mattituck Sill; SB, Smithtown Bay)

Seasonal hypoxia has been frequently reported around the US coastal areas, for example, in the northern Gulf of Mexico (Justić et al., 1996; Rabalais et al., 2002), the Neuse River estuary (Buzzelli et al., 2002), the Chesapeake Bay (Kemp et al., 1992 and 2005; Hagy et al., 2004), as well as in certain tributaries (Kuo and Neilson, 1987; Breitburg et al., 2003) and the New York Bight (Swanson and Parker, 1988). Kemp et al. (1992) suggested that any reduction in nutrient loading to the Chesapeake Bay would yield rapid but proportionally smaller increase in oxygen concentration. Hagy et al. (2004) also pointed out that the long-term increase in hypoxia occurred concurrently with the long-term increase in nitrate loading into the Chesapeake Bay. It is believed that nutrient over-enrichment results in the depletion of DO near bottom in shallow waters because the enhanced primary production with coastal eutrophication often leads to problems such as a seasonal formation of hypoxic condition (National Research Council, 2000). Therefore, environmental mitigation efforts have been directed at reducing the amount of nutrient loadings into a system. Kemp et al. (2005) showed that the Susquehanna River concentration of total nitrogen entering the Chesapeake Bay has slightly declined since 1990 due to improved watershed land management (Sprague et al., 2000). However, Hagy et al. (2004) found that more extensive hypoxia was observed in recent years than would be expected from the observed relationship.

Long Island Sound (LIS) (see Figure 1) has traditionally suffered from hypoxic conditions, which have been observed in the western sound since the early 1970s. Hypoxia in LIS became more severe toward the end of the 1980s (Parker and O'Reilly, 1991). In 1998 the states of Connecticut and New York and the Environmental Protection Agency (EPA) adopted a plan for Phase III Actions for Hypoxia Management, with the aim of managing nitrogen targets through a development of a Total Maximum Daily Load (TMDL) (USEPA, 1998). The Long Island Sound TMDL (LIS TMDL) management team recognized that hypoxia is not driven by daily or short-term nitrogen loadings, but may be a function of annual loading rates. As a result, the LIS TMDL is defined as an allowable annual load of nitrogen into the sound. However, O'Shea and Brosnan (2000) suggested that bottom DO in LIS seems to be more associated with thermal stratification than point and non-point nutrient loadings into the western Narrows during the summers of 1963-1999. Numerical model results have also shown that the

concentration of DO in the western LIS is primarily driven by stratification (HydroQual Inc., 1995). In addition, Anderson and Taylor (2001) examined several physical and biological processes, and found that bottom DO is mainly driven by physical processes, namely, those controlling the density structure of the water column. There are other previous studies which have found other mechanisms that control DO during summer in LIS, such as horizontal transport of oxygen (Torgersen et al., 1997) and biological uptake (Welsh and Eller, 1991).

Despite efforts reducing nitrogen loadings and upgrading sewage treatment plants, hypoxia has not decreased, but keeps emerging from the Narrows to the Central Basin. This suggests that our current understanding of DO dynamics is incomplete, and besides the mechanisms which have already been identified there may be processes that need to be identified and old ones re-examined. All previous studies have concentrated their efforts on the western sound, but no study has been published to characterize the bottom DO over the whole sound. Our lack of understanding in the variability of DO could be stemming from the lack of examination of the whole sound. In this study, historical hydrographic survey data are re-analyzed to determine temporal and spatial features of bottom DO throughout the sound. We also re-examine the relationship between hypoxia and total nitrogen, plus other variables. The paper is organized in the following manner: section 2 briefly describes the area of study. The details of data processing including Principal Component Analysis (PCA) and Self-Organizing Map (SOM) analysis are given in section 3. Temporal and spatial variations of the bottom DO including the patterns of SOM analysis are described in section 4. The bottom DO is examined in relation with the density stratification and temperature. Interannual variability of hypoxic volume is also determined in relation to total nitrogen, wind speed, chlorophyll *a,* and riverine discharge in section 4. Factors influencing the bottom DO variability including implications for hypoxia management are discussed in section 5, and results are summarized in section 6.

2.2 Study Area

LIS is approximately 150 km long and 20 km wide with an average depth of 20 m. It is a weakly stratified system compared to typical estuaries such as the Chesapeake Bay, and a major river is located near the eastern end that is connected to the Atlantic Ocean through the Race (Figure 1). The western end is connected to the lower Hudson River via a tidal strait, the East River, where tidal currents exceed 1 m/s (Blumberg and Pritchard, 1997). Owing to complex bathymetry, LIS is made up of four major basins which are separated by various sills and shoals affecting the circulation of bottom waters as shown in Figure 1. The Eastern Basin lies between Mattituck Sill and the Race forming a narrow and deep channel (~90 m). The Central Basin, from Mattituck Sill to Stratford Shoal, is characterized by an asymmetrical V-shaped cross section with a deep channel (~40 m) on the southern side and a gradual slope on the northern. The Western Basin, with a deep channel continuing to the eastern part of the Narrows, is separated by the Cable and Anchor Reef (Vieira, 2000). Tidal currents are strong in LIS, ranging from about 0.5 m/s in the central basin to 1 m/s at the eastern end (Vieira, 1990). Freshwater flow enters into the Sound from runoff and drainage along the coast of Long Island, New York, and Connecticut. The discharges of three major rivers (i.e., Thames, Housatonic, and Connecticut) comprise most of the freshwater input (90%) into LIS, and the Connecticut River alone contributes more than 70% of the freshwater influx (Lee and Lwiza, 2005).

2.3 Data and Methods

2.3.1 LIS data

The Connecticut Department of Environmental Protection (CTDEP), Bureau of Water Management, initiated the LIS Ambient Water Quality Monitoring program in January 1991 to establish a database for monitoring water quality in the sound. The monitoring data are collected almost every month including hydrographic and biogeochemical properties: temperature, salinity, density, DO, chlorophyll *a*, nutrients, suspended sediments, and photosynthetically-active radiation (PAR). Hydrographic parameters (temperature, salinity, and density) are measured using a Seabird SBE-19

CTD equipped with fluorometric, PAR and DO sensors. Water samples are also analyzed in a laboratory for biogeochemical parameters. All these properties are measured year-round throughout the sound, as shown in Figure 2, but intensively sampled during the summer season, with up to 49 stations per survey. Most of surveys are done once in a month, and two surveys per month are carried out during the summer season (June-August). Because surveys with more than 17 sampling stations became more common after 1994, the analyses in this study are conducted using data collected between 1995 and 2004.

Time series of surface data are constructed by taking water column data available between 2 and 3 m depth in every station, and bottom data are produced by using the data nearest to the bottom. Surface and bottom chlorophyll *a* data are constructed on the basis of laboratory processed data and filled in with data from a fluorometric sensor. Bottom DO data are also generated primarily with values measured by the Winkler method, and missing data are filled with available DO sensor data, which are calibrated using Winkler titration onboard the survey ship (Kaputa and Olsen, 2000). Temporal gaps in bottom DO, which are less than 2 months, are linearly interpolated only prior to applying optimal interpolation (OI). Time series of summer bottom DO are optimally interpolated on a 0.02^{o} longitude-latitude grid (931 grid-points) in order to identify patterns covering the whole sound. Length scales in OI are determined by using the maximum distance between minimum distances of sampled stations in a given month.

SOM analysis is then applied on the OI data of summer bottom DO, which comprised 70 surveys from June to September for 1995-2004. The volume of hypoxic water is calculated by first determining the thickness of the bottom layer at OI grid-points under hypoxia multiplied by the total affected area. The amount of mean spring total chlorophyll *a* is determined by multiplying the depth-averaged chlorophyll *a* concentration by water depth at each OI grid-point and the total surface area of LIS. Since nutrients are only measured continuously at 17 major stations, mean spring total nitrogen is defined as the average of total nitrogen concentration (ammonia, particulate nitrogen, total dissolved nitrogen, nitrite, and nitrate) in surface water at those stations from February to May.

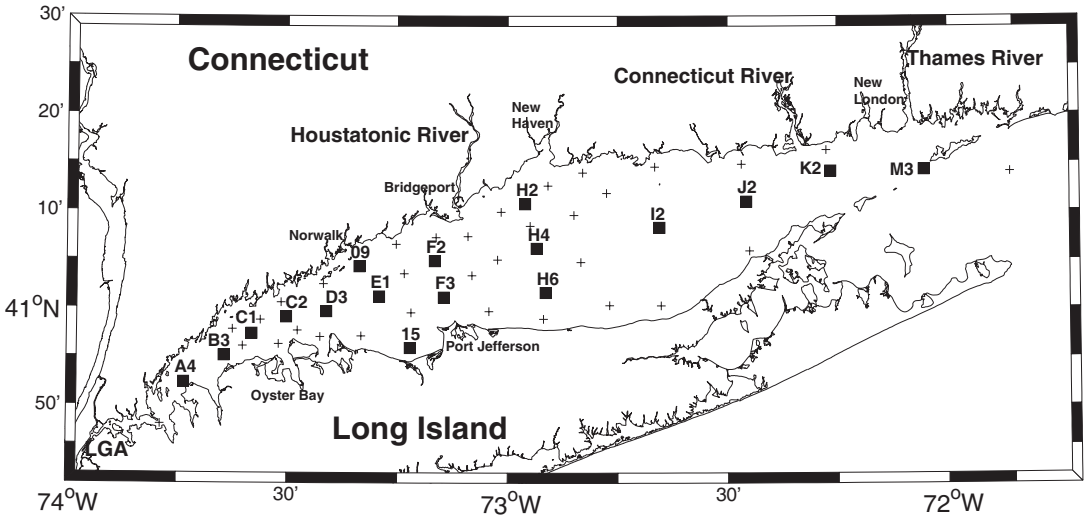

Figure 2-2. The Connecticut Department of Environmental Protection water quality sampling stations (+) in Long Island Sound (square markers indicate the positions of major stations).

2.3.2 Wind and freshwater discharge

In order to estimate the contribution of wind in vertical mixing, we use wind data from Sikorsky Memorial Airport, Bridgeport, Connecticut (WMO ID 72504) to represent the wind condition over the sound. Daily mean wind speed is obtained from National Oceanic and Atmospheric Administration (NOAA) National Climate Data Center (NCDC) historical data archives. Daily measurements are averaged to represent the monthly and summer wind conditions in LIS. In order to determine the effects of freshwater input, monthly freshwater discharge data were retrieved from the U.S. Geological Survey (USGS) website (URL http://nwis.waterdata.usgs.gov/nwis/). Most of freshwater from major rivers entering LIS flows through the Connecticut coast, via the Connecticut River (USGS site number 01184000), the Housatonic River (01205500), and the Thames River which combines the input of the Quinebaug (01127000), the Shetucket (01122500), and the Yantic Rivers (01127500). Monthly discharge rates from these rivers are combined to represent the freshwater discharge into LIS.

2.3.3 Cluster analysis

Principal Component Analysis (PCA)

PCA is used to examine the structure of summer DO interannual variability in the bottom waters. The data matrix includes 17 major stations with seven variables, i.e., DO, river discharge, wind speed, bottom temperature, surface total nitrogen, surface chlorophyll *a*, and density stratification. Rows (objects) represent stations repeated over time. From the PCA of all the variables for each station we plot principle components (based on the first two modes) and eigenvectors of the anomalies on the same scale. This type of a plot is commonly known as a bi-plot (Reyment and Joreskog, 1996), and it is useful in examining relationships between several variables simultaneously. However, one has to be careful in interpreting the results with this kind of a matrix, because relationships due to space or time cannot be easily separated.

Self-Organizing Map (SOM)

Since the DO dynamics might be nonlinear in nature, we apply a nonlinear analysis in addition to the PCA described above. SOM is an artificial neural network based on unsupervised learning (Kohonen, 2001). It is a nonlinear cluster analysis mapping high-dimensional input data onto a two-dimensional output space while preserving the topological relationships between the input data (Liu and Weisberg, 2005). Because SOM is an effective tool in extracting patterns from large data sets, it has been widely used in various fields of studies ranging from sciences to economics (Kaski et al., 1998; Oja et al., 2002). SOM analysis has also been applied to oceanography by Liu and Weisberg (2005) for description of ocean current variability, Richardson et al. (2003) to extract sea surface temperature from satellite data, and Risen et al. (2004) to identify wind regimes. The application of SOM in this study is based on a software package SOM Toolbox 2.0 for Matlab. It is an implementation of the SOM and its visualization in the Matlab computing environment (Vesanto et al., 2000). The SOM Toolbox can be obtained from the Helsinki University of Technology, Finland: URL at http://www.cis.hut.fi/projects/somtoolbox.

2.4 Results

Figure 3 shows the time series of bottom DO at stations A4, 09, H2, and J2 located in each basin from the Narrows to the Eastern Basin for 1995-2004. It is clearly shown that the variation of bottom DO is mainly dominated by seasonal fluctuations at all stations, i.e., maximum bottom DO in late winter (February-March) and minimum bottom DO in summer (July-September). There is a strong longitudinal gradient in variation of bottom DO from east to west. The range of bottom DO is largest in the Narrows (i.e., 0.1~14.8 mg/l at station A4), and it tends to decrease in an eastward direction toward the Race (i.e., 6.6~12.2 mg/l at station M3). There is no clear indication for long-term trends in increasing or decreasing of bottom DO throughout the sound. However, hypoxic condition (less than 3 mg/l of DO) occurs every summer at station A4, but less frequently as one goes further east to the area near station H2. Hypoxia does not

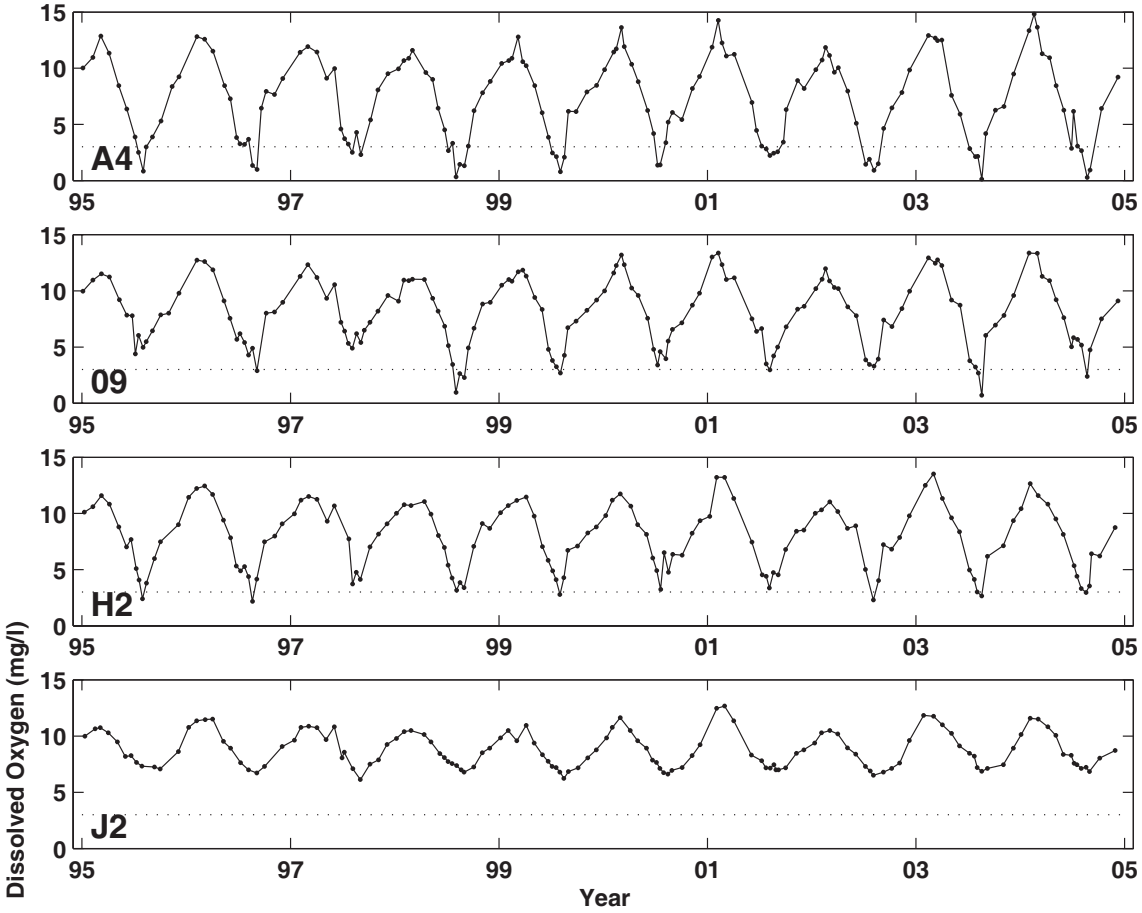

Figure 2-3. Time series of bottom dissolved oxygen (mg/l) at stations A4 (the Narrows), 09 (the Western Basin), H2 (the Central Basin), and J2 (the Eastern Basin) from 1995 to 2004. The dotted-line indicates the threshold of hypoxic condition (3 mg/l of dissolved oxygen).

occur at stations H4, H6, and I2 in the Central Basin and all stations in the Eastern Basin for the entire record. The onset and duration of hypoxia differ from station to station and year to year. For instance, hypoxia occurs during the summer of 1996 at stations A4, 09, and H2 while it is not observed at stations 09 and H2 in 1997. Station A4 undergoes hypoxic conditions in July and August of 2002, but hypoxia only appears at station H2 in early August and it is not observed at station 09. Although the occurrence of hypoxia varies spatially and temporally in LIS, it is generally observed at stations in the Narrows, Western Basin, and the nearshore area of the Central Basin.

We use PCA to examine the structure of DO. The first principle component explains 30% of the variability and the second mode explains 29%. The third and fourth modes contain 14% and 10% of the total variance, respectively. When the first two modes are plotted against each other in a bi-plot as shown in Figure 4, there is a clear distinction between three groups, i.e., stations from the Eastern Basin, the Narrows, and the rest. The data from the Western and Central basins are intermingled. The stations in the Narrows are characterized by high total nitrogen and high chlorophyll *a*; the Eastern basin contains highly oxygenated water, and Central and Western stations are strongly influenced by wind, bottom temperature, stratification and river discharge. The superimposed Empirical Orthogonal Function (EOF) vectors indicate that bottom DO is high where total nitrogen and chlorophyll *a* are low. All the relationships shown are a function of space not time. For example, the positive relationship between total nitrogen and chlorophyll *a* is a spatial one, i.e., both total nitrogen and chlorophyll *a* decrease with distance from west to east. The temporal relationship between the two variables is negative and the total nitrogen lags approximately a month behind chlorophyll *a* as shown in Figure 5.

In order to analyze the variability of DO over the whole sound, SOM analysis is used to detect specific time-dependent patterns of bottom DO, and to quantify which pattern is frequently observed. After several tests, an SOM array size of 4×3 is selected because it best represents the major features of bottom DO for June-September. The parameters used for the SOM analysis are shown in Table 1 and results of a 4×3 SOM array are shown in Figure 6. Each map in the SOM array represents a typical synoptic state within the data, constructed from the weights on that particular unit. The unit, often

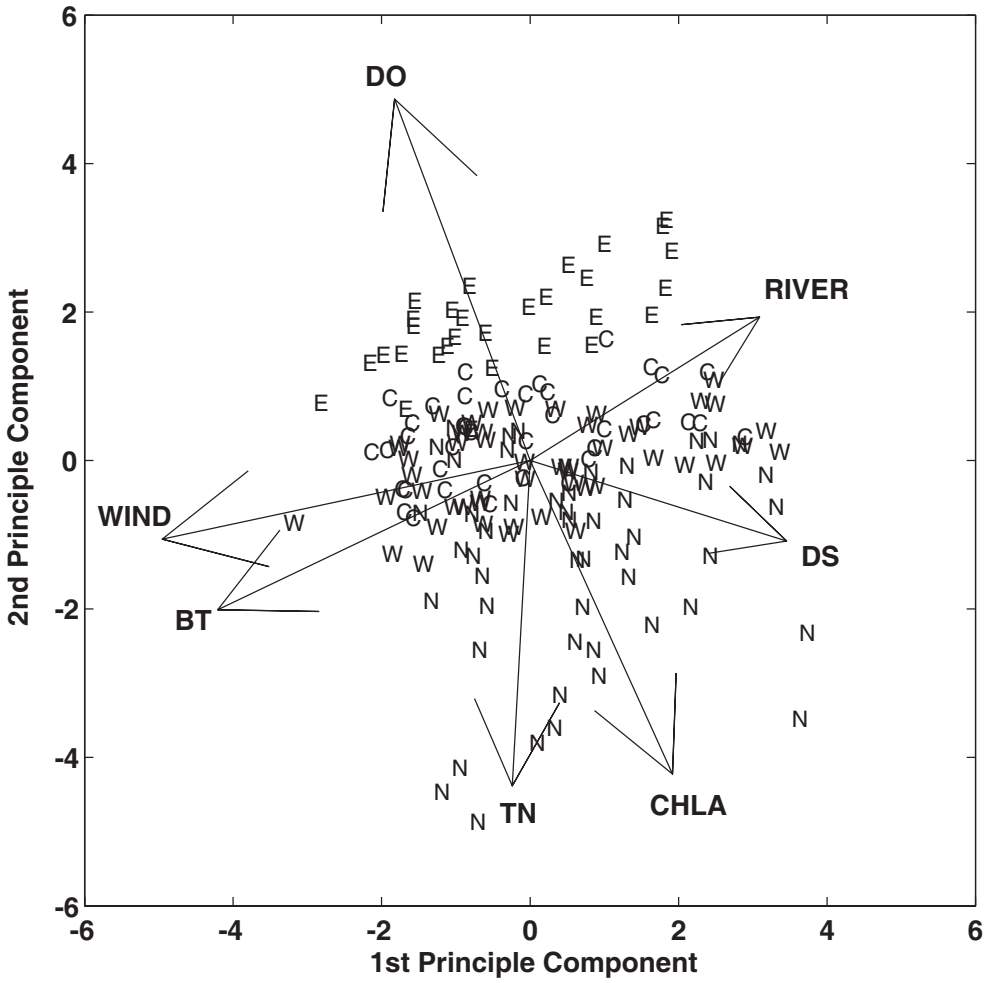

Figure 2-4. A bi-plot of principle components and empirical orthogonal function vectors of bottom dissolved oxygen (DO) in summer, spring chlorophyll *a* (CHLA), spring total nitrogen (TN), summer bottom temperature (BT), summer wind speed (WIND), summer density stratification (DS), and spring river discharge (RIVER) at major stations from 1995 to 2004. Stations in the Narrows are represented by N, C is for the Central Basin, W is for the Western Basin, and E is for the Eastern Basin. There is a good separation between the Narrows stations, the Eastern stations, and the rest of the sound.

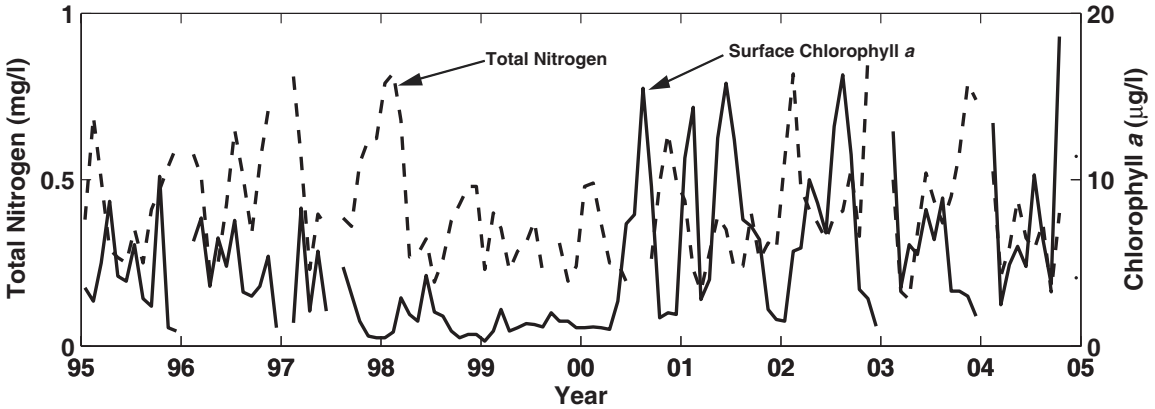

Figure 2-5. Time series of surface total nitrogen (dashed line) and surface chlorophyll *a* (solid line) for station D3 in the Narrows of Long Island Sound from 1995 to 2004.

Table 2-1. Self-Organizing Map (SOM) parameters

Parameter	Value
initialization	linear (default)
training function	batch (default)
map size	4 × 3
map lattice	hexagonal
map shape	sheet
neighborhood function	Gaussian
training length	10

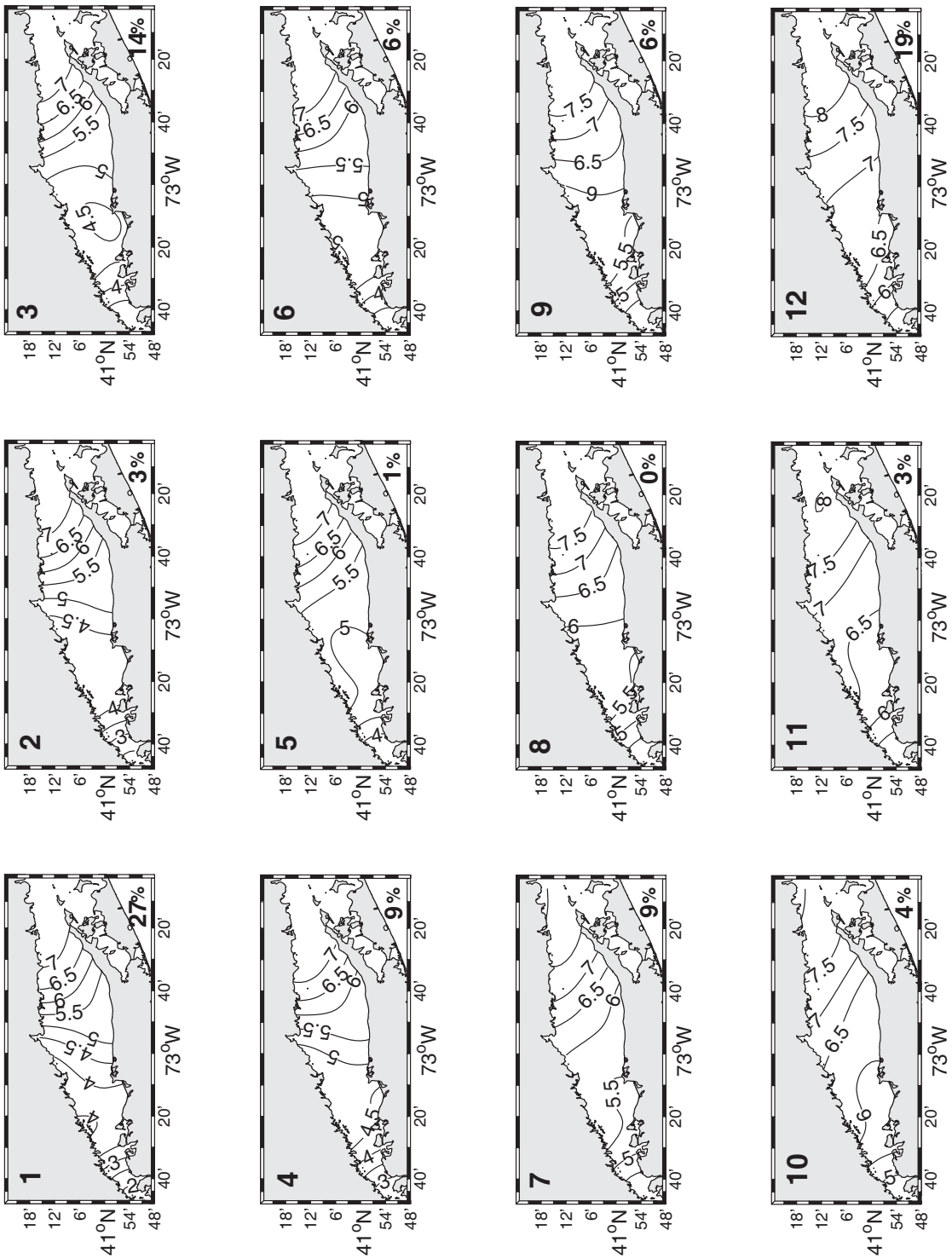

Figure 2-6. A 4×3 self-organizing map (SOM) array of the bottom dissolved oxygen for June-September. The unit of patterns is indicated in the upper-left corner of each map. The relative frequency of units is shown in the lower-right corner of each map as a percentage (%). The bottom dissolved oxygen concentration is contoured every 0.5 mg/l from 2.0 to 8.0 mg/l.

called a node, is indicated in the upper-left corner of each map. The lower numbered maps (the upper-side of the SOM array) exhibit relatively low bottom DO conditions with hypoxic areas while the higher numbered maps (the lower-side of the SOM array) display higher DO levels. All maps indicate strong longitudinal gradients of bottom DO decreasing toward the western sound, which supports the results from PCA. Similar bottom DO patterns are located adjacent to one another and those patterns continuously change across the array. The most dissimilar ones are at opposite ends of the SOM array (i.e., between unit 1 and 12). Once the patterns are characterized, input data are then subjected to SOM unit to find out which patterns they are most similar to. The best matching unit (BMU), or the winning node, can be identified according to the minimum Euclidian distance when that frame is compared to SOM unit. In order to quantify the representation of each unit, relative frequency of occurrence of each pattern is determined as a percentage indicated in the lower-right corner of each map in Figure 6. The most common bottom DO pattern during summer is unit 1 occurring 27% of the input data and showing a pattern with the largest area of hypoxic conditions. Its counterpart, unit 12, represents 19% of the data. There is also a zero frequency at unit 8.

The relative frequency of the input bottom DO data from the BMU evolution can be better viewed monthly as shown in Figure 7. A frequency map for each month highlights the variability of the bottom DO through the summer season. The maps are superimposed on the SOM array so that the coordinates of the frequency map correspond to maps of the SOM array. The relative frequency of patterns in a month is also quantified as a percentage and indicated in each map. The frequency of unit mapping for June is mostly limited to the lower-right of the SOM array such as units 9, 11, and 12 with maximum occurrence of 65% in unit 12. It depicts the bottom DO pattern of early summer with a range of 5.3~8.2 mg/l of DO increasing toward the eastern end. However, frequency map of July shows that units are relatively spread in the upper and left sides of the array with maximum occurrence of 30% at unit 4. It describes the beginning of hypoxic conditions in the Narrows. The most frequent pattern in August is unit 1 with occurrence of 65%. It shows hypoxic conditions in most of the Narrows and suboxic condition (3.5~4.0 mg/l of DO) over the Western Basin except the areas near station 09. It is interesting to note that unit 3 illustrates the isolated suboxic patch (4~4.5 mg/l of

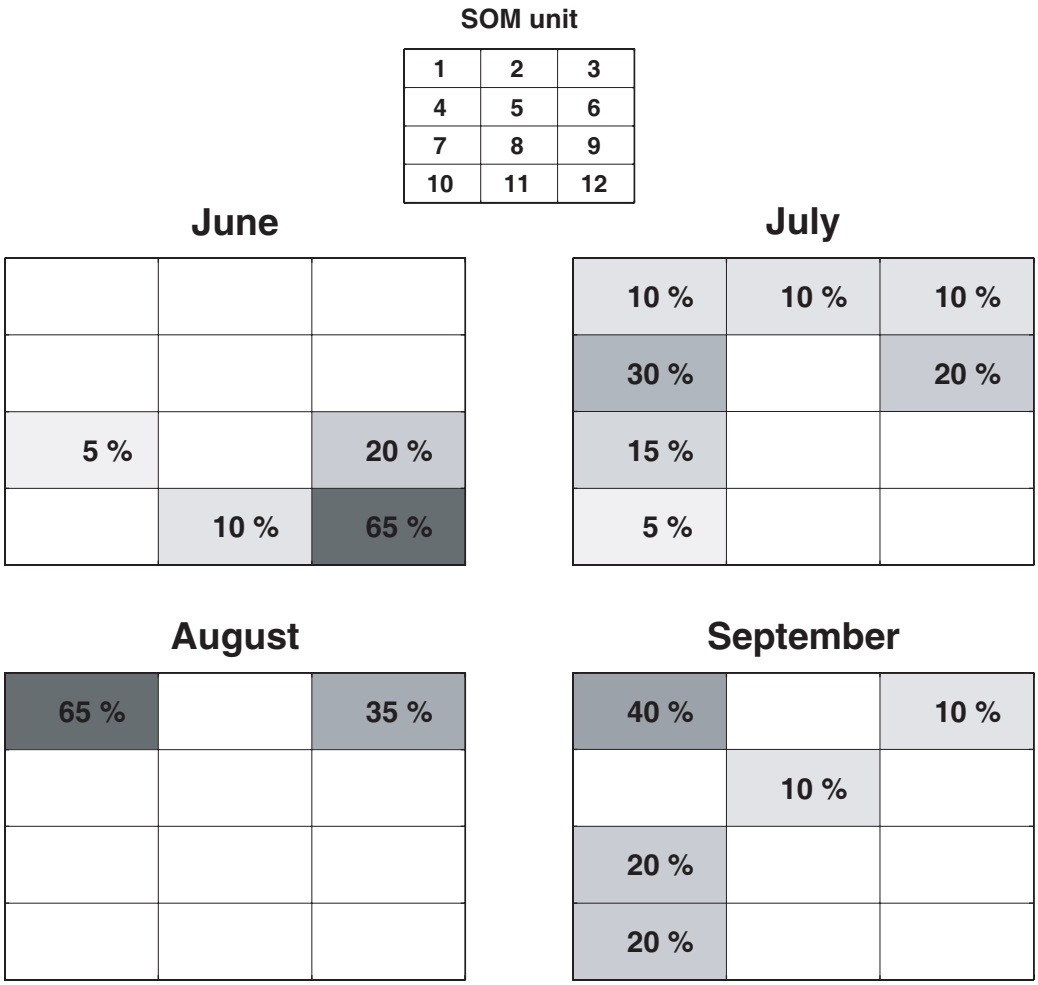

Figure 2-7. Monthly relative frequency map of the 4×3 self-organizing map (SOM) array of the bottom dissolved oxygen from June to September. The coordinates of the each frequency map correspond to SOM unit (top panel) where numbers indicate the unit of patterns in the SOM array (see Figure 6). The percentage in a monthly frequency map accounts for the relative occurrence of each pattern in a given month. For example, unit 1 and 3 are only patterns observed in August and no other units of patterns have occurred.

DO) near Smithtown Bay in the Western Basin, which also frequently occurs (35%). Units 7 and 10 are frequently observed (40%) in September, which are patterns with a range of 4.2~7.6 mg/l of bottom DO. The frequency map still shows unit 1 (40% of occurrence) since September data are often collected in the early part of a month. In general, the SOM analysis is consistent with time series of bottom DO showing that hypoxic conditions appear in July, get fully developed in August, and start to weaken in early September.

To explore the seasonal evolution of DO, the data of bottom DO is analyzed together with temperature, since temperature affects microbial activity and solubility of oxygen. Figure 8 shows results at stations B3, 15, H6, and K2 from the Narrows to the Eastern Basin. Bottom DO in the Eastern Basin (station K2) is almost saturated throughout the year. For the other basins, the bottom DO follows solubility concentrations only for spring, fall, and winter seasons. During summer the bottom DO starts to be under-saturated in June, and it declines linearly with temperature as the season progresses, until it reaches its minimum when temperature is 19~20 °C in August. For stations in the Western Basin (station 15) and the Narrows (station B3) the average rate of change of DO with temperature is approximately 1 mg/l per degree Centigrade, and the rate decreases to zero for stations in the Eastern Basin. What is intriguing is that although temperature may rise up to about 23 °C, the temperature at which minimum bottom DO is observed (19~20 °C) does not vary much. After reaching the minimum concentration, bottom DO recovers quickly within two weeks, and by October it is almost saturated. At first we thought the recovery was driven by wind mixing, because wind speed picks up at the beginning of fall season. Upon closer examination of the time of initiation of DO recovery, it is seen that in most cases the recovery starts before the increase in the wind commences. This result is very surprising, because the traditional understanding for the reason for the DO recovery is that it is mainly driven by wind mixing.

Following the examination of the annual evolution of DO, we analyzed the relationship between bottom DO and temperature during summer, i.e., June-August data. Table 2 shows that the correlation between the two variables is significant at all stations, but it tends to be weaker at shallow stations (<15 m), where mean temperature is

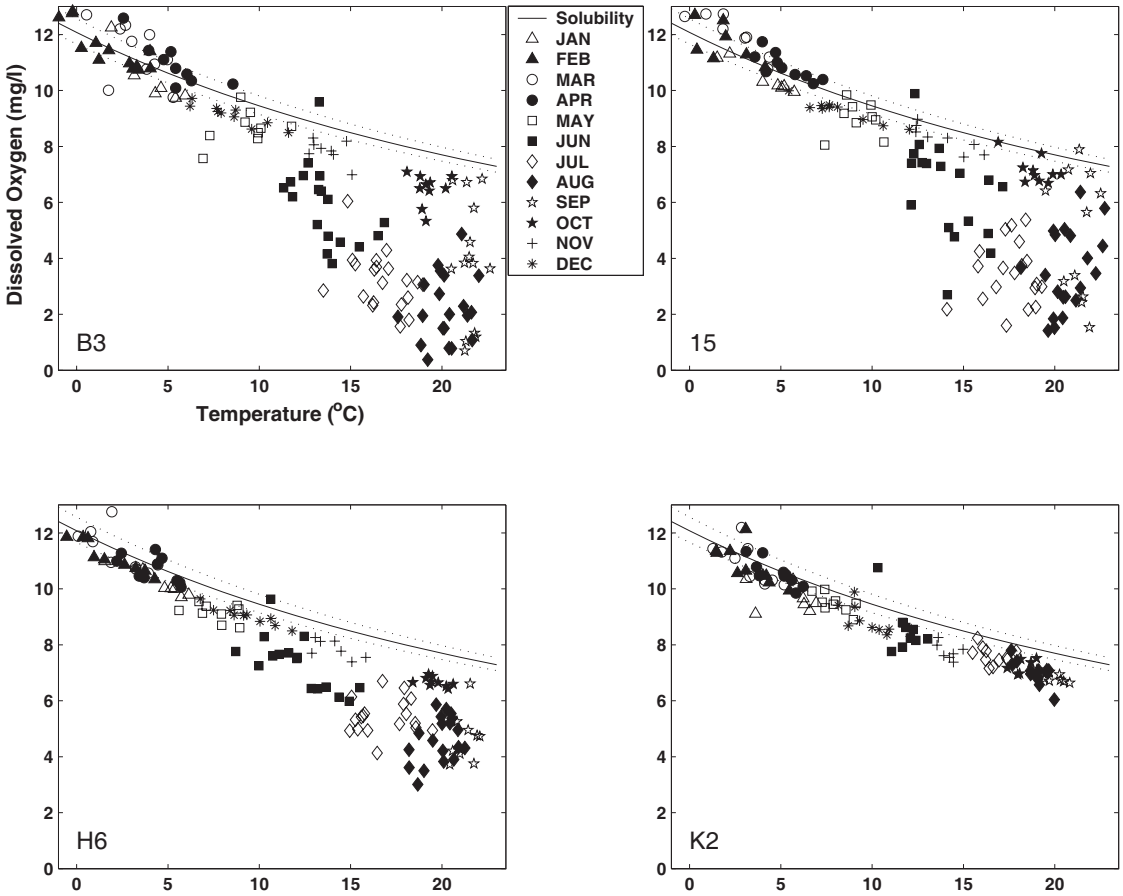

Figure 2-8. The relationship between the bottom dissolved oxygen (mg/l) with bottom temperature (°C) at stations B3, 15, H6, and K2. The solid line indicates the mean solubility and dotted lines are the maximum and minimum solubility depending on salinity.

Table 2-2. Correlation coefficients between bottom temperature (BT) and bottom dissolved oxygen (BDO), and mean temperature for the summer season (June-August).

region	station	depth (m)	correlation coefficient between BDO and BT	mean temperature (°C)
Narrows	A4	32.6	-0.66 ($p<0.01$)	17.6
	B3	18.0	-0.76 ($p<0.01$)	16.9
	C1	19.8	-0.80 ($p<0.01$)	16.9
	C2	32.4	-0.87 ($p<0.01$)	16.6
	D3	40.9	-0.89 ($p<0.01$)	16.5
Western Basin	09	9.1	-0.58 ($p<0.01$)	17.8
	E1	38.1	-0.89 ($p<0.01$)	16.3
	15	15.3	-0.57 ($p<0.01$)	17.6
	F2	19.7	-0.83 ($p<0.01$)	16.9
	F3	40.9	-0.87 ($p<0.01$)	16.6
Central Basin	H2	13.9	-0.74 ($p<0.01$)	17.6
	H4	23.7	-0.88 ($p<0.01$)	17.3
	H6	41.4	-0.79 ($p<0.01$)	16.5
	I2	27.3	-0.86 ($p<0.01$)	17.7
Eastern Basin	J2	21.8	-0.87 ($p<0.01$)	17.3
	K2	37.7	-0.82 ($p<0.01$)	15.7
	M3	72.6	-0.82 ($p<0.01$)	15.2

relatively higher. For example, stations 09, 15, and H2 show weaker correlation coefficients (r) between -0.57 and -0.74, and higher mean temperatures (17.6~17.8 °C). It is interesting to note that station A4, albeit deep, exhibits characteristics similar to shallow stations; r is -0.66 and the mean temperature is 17.6 °C. In contrast, relatively stronger correlations ($r \leq -0.76$) between bottom DO and temperature are shown at deep stations (>20 m) accompanying the lower mean temperature (less than 17 °C). However, some stations, e.g., stations I2 and J2 exhibit relatively higher mean temperature with stronger correlation.

Since stratification plays a crucial role in the variability of DO, the saturation of DO is also examined with density stratification for June-August. The solubility of DO is calculated using a formula by Weiss (1970) in order to remove effects of temperature and salinity. Figure 9 clearly indicates that bottom DO in the Eastern Basin (stations J2, K2, and M3) is always saturated despite density stratification changes. The relationship between the two variables is statistically significant only at the westernmost and shallow stations, i.e., A4, 09, 15, and H2, where the bottom temperature is weakly correlated with DO and the mean temperature is relatively high (see Table 2). In contrast, the saturation of bottom DO barely co-varies with stratification at deep stations, where stratification tends to be greater (> 1 kg/m^3) than in shallow stations. Moreover, the mean saturation of DO decreases in a westward direction while the stratification changes little from one station to another.

Nixon et al. (1995) showed that primary production is the major source of organic carbon, whose decomposition leads to reduced oxygen levels in the bottom water (Rabalais et al., 2002). Anderson and Taylor (2001) also suggested that the export production from surface waters appears to be more important in fueling biological oxygen demand (BOD) in bottom water than allochthonous inputs of organic matter. Hence, we examine the relationship between hypoxia and spring (February to May) primary production, summer (July to August) wind speed, maximum spring discharge, and spring total nitrogen. The volume of hypoxic condition is determined using the OI data. Figure 10(a) shows the linear relationship between the maximum hypoxic volume and mean spring total chlorophyll *a* for the whole sound, which is not significant (r^2=0.19, $p>0.05$). Despite having the highest primary production in 2001, the volume of hypoxic

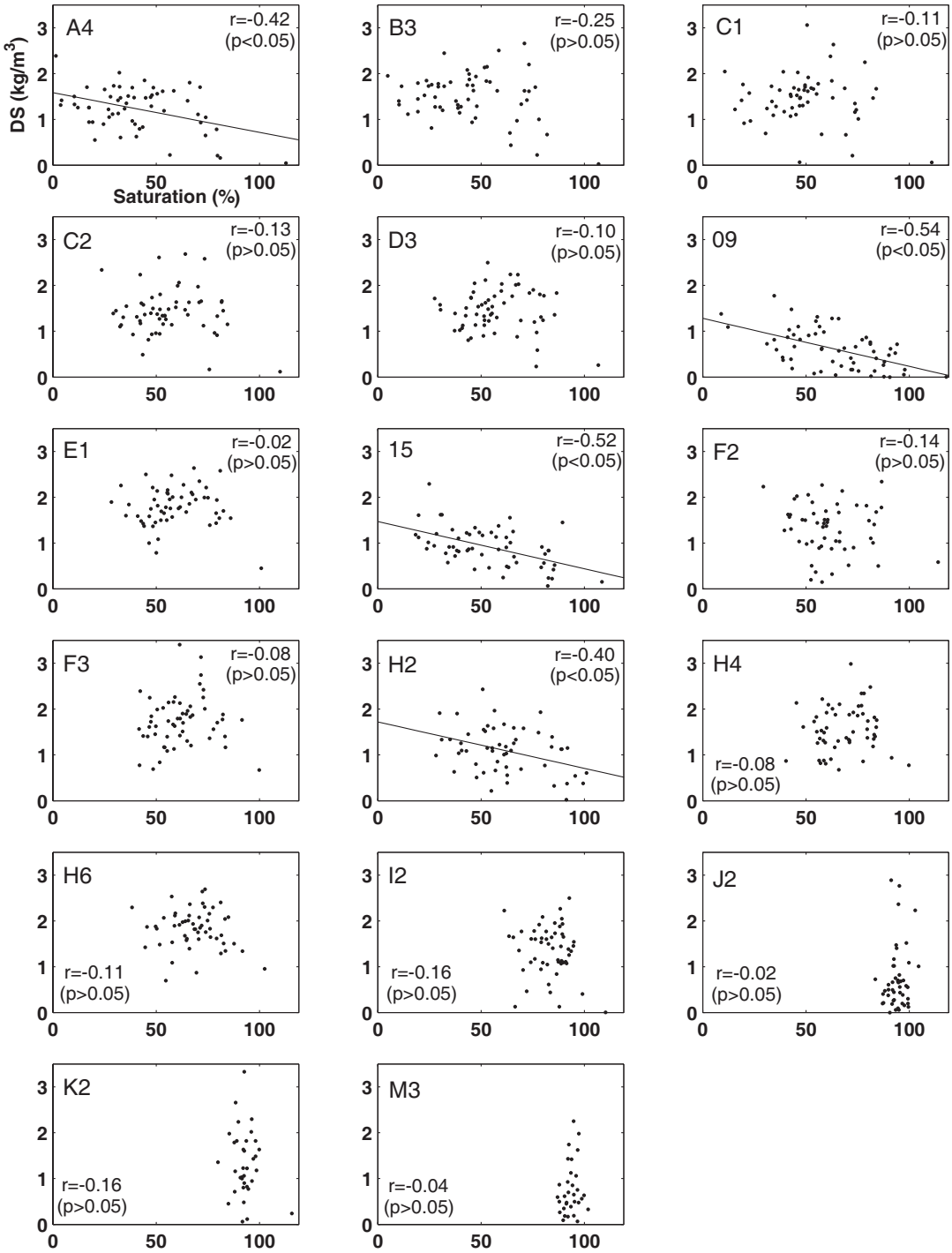

Figure 2-9. The relationship between the density stratification (DS) calculated as a difference between surface and bottom values (kg/m^3), and the saturation of bottom dissolved oxygen as a percentage (%) for June-August. The name of station is indicated in the upper-left and the correlation coefficient (r) is shown in the upper-right or the lower-left. A solid line indicates the linear relationship when the slope is significantly different from zero ($p<0.05$).

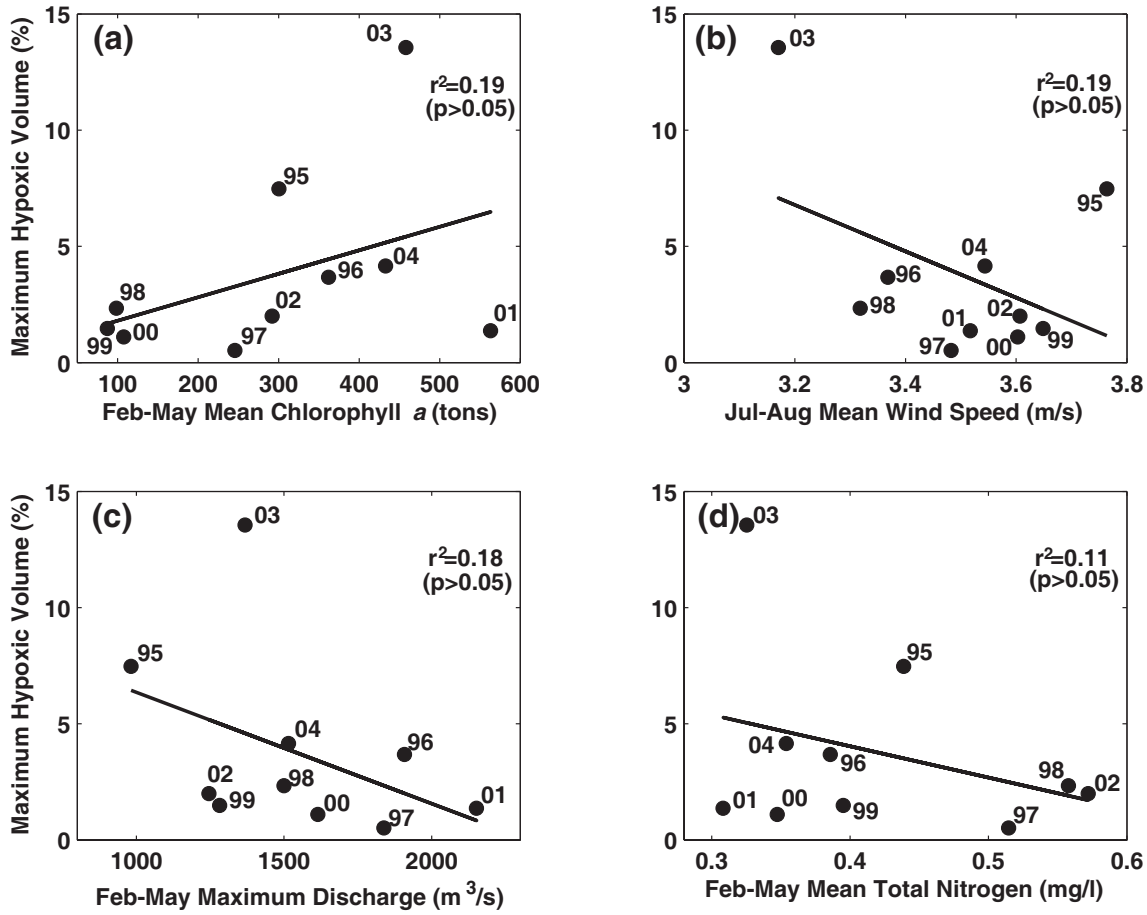

Figure 2-10. The relationship between the maximum hypoxic volume as a percentage (%) and (a) mean spring (February-May) total chlorophyll *a* for the whole sound (ton), (b) mean summer (July-August) wind speed (m/s), (c) maximum spring (February-May) discharge into Long Island Sound (m^3/s), and (d) mean spring (February-May) total nitrogen (mg/l), from 1995 to 2004. The solid lines indicate the least-squares fit from linear regression and the coefficient of determination (r^2) is shown in the upper-right.

condition was less than 1.5% of the total volume, whereas hypoxia occupied about 14% of the sound in 2003 with the lesser primary production. Figure 10(b) shows the average of wind speed during summer is negatively correlated with the hypoxic volume, with a coefficient of determination of r^2=0.19 ($p>0.05$). Also, Figure 10(b) helps to explain why year 2001 appears to be an odd year. The mean summer wind speed in 2001 was medium, i.e., wind mixing minimized the effect of spring biomass production, whereas the weak wind in 2003 could not overcome stratification. Therefore, the effect of spring primary production and wind mixing in summer is an important factor in determining the maximum volume of hypoxic condition. Although hypoxia in other estuaries is strongly associated with freshwater input (e.g., Kemp et al., 2005), Figure 10(c) indicates that there is a weak negative relationship between the maximum volume of hypoxia and the amount of freshwater discharge into LIS, r^2=0.18 ($p>0.05$). The relationship is worse with the mean spring total nitrogen yielding r^2=0.11 ($p>0.05$). Figure 10 clearly illustrates that the individual relationship for every variable we have considered with hypoxic volume is weak. Next we decided to examine the combined effect of all the variables. Multiple linear regression using spring chlorophyll *a*, summer wind speed , spring river discharge and spring total nitrogen produces a strong relationship with r^2=0.92 ($p<0.01$) as shown in Figure 11. When total nitrogen is removed the coefficient of determination drops slightly to r^2=0.84 ($p<0.01$). Surprisingly, the largest change is detected when river discharge is excluded, with the coefficient of determination dropping to r^2=0.31 ($p>0.05$).

2.5 Discussion

The SOM analyses (Figure 6 and 7) have revealed that unit 1, i.e., the severe hypoxic condition, is the most frequently occurring pattern during summer in LIS. It is interesting to note that there is a region near station 09, the shallowest station, showing a higher concentration of DO compared to surroundings. Table 2 shows the highest mean temperature with a weak correlation of bottom DO and Figure 9 exhibits the strongest relationship of bottom DO with density stratification at station 09. This means that vertical mixing tends to play an important role in the variability of DO at shallow stations.

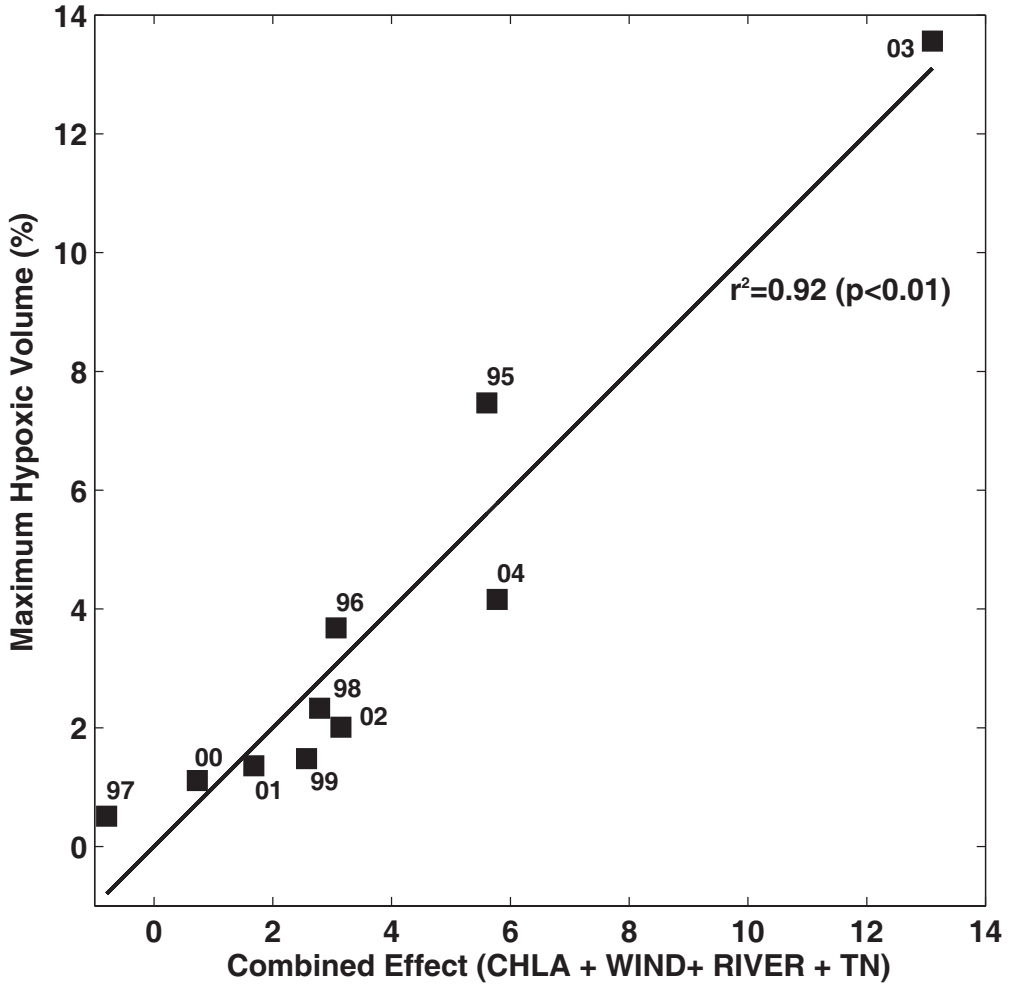

Figure 2-11. Multiple linear regression showing the relationship between the maximum hypoxic volume as a percentage (%) and the combined effect of four variables from the Figure 10, i.e., (i) mean spring total chlorophyll *a* for the whole sound (CHLA), (ii) mean summer wind speed (WIND), (iii) maximum spring discharge into Long Island Sound (RIVER), and (iv) mean spring total nitrogen (TN). The solid line represents the least-squares best fit from linear regression with the coefficient of determination (r^2) shown in the upper-right.

In contrast, unit 3 demonstrates the suboxic patch (4~4.5 mg/l of DO) near Smithtown Bay in the Western Basin, which exhibits the lower DO compared to surroundings. In the central area of the Western Basin near stations F3 and E1, bottom water with a range of 3-4 mg/l of DO was observed in August of 1995, 1997, 1999, 2001, and 2004 (not shown). It is possible that the bottom water becomes stagnant due to the complex bathymetry because these stations are located along the deep channel (~40 m) in the Western Basin which is separated by shoals (see Figure 1). Its location coincides with that of a cold water pool that usually occurs in the bottom of the Western Basin during summer (e.g., Gay et al, 2004; Crowley, 2005). Hence, the bottom water is likely to be isolated from surroundings and inhibited from vertical mixing with oxygenated water.

Previous studies (HydroQual Inc., 1995; O'Shea and Brosnan, 2000; Anderson and Taylor, 2001) have shown that stratification or vertical mixing was an important contributing factor to the variability of bottom DO in the western LIS. However, this characteristic is not universal to all stations in LIS. Only stations such as A4, 09, 15, and H2 exhibit a strong relationship between bottom DO and stratification (see Figure 9). This implies that bottom DO is indirectly related with bottom temperature but has no functional relationship with stratification at deep stations. Solubility seems to control bottom DO in the Eastern Basin (see Figure 8). Figure 4 suggests that the factors involved in controlling summer bottom DO differ from region to region in LIS. This longitudinal gradient may stem from the differences in primary production, nutrient, hydrographic properties and dynamics. For example, nitrogen loading from sewage treatment plants in the densely populated areas around the western LIS may stimulate primary production. The longitudinal distributions of DO and other scalar properties (e.g., nutrients, temperature, and salinity) possibly occur through the advection of fronts and the processes involved in exchange with adjacent water (Lee and Lwiza, 2005). Therefore, findings in previous studies may be insufficient to adequately describe the variability of bottom DO for the whole sound.

Our results indicate that the bottom DO begins to be under-saturated in June, which coincides with the maximum density stratification and weak wind speed. This supports what was observed by Welsh and Eller (1991) about the period of oxygen depletion being associated with the period of stratification. However, the stronger density

stratification observed at deep stations is not strongly associated with changes in bottom DO. Undoubtedly stratification hinders transport of oxygen to the bottom layer, but intensification of stratification does not necessarily result in further depletion of oxygen. Hence, biological uptake is more likely a major factor that controls the variability of DO at deep stations during summer. Nutrient concentrations in LIS clearly affect the upper limit of phytoplankton biomass, which accumulates during the spring bloom (Riley 1952). The influence of nutrients on the onset of spring blooms, however, may be diminished during warmer winters. The long-term data set of the CTDEP indicates that during abnormally warm winters (i.e. 1998 – 2000), there is little if any detectable spring bloom and nutrient concentrations remain elevated from January to March in LIS (see Figure 5). Such years tend to be associated with weak hypoxia. Phytoplankton contribute to BOD in several ways. When DO demand exceeds gross photosynthetic production under low light conditions, and phytoplankton continue to respire, they become oxygen consumers rather than producers (Cole et al., 1992). Therefore, at night phytoplankton below the photic zone can become a major component of the BOD (Jensen et al., 1990). In addition, since they are the major food source for herbivores, they indirectly fuel BOD by the zooplankton. Jensen et al. (1990) showed that the combined effect of phytoplankton and bacteria may account for 64-83% of total community BOD. Hence, processes which stimulate primary production and vertical export of particulate organic carbon (POC) to bottom waters will enhance BOD at depth and contribute to hypoxia.

Phytoplankton and bacterioplankton are a major source of BOD (Anderson and Taylor, 2001; Welsh and Eller, 1991), and bacteria are presumably the primary consumers of organic matter produced at the surface. The bacterial decomposition can be enhanced by the increase of water temperature, which eventually results in the higher BOD level since temperature is an important factor controlling bacterial abundance and production (Staroscik and Smith, 2004). Except for the Eastern Basin, the strong correlation between temperature and DO may indicate the relationship of bottom DO with the bacterial activity during summer. Minimum bottom DO occurs in LIS when the temperature is approximately 19~20°C in early August although temperature may rise up to about 23°C in September (see Figure 8). This suggests that 20°C may be the optimum temperature for maximum estuarine bacterial production as proposed previously by Shiah

and Ducklow (1994a). Shiah and Ducklow (1994b) demonstrated that substrates become limiting when higher temperatures allow faster maximum bacterial growth, because cells require greater rates of substrates supply. When temperature exceeds 20°C, rates of microbial production and respiration slow down because organic matter gets depleted. However, it is not clear how the timing of organic matter depletion would coincide with 20°C every year. Another, alternative explanation is that bacterial biomass can be influenced by grazing (Shiah and Ducklow, 1994a). Anderson and Taylor (2001) also showed that bacterial biomass in LIS reached maximum values in July and early August, and consequently become low and relatively constant thereafter in bottom waters.

Examining the role of bacterial biomass in regulating DO as discussed above is important, because, the recovery from minimum DO levels in late summer or early fall has generally been accepted as a result of increased wind mixing from summer low. However, our study shows that the increase of bottom DO from the minimum usually begins in mid-August, well before the wind speed starts to increase. This shows that the recovery is not necessarily driven by increased mixing. It seems to support the argument of bottom DO budget being driven by one or a combination of the following: (i) reduced bacterial activity, (ii) leakage of oxygen from the surface layer due to background diffusion, and (iii) horizontal exchange.

Practical implications of understanding DO dynamics are finding ways of reducing the frequency and the extent of hypoxia to the minimum. Our results show that hypoxic volume is weakly correlated to summer wind speed, spring total nitrogen, spring chlorophyll *a*, and maximum river discharge. We used spring values for total nitrogen and chlorophyll *a* because that is when maximum concentrations of chlorophyll *a* occur, implying maximum contribution to the organic carbon pool. Maximum river discharge was applied in order to represent major flood events. Interannual variability of total nitrogen has the weakest coupling because nitrogen concentrations are driven by the phytoplankton biomass (see Figure 5). At first the fact that maximum river discharge is negatively correlated to the hypoxic volume is surprising because we thought high volume of freshwater input would lead to strong stratification, thus cutting off the bottom water early in spring. However, the negative correlation seems to indicate that extreme river discharge events may act to enhance estuarine circulation, which brings in more

oxygen to the bottom water. What is even more intriguing is that the river discharge which had a weak correlation (r^2=0.18) with hypoxic volume had the largest impact when excluded from multiple regression. Since the combined effect of all four factors produces a very strong correlation, it underscores the fact that these factors interact and may act synergistically to influence the DO balance in ways we have yet to fully understand.

The results may explain also why recently LIS has experienced severe hypoxic conditions despite efforts in waste management plans. The LIS TMDL management initiative calls for a reassessment phase whereby response to nitrogen reduction is evaluated. Interannual variability in summertime bottom DO confounds this assessment and necessitates an evaluation of factors controlling this interannual variability. Since the TMDL goals (not just for LIS, but most regions experiencing hypoxia in the United States) are based on only one factor (nitrogen load) and ignore other important factors, the regional management teams will most probably continue to be frustrated by not being able to accurately evaluate the response. The variability of the combined effect of late winter and spring total nitrogen, spring chlorophyll *a*, spring river discharge, and summer wind condition can explain more than 90% of the variability in summer-time hypoxia in LIS. We want to emphasize that this does not mean that regulating nitrogen load is not important. It is the only choice we have because we have no control on the other variables. However, in order to be able to properly assess the response of the ecosystem to nitrogen reduction, we first must have a systematic way of accounting for the effect introduced by the interannual variability of other factors. It is tempting to think that if we know the amount of nitrogen in the water then we can determine primary production, but the coupling between nutrients and phytoplankton biomass is strongly influenced by meteorological forcing. As mentioned earlier, it has been shown that warm winters can adversely affect spring blooms (Keller et al. 1999; Keller et al. 2001; Oviatt et al. 2002). Also, our results show that efforts toward reducing nitrogen loading so far have not had any impact on the frequency or severity of hypoxia. This indicates that nitrogen levels in LIS during late winter and spring are still too high to limit primary production. In order for the TMDL goal to succeed, nitrogen levels have to be lowered such that they can measurably reduce the organic carbon pool.

This study has shown that processes involved in the dynamics of DO are more complicated and they often interact all year around. Water quality data collected on weekly to monthly basis as in most of research programs are probably inadequate because the residence time of particles in LIS is on the order of a few days (Aller and Cochran, 1976). In addition, it has been shown that, at the highest observed BOD rates, DO in bottom waters would be completely depleted in less than 3 days (Anderson and Taylor, 2001). Therefore, in order to understand the mechanisms controlling the dynamics of DO in LIS better, future research work needs to include other areas (tidally dominated and non-tidally dominated), and surveys should be conducted at higher frequency to capture those processes that occur at timescales on the order of days. There are still uncertainties in biological uptakes, for example, sediment oxygen demand since benthic communities may account for the higher proportions of the BOD (Aller, 1994), and the role of grazing on bacteria. Previous modeling efforts (e.g. HydroQual, Inc., 1995) have mainly focused on the physics (mixing and stratification) and simple oxygen balance with biological consumption rates that need to be re-evaluated.

2.6 Summary

The variability of bottom DO has been examined in relation to temperature and density stratification over the whole sound. No clear indication is shown in long-term increase or decrease of bottom DO, but there is a strong longitudinal gradient in variation of bottom DO from east to west. SOM analysis demonstrates that hypoxia occurs in the Narrows every summer and is less frequently observed in the Western Basin. Hypoxia, however, does not develop at some stations in the Central Basin nor at any station in the Eastern Basin for the entire record. Contrary to previous studies, for the first time we have shown that there is a large spatial variability in the primary factor which controls the bottom DO. For example, the westernmost and shallow stations are largely affected by density stratification, whereas biological processes possibly dominate the variability of bottom DO at other stations (except the Eastern Basin where DO is controlled by solubility). Secondly, our results indicate that the variability of hypoxic volume is a

function of primary production in spring which acts as a source of organic carbon pool. Third, we have shown that although the hypoxic condition is initiated by strong stratification and weak wind speed, its recovery is not necessarily controlled by increased mixing. We propose three mechanisms that might be responsible for abetting recovery, i.e., horizontal exchange, background vertical diffusion and diminished microbial activities. While the first mechanism can act alone to bring in oxygenated water to a hypoxic location, the latter two have to act in tandem. Last but not least, this analysis has exposed a major flaw in the current TMDL policy evaluation. Neglecting the influence of spring bloom production and basing the policy on nitrogen load alone makes it difficult for the management teams to evaluate the response. Therefore, there is a need to include those biogeochemical processes missing in the current models, e.g., role of spring bloom, microbial activity in the water column and the sediment and diagenetic mobilization, and to determine how they interact with physical factors (especially advection) and the competition between vertical mixing and stratification.

Chapter 3

Interannual Variability of Temperature and Salinity in Shallow Water: Long Island Sound, New York

Abstract

Variabilities of temperature and salinity over Long Island Sound (LIS), New York, are examined using observations from 1991 to 2002. There is a strong seasonal variation in the temperature and its interannual variability is characterized by a higher variance during winter than summer. The salinity exhibits regular seasonal patterns driven by freshwater input, but there is a long-term change throughout the Sound. Anomaly maps for the temperature and salinity indicate strong longitudinal gradients increasing in the westward direction. Empirical orthogonal function analyses indicate that the first modes of the temperature and salinity anomaly can explain 87% and 89% of the total variances, respectively. The first mode principle components of the temperature and salinity anomaly contain quasi-biennial periodicities. The salinity anomaly also contains an additional signal at a decadal time scale. Seasonal variations in the temperature and salinity are primarily associated with heat flux and freshwater discharge. However, the surface heat flux anomaly only accounts for 17% of the total variance of the time rate change of the temperature anomaly and the freshwater discharge anomaly explains 25% of the variance of the salinity anomaly. Contrary to traditional paradigms about estuaries, this result shows that forcings other than local processes control the interannual variabilities of the temperature and salinity in LIS, most probably through horizontal exchanges. The significant correlation between the salinity anomaly and the Gulf Stream (GS) position suggests that the interannual variability of salinity in LIS is possibly connected to shelf-slope water properties associated with changes in the GS position.

3.1 Introduction

There has been increasing attention to understand interannual variability of physical environments between ocean and atmosphere. Previous analyses of ocean temperature anomaly in the North Atlantic have revealed variability of sea surface temperature (SST) and sea surface salinity (SSS) on a decadal timescale (e.g., Halliwell, 1997; Mignot and Frankignoul 2003). Evidence presented for the variability of SST and SSS in the North Atlantic is mostly associated with surface heat flux (Halliwell, 1997; Mignot and Frankignoul 2003), wind patterns (Halliwell and Mayer, 1996; Kushnir, 1994), and North Atlantic Oscillation (NAO) (Czaja and Frankignoul, 2002; Robertson et al., 2000). Observations also show that SST and SSS anomaly in the North Atlantic during wintertime keep reemerging in the upper mixing layer in a persistent manner (Alexander et al., 2001; Watanabe and Kimoto, 1999). However, recent studies have shown that anomalous ocean circulation is responsible for the variability of SST on decadal time scales in the North Atlantic, especially in the Gulf Stream (GS) region (Dong and Kelly, 2004; Halliwell, 1998) and the North Atlantic subpolar gyre (Verbrugge and Reverdin, 2003). Halliwell (1998) suggests that SST anomaly in the GS region is primarily associated with changes in horizontal heat advection and entrainment heat flux. Dong and Kelly (2004) performed numerical experiments to simulate the heat balance in the GS region from November 1992 to December 1999. They found that interannual variations in heat content are dominated by anomalous advection of geostrophic currents.

Our knowledge on how estuaries and other shallow coastal waters respond to climate variability is not as clear since few studies have focused on interannual variation of physical properties in shallow waters. Several studies have examined how interannual temperature variability may regulate marine ecosystem structures in shallow waters. For example, it is has been shown that a increase of water temperature may be responsible for reduced primary production in estuaries (e.g., Keller et al., 1999; Oviatt, 2004; Oviatt et al., 2002; Stachowicz et al, 2002) and shelf regions (e.g., Redalje et al., 2002; Roemmich and McGowan, 1995). Oviatt et al., (2002) showed that phytoplankton bloom was negatively correlated with warm water temperature in Narragansett Bay, Rhode Island, which led to the absence of bloom in the El Niño-induced warm winter of 1998. Keller et

al. (1999) found that during warm conditions, there was relatively low phytoplankton biomass associated with high zooplankton abundance. Oviatt (2004) recently showed that during warm winters, winter-spring bloom is suppressed and zooplankton abundance increases, while nutrient levels remain high. Stachowicz et al. (2002) reported that the warm winters facilitate the invasion of nonindigenous ascidian species into eastern Long Island Sound (LIS). All these studies underscore the importance of temperature as an ecological regulator.

Previous studies (Lentz et al., 2003; Mountain et al., 1996; Mountain and Manning, 1994; Taylor and Mountain, 2003; Umoh and Thompson, 2003) suggest that the variability of temperature and salinity along the northeastern U.S. coast are primarily connected to local surface heat flux and freshwater discharge, respectively. Advective processes are addressed as a secondary forcing. Mountain et al. (1996) found that the interannual variability of water temperature in the Gulf of Maine was correlated with surface heat flux variations. Mountain and Manning (1994) showed that the variability of surface salinity in the Gulf of Maine is primarily due to the changes in local freshwater input via runoff and precipitation during 1979-1987. Taylor and Mountain (2003) also suggested that the springtime temperature variability in the northern Mid-Atlantic Bight during the 1956-1973 periods was caused mainly by surface heat flux. This might be true in regions where advective processes are small, but it is not known if that holds true in environments where horizontal exchanges may be important, e.g., estuaries.

The conventional wisdom about seasonal variations of temperature and salinity being mainly driven by local forcings are essentially correct, however, it is not clear yet as to what drives anomalous increase (or decrease) of these properties in coastal shallow waters. Previous studies have not examined shallow water systems (including estuaries) to determine how interannual variabilities of temperature and salinity are related to local or external forcings. As a first step towards answering this question, this study examines characteristics of temperature and salinity variability in a shallow water system, and attempts to associate different time scales with possible forcing mechanisms. We have used water quality monitoring data from LIS as a case study.

Monthly hydrographic survey data collected by the Connecticut Department of Environmental Protection (CTDEP) are examined to determine temporal and spatial

characteristics of the temperature and salinity in LIS. Empirical orthogonal function (EOF) analysis is used to identify spatial structures of the depth-averaged temperature and salinity. We also evaluate the role of advective processes in the heat balance, and the relationship between salinity and riverine discharge to determine whether they are consistent with local effects approach. The paper is organized in the following manner: section 2 briefly describes the area of study. The details of data processing including surface heat flux and effective degrees of freedom are given in section 3. Temporal and spatial structures of the temperature and salinity are described in section 4. The role of horizontal exchange in variation of anomalous temperature and salinity is also examined in section 4. Discussion on possible links to factors influencing the anomalous temperature and salinity variability is presented in section 5, and results are summarized in section 6.

3.2 Study Area

LIS is about 150 km long, 20 km wide, and 20 m deep. It is the sixth largest estuary in the United States. Its bathymetry is characterized by an asymmetrical V-shaped cross section with a deep channel (~40 m) on the southern side and a gradual slope on the northern side. There are several north-south oriented shoals that separate LIS into eastern, central, and western basins. Tidal currents are strong, ranging from about 0.5 m/s in the central basin to 1 m/s at the eastern end. The mean circulation, on the other side, is relatively weak approximately 0.1 m/s or less (Veira, 2000). The LIS circulation exhibits the traditional sense of a 'two-layered' estuarine flow; though, the 'lower-layer' flow does not always stay underneath. Oceanic water enters LIS at the eastern margin of LIS through the Race underneath outgoing less saline water (see Figure 1). As it enters the central basin, the oceanic flow occupies the southern side of the channel from top to bottom, while the outgoing water is restricted to the channel along the Connecticut shore. In the central basin the westward flow occupies the main channel, allowing the lighter water to flow out above it at lower speed. In the western basin, the classical estuarine circulation is fully developed (Veira, 2000). Freshwater flow enters into the Sound from

runoff and drainage along the coast of Long Island, New York, and Connecticut. The discharges of three major rivers (i.e., Thames, Housatonic, and Connecticut) comprise most of the freshwater input (90%). The Connecticut River solely contributes more than 70% of the freshwater influx to the Sound with mean annual flow of 475 m^3/s. Precipitation (110 cm/y) is distributed evenly throughout the year, slightly exceeding the annual evaporation (93 cm/y) in LIS (Thomas et al., 2000).

3.3 Data and methods

3.3.1 LIS water column data

The Connecticut Department of Environmental Protection (CTDEP), Bureau of Water Management, initiated the LIS Ambient Water Quality Monitoring program in January 1991 to establish a database for monitoring water quality in the Sound. The monthly monitoring data include the following water column properties: temperature, salinity, density, oxygen and chlorophyll *a*. These data are collected using a Seabird SBE-19 CTD equipped with dissolved oxygen (DO) and photosynthetically-active radiation (PAR) sensors. These properties are measured throughout the Sound, but intensively sampled during summer season with up to 49 stations per survey.

Time series of the monthly data during 1991-2002 were constructed by averaging whole water column data at every station, and a few gaps in the monthly data were linearly interpolated. Prior to applying EOF analysis, the time series were optimally interpolated on a 0.04º longitude-latitude grid in order to obtain a spatial structure covering the whole Sound. Length scales of the optimal interpolation varied between 5 and 25 km at intervals of 5 km depending on the number of sampled stations in a given month. The number of stations per survey ranged from 4 to 49 stations per month. Months with few stations (less than12 stations) were more prevalent before 1994. The water column data used for most of our study were taken from five major stations, i.e., B3, D3, F3, I2 and M3, indicated by squares as shown in Figure 1. Monthly freshwater

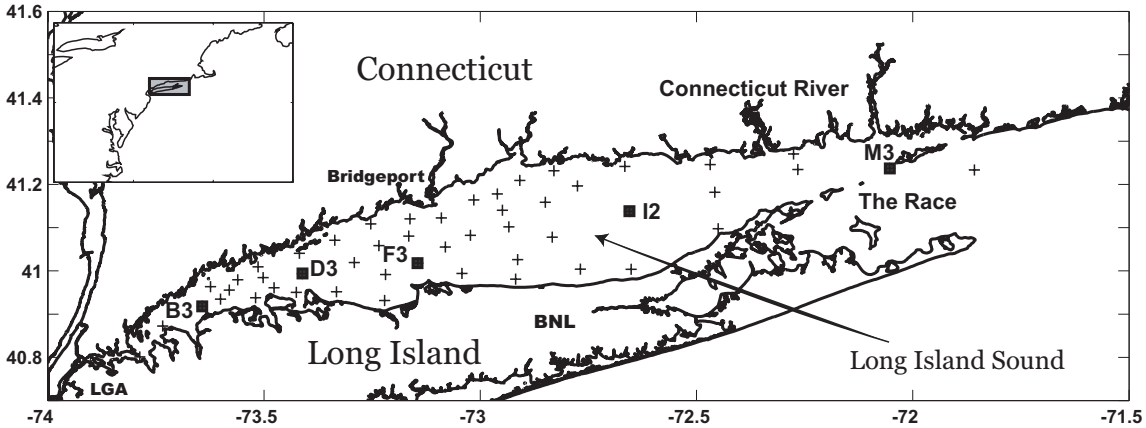

Figure 3-1. Long Island Sound ('+' represents CTDEP sampling stations. Square markers indicate the names of stations where the water column data were selected for this study).

discharge data of the Connecticut River were retrieved from the water resources database at the U.S. Geological Survey website (URL http://nwis.waterdata.usgs.gov/nwis/).

3.3.2. Climate data and surface heat flux

In order to estimate the contribution of local forcings in temperature, we applied simple heat budget formulae to calculate net surface heat flux through the sea surface in LIS. Daily measurements of air temperature, barometric pressure, relative humidity, wind speed, and cloud cover were obtained form National Oceanic and Atmospheric Administration (NOAA), National Weather Service (NWS) and National Climate Data Center (NCDC) historical data archives from 1990 to 2002. Most data such as cloud cover, relative humidity, air temperature, sea level pressure, and wind speed were obtained from the Bridgeport Sikorsky Memorial Airport (BDR), Connecticut. Where the BDR data were missing for a period longer than a week, the gaps were filled by data from the nearest stations available. For example, the relative humidity data from Brookhaven National Laboratory (BNL) were used for January and February of 1997, and cloud cover data from La Guardia Airport (LGA) in New York were also used for the period of 1990-April 1996. Hourly measurements of solar radiation data from BNL were daily averaged to represent the insolation in LIS. Most gaps (less than a week) in the climate data were linearly interpolated. However, the solar radiation data for the whole of 1994 were not available, and the gap was not interpolated.

Estimation of net surface heat flux is based on the bulk formulae. The components of net surface heat flux (Qt) consist of following:

$$Q_t = Q_s + Q_l + Q_h + Q_e \tag{3-1}$$

where, Q_s is surface heat flux due to incoming solar radiation, Q_l is long wave radiation, Q_h is sensible heat flux due to temperature difference between ocean and atmospheric boundaries, and Q_e represents latent heat flux. Estimation of the short wave radiation was adjusted using the albedo representing latitude of 41ºN (Payne, 1972). The long wave

radiation flux was calculated using the bulk formula of Berliand and Berliand (1952) recommended by Fung et al. (1984) with a cloud correction factor from Bunker (1976). The sensible and latent heat fluxes were estimated by the bulk formulae of Tropical Ocean-Global Atmosphere Coupled-Ocean Atmosphere Response Experiment (TOGA/COARE) (see Fairall et al., 1996). It should be noted that the equation is only true for local heat balance, because it does not include advective heat flux (Q_v).

3.3.3 Effective degrees of freedom

Time series data tend to contain a strong auto-correlation, which reduces the number of independent observations. In order to obtain meaningful statistics, it is critical to evaluate the effective number of degrees of freedom using information on the coherence and correlation of data (Emery and Thomson, 2001). Effective degrees of freedom (N*) as given by Chelton (1983) is:

$$N^* = \frac{N}{\left(\sum_{\tau=-\infty}^{\infty} \rho_{xx}(\tau)\rho_{yy}(\tau) + \rho_{xy}(\tau)\rho_{yx}(\tau) \right)} \tag{3-2}$$

where N is data record length, ρ_{xx} and ρ_{yy} are normalized auto-covariance for variables at particular lag τ. ρ_{xy} and ρ_{yx} are normalized cross-covariance.

3.4 Results

3.4.1 Temperature

The depth-averaged temperature in central LIS (station I2) is mainly dominated by seasonal variation as shown in the first panel of Figure 2. The minimum temperature mostly occurs in February, and the maximum occurs in September. The range of the

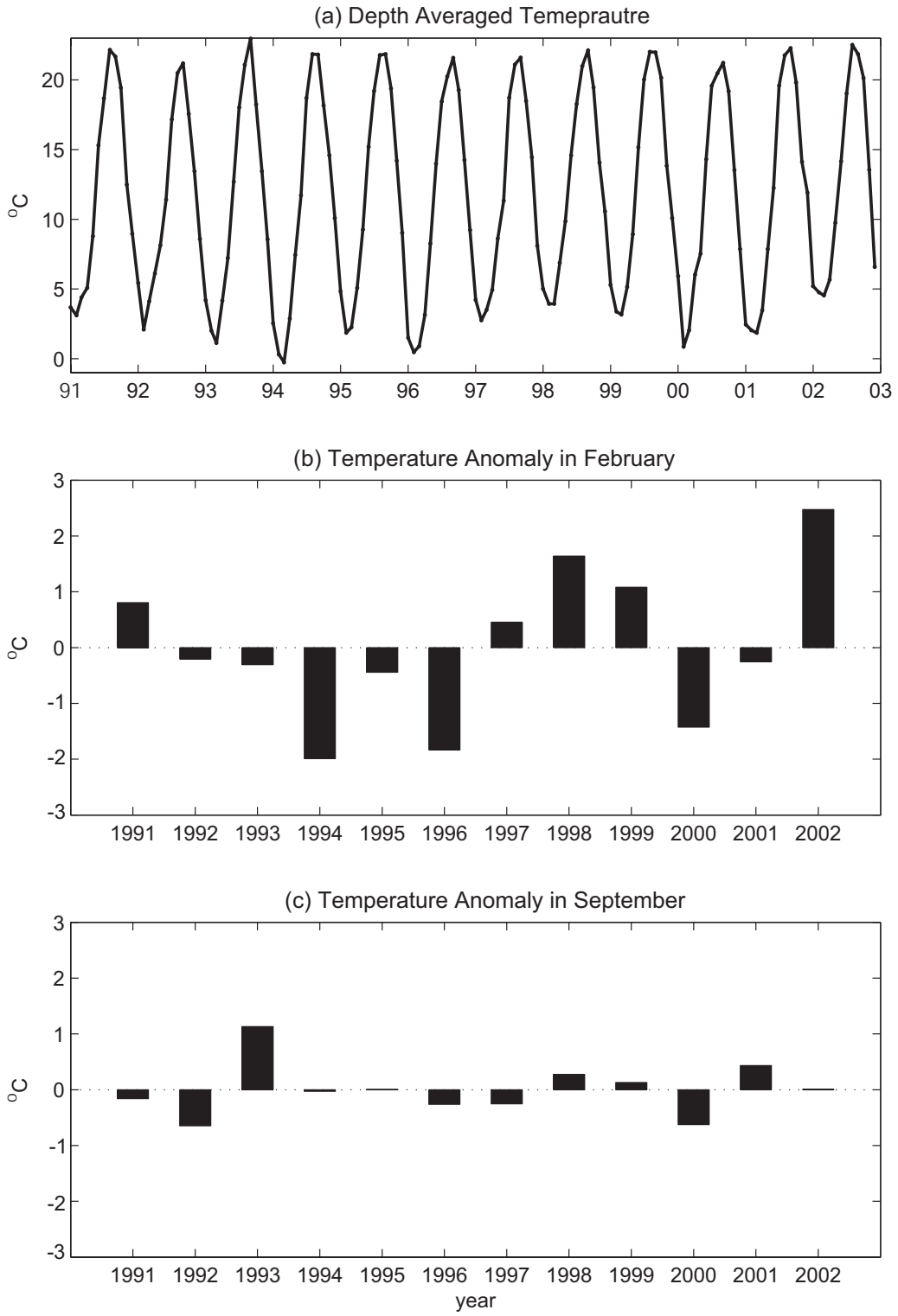

Figure 3-2. Central LIS - Station I2: (a) depth-averaged temperature (b) February temperature anomaly, and (c) September temperature anomaly.

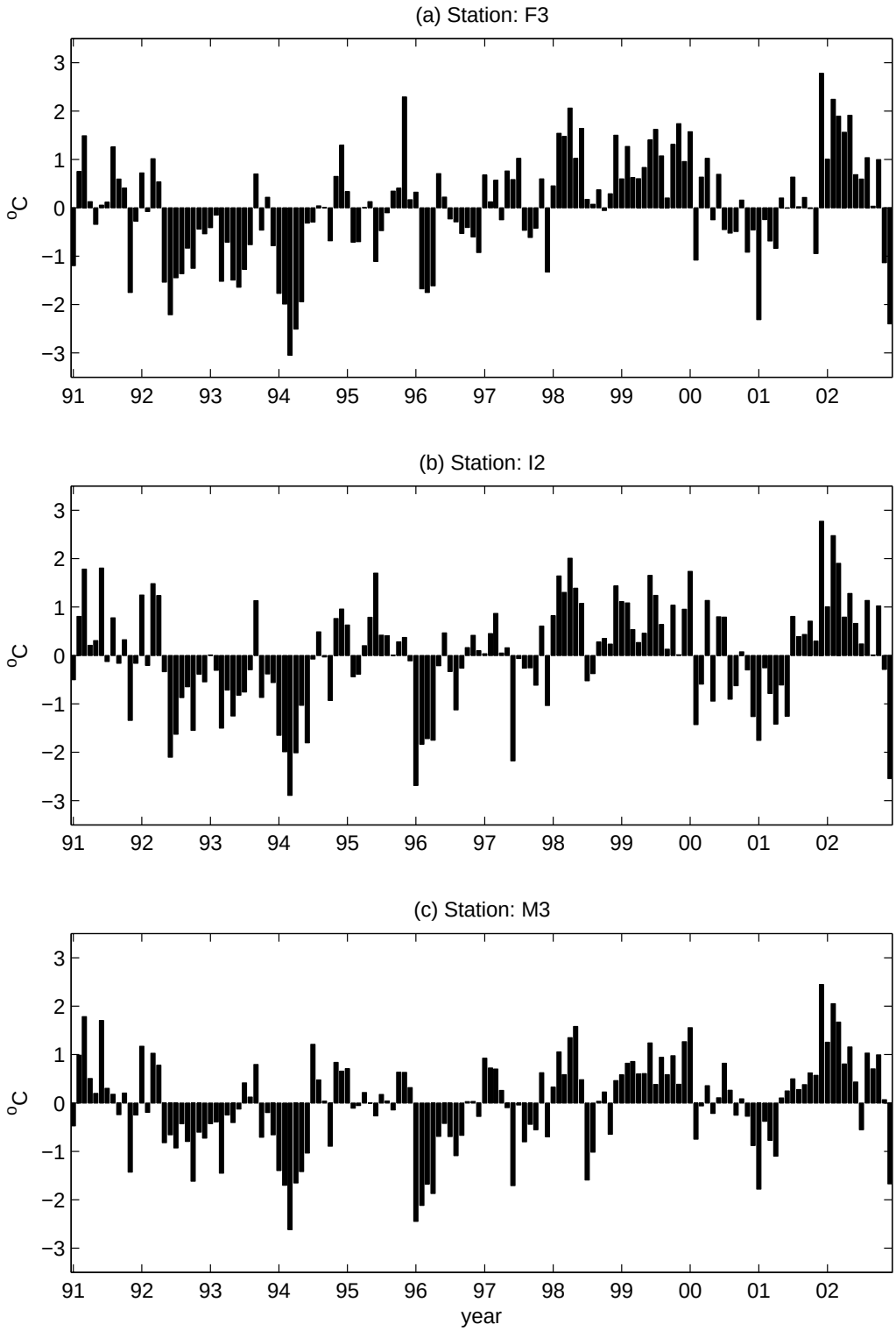

Figure 3-3. Depth-averaged temperature anomalies at (a) station F3, (b) station I2, and (c) station M3.

minimum and maximum temperature is higher in the western Sound (-0.7 to 22.6 ºC) than in the eastern part (1.0 to 20.5 ºC). This means that the temperature of eastern LIS is relatively warmer in winter seasons and cooler in summer seasons than that of western LIS. In general, the winter temperature tends to decrease for the 1991-1993 period, and keeps increasing until 1999. After a short decline in 2000, the temperature notably increased again to the end of data record for winter seasons. One intriguing feature of the depth-averaged temperature is that it shows higher variance in winter, while in summer it fluctuates very little from one year to the next as illustrated in the second and third panels of Figure 2. For instance, the variance of the depth-averaged temperature at station I2 is 1.9 ($ºC^2$) in February and 0.2 ($ºC^2$) in September.

In order to examine the variability of temperature more closely, we remove the seasonal climatology from the depth-averaged temperature data as shown in Figure 3. It is interesting to note that the magnitude and duration of the anomalies in eastern LIS appear different from western LIS. For example, station F3 shows stronger negative anomalies from the summer of 1992 to early 1994 than station M3, while strong negative anomalies at station M3 in the winter of 1996 were drastically reduced at station F3. This anomalous differential heating or cooling along the Sound could be due to anomalous surface heat fluxes (latent and sensible), horizontal exchanges (advection and diffusion), differences in water depth (heat content), or combination of both.

To extend the analysis of the longitudinal variance of the temperature anomaly further, an EOF analysis is used to determine how the pattern of variability is distributed and its evolution with time. Figure 4 shows the spatial pattern of the first EOF mode and its time coefficient of the depth-averaged temperature anomaly. The first mode accounts for 87% of the total variance of the depth-averaged temperature anomaly. The spatial pattern demonstrates the lower amplitude along the thalweg, and the higher amplitude along the shoal areas. Also, it shows lower longitudinal amplitude in eastern LIS, and higher amplitude in western LIS except at western boundary itself, which is most probably due to reduced tidal exchange through the East River. The time coefficient of the first mode of EOF shows large negative values in winter seasons of 1994, 1996, and 2001, and positive values in winter seasons of 1992, 1998, and 2002. The major events

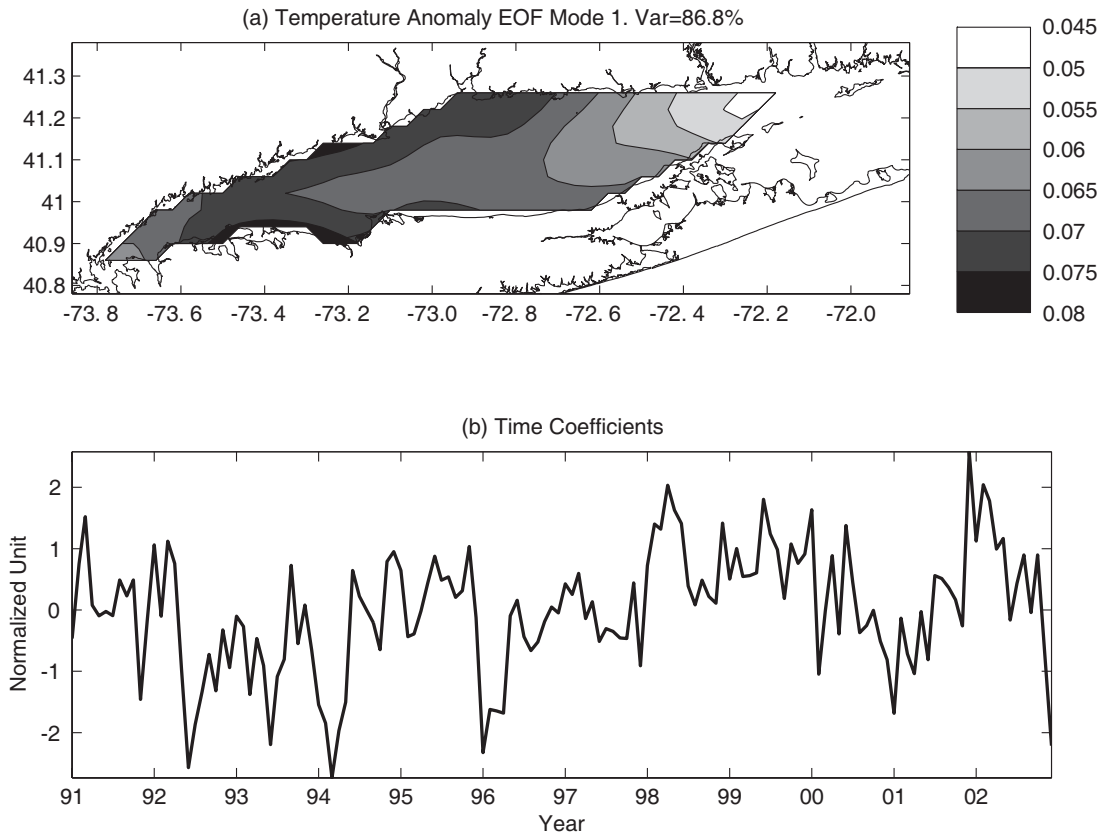

Figure 3-4. Depth-averaged temperature anomaly (a) spatial pattern of the first EOF mode and (b) time coefficient.

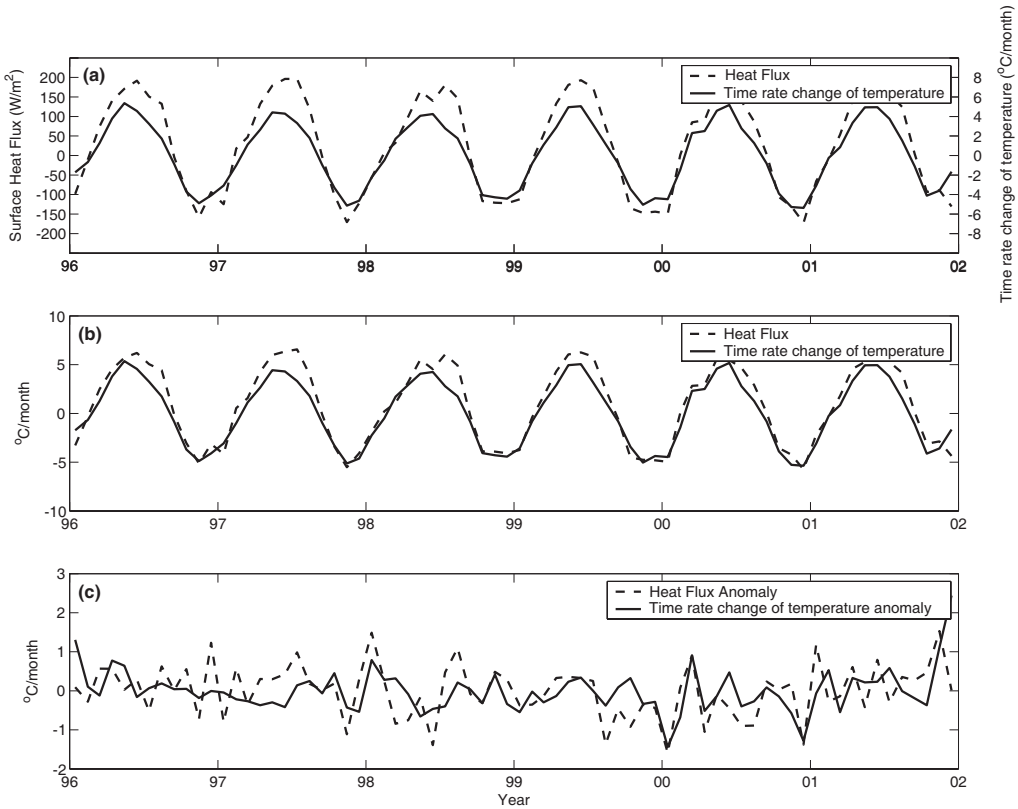

Figure 3-5. (a) Net surface heat flux (dashed) and the time rate change of temperature (solid), (b) same as (a), but units of both data are given in ^{o}C/month, and (c) surface heat flux anomaly (dashed) and the time rate change of temperature anomaly (solid) based on (b) in Long Island Sound.

are spaced at approximately two years apart, but it is not immediately clear what drives this quasi-biennial variability.

Since seasonal temperature is mostly driven by surface heat flux in various regions, we examined a role of net surface heat flux and its anomaly in temperature variation. Prior to calculating net surface heat flux, the temperature and density are averaged over the whole Sound to obtain one number for each variable. Figure 5(a) shows that the seasonal net surface heat flux is highly correlated with the time derivative of temperature in LIS for 1996-2001. The variation of the heat flux (Q_t) explains 95% of the time derivative of the temperature $(\partial T / \partial t)$. The heat content increases in spring/summer when the surface heat flux is positive, and decreases in fall/winter when the surface heat flux is negative. In order to compare these two variables quantitatively, the heat flux is divided by the density, specific heat, and mean water depth of LIS (20.4 m) as shown in Figure 5(b). It demonstrates that the heat flux and the change of the temperature are balanced during fall/winter seasons, but the time rate change of the temperature in LIS is lower than the heat flux coming from the surface during spring/summer seasons. When the seasonality is removed, the effect of the surface heat flux on the time rate change of the temperature anomaly variation is greatly reduced. As shown in Figure 5(c), the anomaly of net surface heat flux $(Q_t^{'})$ only accounts for 17% of the total variance of the time derivative of the temperature anomaly $(\partial T^{'} / \partial t)$ for 1996-2001 when all months are considered. The explained variance increases to 30% when only winter months (January-March) are considered.

3.4.2 Salinity

In this section, we explore variability and balance of the depth-averaged salinity in LIS with freshwater discharge and possible connections to shelf-slope water properties. Before we begin analyzing the freshwater discharge, which primarily contributes to seasonal variability of salinity in costal regions, a role of precipitation on variability of salinity is examined. Precipitation does not seem to play a significant role in the salinity variability and the freshwater runoff in LIS (not shown). The river runoff in LIS can

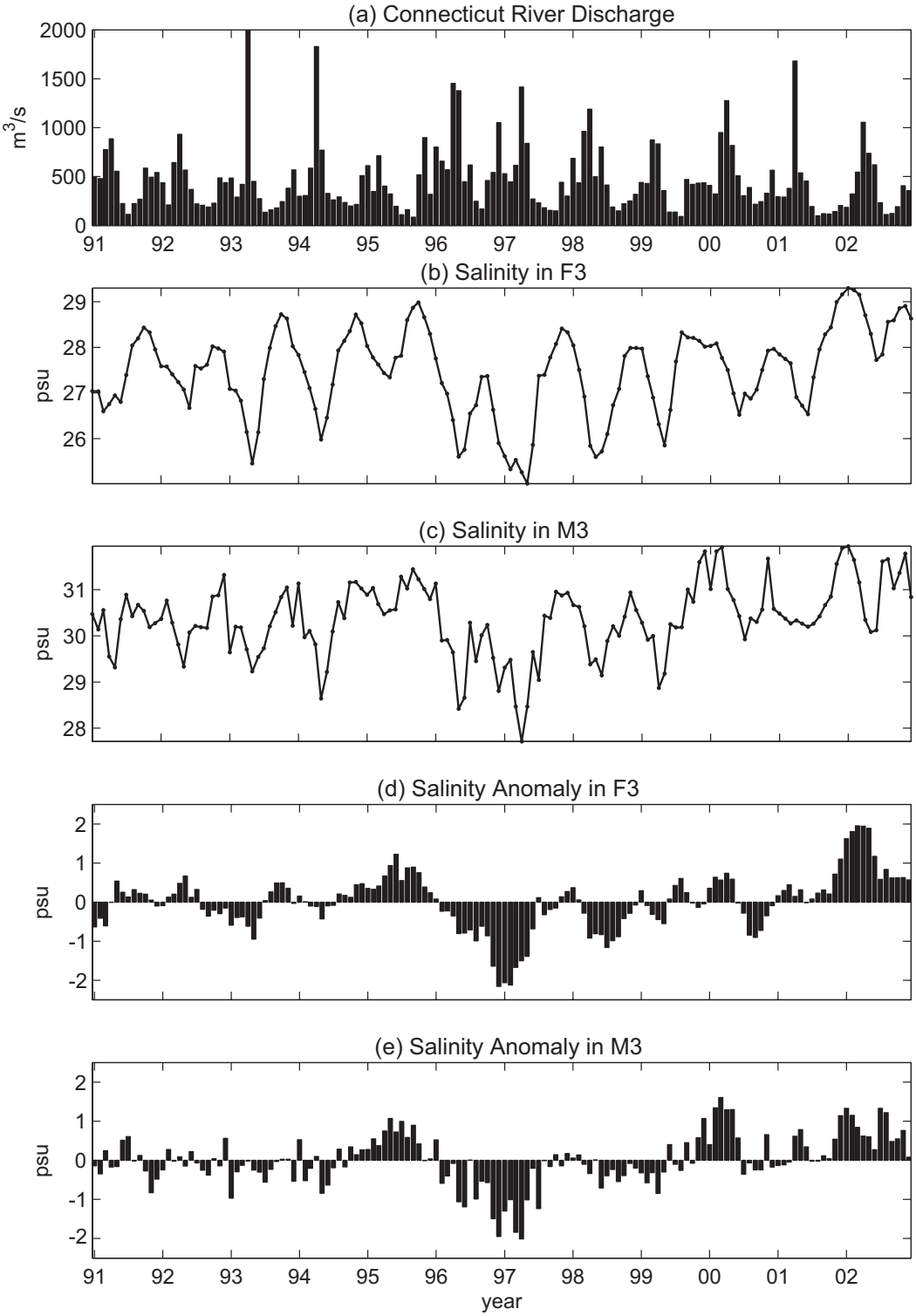

Figure 3-6. (a) Connecticut River discharge, depth-averaged salinity at (b) station F3 and (c) station M3, and depth-averaged salinity anomaly at (d) station F3 and (e) station M3.

justifiably be represented by the Connecticut River discharge, because it comprises 70% of the total freshwater discharge in LIS. The first panel of Figure 6 shows monthly time series of the Connecticut River discharge (m3/s) from 1991 to 2002. The depth-averaged salinity in LIS does not exhibit smooth sinusoidal fluctuations as the temperature (c.f., Figure 2), however, regular seasonal patterns are present as shown in the second (station F3) and third (station M3) panels of Figure 6, i.e., the salinity minimum mostly occurs in spring, and the maximum in the fall due to the decreased rate of riverine discharge.

Besides strong seasonality, observations show two conspicuous characteristics of the salinity between the central LIS (second panel) and the eastern LIS (third panel). One is the similar trend of salinity variability between stations F3 and M3 on a longer time scale (> 2 years). Another is sub-seasonal fluctuations, which only occur in station M3. In general, water becomes less saline as it gets farther west, an indication of the distance from the estuary mouth and very little contribution from the East River and the Harlem River. The depth-averaged salinity at station M3 varies from 29 to 32, which is likely controlled by the exchange of saltier water from outside the Sound, because the water is significantly diluted inside the Sound to a range of 25 to 29. Since the salinity is strongly affected by the seasonal freshwater discharge into LIS, it can be seen that the continuous decrease from the fall of 1995 to the spring of 1996 corresponds to the increase in discharge during the same period. The reverse effect on the continuous increase of salinity occurs from the spring of 1997 to 2002.

After removing seasonality, anomalies of the depth-averaged salinity in stations F3 and M3 reveal more details of variability shown in the fourth and fifth panels of Figure 6, respectively. There is a strong negative phase in the winter of 1997 and a strong positive phase in the winter of 2000 and 2002. On a longer timescale, the salinity starts to decrease in the spring of 1995 and bounces back to average condition in the summer of 1997 throughout the Sound. It is interesting to note that the variability of high-frequency signals is different from one station to another, with a pattern similar to the temperature anomaly described earlier. For example, the strong negative anomaly in the summer of 1998 at station F3 is not well observed in station M3. Strong 1999-2000 winter positive anomalies are shown in M3, but they are notably reduced in station F3.

Table 3-1. Relationship between anomaly of monthly Connecticut River discharge and depth-averaged salinity anomaly from 1991 to 2002.

Station	Correlation coefficient (r)	Effective degrees of freedom (N*)	p
B3	-0.42	47.8	< 0.01
D3	-0.43	46.8	< 0.01
F3	-0.44	55.1	< 0.01
I2	-0.51	59.0	< 0.01
M3	-0.33	74.8	< 0.01

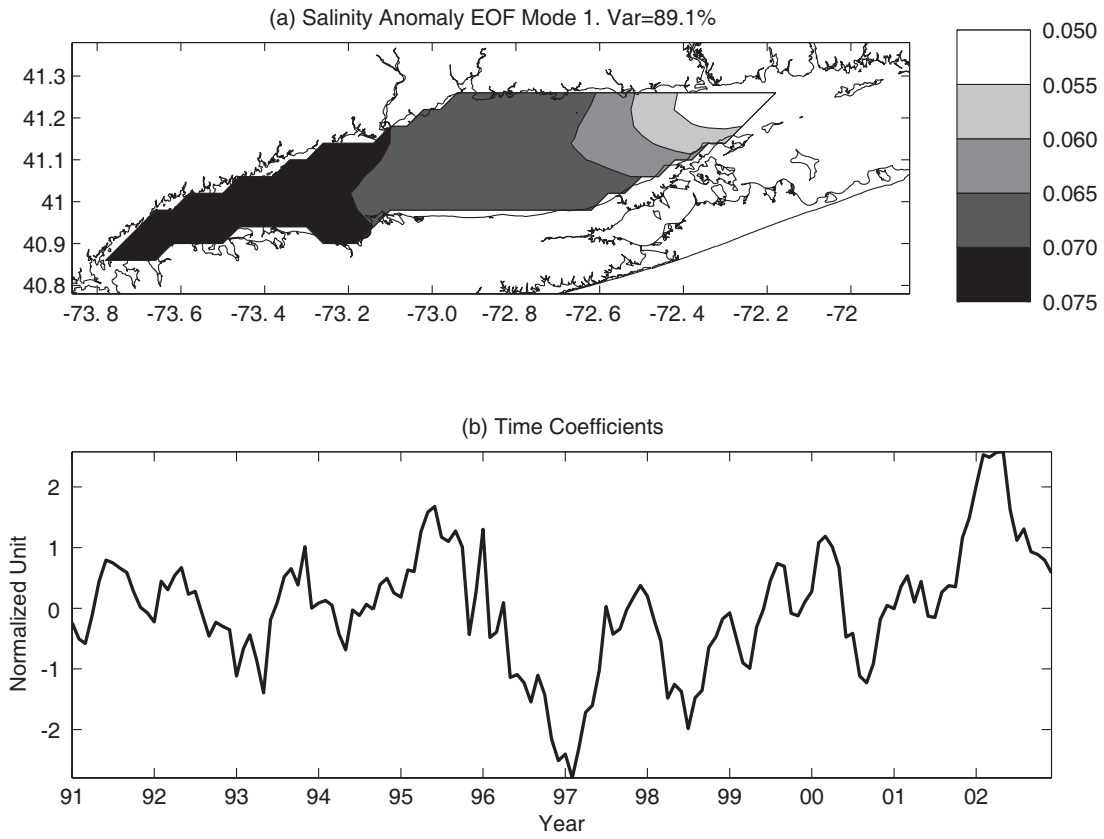

Figure 3-7. Depth-averaged salinity anomaly (a) spatial pattern of the first EOF mode and (b) time coefficient.

There is also evidence of systematic periodicity in a high-frequency scale (3-5 month period) at station F3 between 1999 and 2000.

In order to examine the variance of salinity anomaly, an EOF analysis is used to determine spatial distribution and temporal change (Figure 7). The first mode explains 89% of the total variance of the salinity anomaly in LIS. The spatial structure of the first mode is similar to the first mode of the temperature anomaly as shown earlier in Figure 4. The spatial pattern has large amplitude in western LIS, which decreases with distance to the east. The principle component of the first mode shows large negative values in the winter of 1997 and positive values in the winter of 2002. The principle component exhibits two major periodicities, quasi-biennial and decadal. The latter can barely be seen because the length of record is hardly long enough to resolve it.

The average of freshwater runoff in the high discharge season (March-May) is approximately 7.1×10^9 m^3 and 1.8×10^9 m^3 in the low discharge season (July-September) from the Connecticut River. In order to estimate how much anomalous freshwater input accounts for the variability of the salinity in LIS, we calculated the correlation coefficients between the riverine discharge anomaly and depth-averaged salinity anomaly over twelve years from 1991 to 2002. Results for the selected five stations such as B3, D3, F3, I2, and M3 are shown in Table 1. All maximum peaks in the cross-correlation correspond to a one-month lag of the salinity anomaly. All correlations are statistically significant ($p<0.01$) for their respective effective degrees of freedom (Chelton, 1983). The anomalous riverine discharge explains at most 25% of the depth-averaged salinity anomaly in central Sound. This result strongly suggests that, like the temperature anomaly, the salinity anomaly is dominated by external forcings.

If local forcings are not dominant in controlling interannual variabilities of heat and salt then the only other source of variability must come from outside LIS. We propose here that the external variability is connected to the variability in LIS through horizontal exchange mainly via the eastern end. The adjacent shelf-slope water in the Mid-Atlantic Bight (MAB) would be the most obvious source to examine, but there are no regular long-term salinity records available. However, shelf-slope water properties have been shown to be a byproduct of mixing between Labrador Sea water and the GS water (Rossby, 1999; Rossby and Benway, 2000; Rossby and Gottlieb, 1998; Schollaert

et al., 2004). Therefore, we chose to use the GS position as a proxy variable to represent the shelf-slope water properties. The monthly GS index (the first EOF mode of the GS north wall position) data by Taylor and Stephens (1998) were obtained from Plymouth Marine Laboratory, United Kingdom, through their web site (URL http://www.pml.ac.uk/gulfstream/data.htm). In order to verify whether shifting of the GS position is statistically related to the water properties in LIS, the correlation between the anomaly of the GS index and the salinity anomaly in the easternmost station M3 was calculated. The maximum peak in the cross-correlation corresponds to a zero lag with the correlation coefficient (r) of 0.40. The correlation with the GS position is statistically significant ($p<0.05$) for $N^*=23$, the effective degrees of freedom (Chelton, 1983). We also considered effects of large-scale atmospheric processes such as NAO in order to determine whether fluctuations of the westerlies are connected to the variability of the salinity anomaly in LIS. The relationship between monthly NAO index and the station M3 salinity anomaly is not statistically significant ($r=0.17$, $N^*=80$, and $p>0.05$), but the peak of cross-correlation corresponds to a 12-month lag of the salinity (not shown). We attempted to relate the depth-averaged temperature anomaly to the GS index, but relationship is not well resolved most probably because temperature is not totally conservative in shallow waters.

3.5 Discussion

Since EOF analyses of the temperature and salinity anomalies show that the variances tend to gradually decrease in the eastward direction, we also examined variances of oxygen and chlorophyll a anomalies for five selected stations from western to eastern stations (not shown). There is a similar trend for anomaly variances of other variables decreasing in the eastward direction, which indicates strong longitudinal gradients of anomalies from east to west. The maximum variance of anomaly occurs at the westernmost station B3, and the minimum is found at the easternmost station M3. It is not immediately clear what causes the westward ‘amplification’ of anomalies, but it most probably occurs through advection of thermohaline fronts where gradients are strong,

especially in western LIS (see Gay et al., 2004). An alternative cause might be due to increased influence of anthropogenic activities in the densely populated and heavily industrialized areas around western LIS.

Previous studies have suggested that processes driving variability of temperature in coastal areas and open ocean are dominated by local heat fluxes (e.g., Halliwell, 1997; Large, 1996; Mignot and Frankignoul 2003; Mountain and Manning, 1994, Mountain et al., 1996; Taylor and Mountain, 2003; Umoh and Thompson, 1994). It is generally accepted that seasonal variabilities of temperature and salinity in shallow water systems are driven by local forcings, such as surface heat flux and freshwater discharge. This implies that the surface net heat flux (Q_t) controls the rate of the temperature change $(\partial T / \partial t)$ in LIS. The analysis presented in this study has revealed that the seasonal fluctuation of the depth-averaged temperature is indeed primarily driven by the surface heat flux. However, there is a strong discrepancy between the heat flux and the time rate change of the temperature during spring/summer (cf. Figure 5(b)). Moreover, Figure 5(c) clearly shows that the interannual variability of the temperature in LIS is not driven by the local heat flux. The heat loss during spring/summer and the heat flux anomaly not explained by the local forcing in this study evidently is due to those processes which were not considered, such as large atmospheric oscillations, horizontal diffusion and advection across the boundaries.

We could not conduct analyses to include horizontal fluxes directly, because velocity data were not available. However, recent numerical modeling efforts (Crowely, 2005; Gay et al, 2004) and an observational study (Codiga and Aurin, 2007) have examined the rate of horizontal exchanges between LIS and adjacent waters. Modeling studies show that the horizontal exchanges at the eastern end are between 1.8×10^4 m^3/s ~2.0×10^4 m^3/s. Codiga and Aurin (2007) estimated mean exchange volume transports at eastern LIS from November 2002 to April 2004 to be approximately $2.8\pm0.5\times10^4$ m^3/s, which is similar to the numerical modeling results. This observational result is based on twelve months velocity data from ADCP mounted on a ferry between New London, Connecticut and Orient Point, New York. They found the high exchange volume transport during spring/summer and the low transport during winter. The peak in the exchange volume transport is observed in March-April, approximately 44,000 m3/s,

which clearly illustrates that the amount of volume of water exchanged in a month through the eastern boundary is much greater than the volume of LIS. Since there are temperature differences between LIS and adjacent shelf waters, the large volume of transport implies large heat loss from LIS during spring/summer when stratification inhibits vertical mixing, because the water coming from outside is relatively cooler. The large volume exchange led us to examine how properties of the shelf-slope water are likely to affect the interannual variability of temperature. Likewise, local freshwater sources cannot explain interannual variability of salinity, for example, there was no significant change in riverine discharge that could account for the general increases in the salinity during 1997~2002. Therefore, horizontal exchange processes seem to play a big role in the interannual variability of the salinity anomaly in LIS.

The shelf-slope water properties have been shown to vary from year to year in the Mid-Atlantic Bight (MAB) region. Mountain (2003) found that in February 1993 salinity was less than 34 psu everywhere on the shelf in the MAB, but more saline water (~35 psu) occupied the shelf regions in 1995. Mountain and Manning (1994) also showed that the salinity variability is coherent over the northeast continental shelf regions from the western Gulf of Maine to Cape Hatteras during 1977-1987. Mountain (2003) does not directly mention any relationship with the GS position, however, based on his Figure 6 there seems to be an indication of salinity distribution in MAB being influenced by the GS position, because the GS was located at its northernmost position in 1995 during that decade. The statistical relationship between the salinity anomaly in LIS and the GS position are significant. Although strong regression relationship does not necessarily prove a cause and effect, based on the established relationship between the GS and shelf-slope waters, the connection between the anomalous salinity variability in LIS and the GS position shifts is not implausible.

Several studies have indicated that water properties in shelf-slope regions are associated with the GS position. Rossby and Gottlieb (1998) found that the GS position affects the interannual variability of surface temperature off New Jersey coast. Schollaert et al. (2004) showed that biological productivity in the Slope Sea, between the continental shelf of the eastern US and north wall of the GS, exhibits interannual variability, which is positively related to the migration of the GS. They pointed out that

the Slope Sea water properties are more like the GS water (relatively warm and saline) than the Labrador Sea water (relatively cold and fresh) when the GS is displaced to the north associated with higher chlorophyll concentration. Also, when the GS position is shifted farther north, the Slope Sea water and shelf temperature and salinity increase due to a lesser supply of the cold fresh Labrador Sea water, and when it shifts south the Slope Sea allows more Labrador Sea water into the region thus decreasing its salinity (Rossby, 1999; Schollaert et al., 2004). Hence, it is through this complex interaction in shelf-slope regions that the change in the GS position is able to affect the salinity anomaly in LIS.

There is also considerable indirect anecdotal evidence that interannual temperature and salinity variabilities in coastal regions may be affected by the shelf-slope water in the MAB region. Results from previous studies tend to support the idea of possible connections between the shelf-slope water transport into coastal regions and salt variability in shallow waters. Churchill (1985) found that large parcels of outer shelf and slope water commonly enter the near-shore waters off Long Island (LI) during summer, and suggested that this event is related to the appearance of tropical fish near LI. These spring and summer salty intrusions are considered to be one of the mechanisms that transport the slope water into the shelf (Lentz, 2003). Also, other mixing processes including tide, wind, GS rings, and shelf-slope frontal eddies can also affect the properties of inner shelf regions (e.g. Fratantoni and Pickart, 2003). The effect of the GS is further supported by the work of Hare and Cowen (1996), which describes how the GS-associated flow moves pelagic juvenile bluefish (Pomatomus saltatrix) larvae from their spawning ground in the South Atlantic Bight to the MAB shelf regions.

It is still not clear how often the shelf-slope water is transported into the shallow water regions and how much it is exchanged with surrounding waters. However, Gordon and Aikman (1981) suggested that the salty water intrusions from the GS and slope region may contribute 50% of the salt on the MAB shelf needed to balance the river input. Flagg et al. (1994) observed time scales of a day for some intrusions in the southern MAB, with onshore speeds of 10-20 cm/s. This might explain how the variability in estuaries like LIS might be able to respond quickly to the variation of properties of shelf-slope regions and the GS. Horizontal exchange processes seem to be important in heat and salt balances. Therefore, it makes sense to consider the connection between the

variability of properties in LIS and the shelf-slope water processes associated with the meandering of the GS position which is in turn correlated to NAO and ENSO events (Taylor and Stephens, 1998; Taylor et al., 1998). It has been also proposed that a positive NAO leads to higher salinities and decreases transports of Labrador Sea water causing the GS to move north a year to 18 months later (Rossby and Benway, 2000). NAO is expected to lead the salinity anomaly in LIS by one year since NAO primarily leads the latitudinal GS shifts by one year (Frankignoul et al., 2001; Rossby and Benway, 2000; Taylor and Stephens, 1998). Our results also showed that the peak of the cross-correlation with NAO corresponds to a 12-month lag of the salinity anomaly in LIS, but the relationship was not statistically significant. However, it was argued by Dong and Kelly (2003) that the GS position could be related to the southward shift in the maximum westerlies rather than the Labrador Sea shelf transport. Although the movement of the GS north wall and NAO seem to be inter-related, we examined the effects of NAO and the GS separately. Our results show that the two processes have different relationship to the variability of the salinity in LIS. New questions raised by this study are: (i) What are contributions of cross-shelf and along-shelf transports to anomalous variability in shallow waters like LIS (for example, the GS eddy intrusion onto the shelf, shelf-slope frontal instabilities, or salty intrusions)? (ii) What drives the quasi-biennial and decadal timescales of the temperature and salinity variability in LIS?

3.6 Summary

The average winter temperature in eastern LIS has indeed increased over the last 30 years (see Stachowicz et al., 2002) although the increase in the winter temperature for the last decade is not statistically significant in this study. For the last decade, the temperature has exhibited higher variance in winter seasons, 1.9 ºC, than in summer, 0.2 ºC. Also, the salinity decreased by approximately 2 from 1991 to the spring of 1997, and then increased gradually to 2002 by 3 throughout the Sound. It was found that the variances of anomalies are ‘amplified’ from east to west in LIS which may be caused by frontal movement. EOF analysis shows that the variability for both depth-averaged

temperature and salinity anomalies can be explained by the first modes, which contains 87% and 89% of the total variance, respectively. Time coefficients of the depth-averaged temperature and salinity reveal the strong seasonal and quasi-biennial variabilities in LIS. Low-frequency signal in the salinity was also observed to be on a decadal time scale. As expected from previous studies, local forcings dominate the seasonal variations in temperature and salinity in LIS. However, the net surface heat flux explains only 17% of the total variance in the interannual variability of the temperature, and the riverine discharge anomaly accounts for approximately 25% of the total variance in the salinity anomaly in the central LIS. These results support the notion that, contrary to the traditional paradigms, the interannual variabilities in heat and salt are not driven by the local forcings in LIS, and need to consider other external forcings. There is a significant correlation between the monthly GS position and the depth-averaged salinity in LIS, and the correlation coefficient was approximately 0.40 with no lag at major stations. We propose that the variability of the temperature and salinity in LIS might be connected to the variability of shelf-slope water properties associated with the shifting of the GS position. We did not find any significant correlation between monthly NAO index and salinity, but the peak of cross-correlation corresponds to one year lag. Further study is needed to determine how the shelf-slope water exchanges properties with the Sound, under what conditions, and on what time scales.

Chapter 4

Factors driving bottom salinity variability in the Chesapeake Bay

Abstract

The long-term variability of bottom salinity in the Chesapeake Bay is examined using observations from 1985 to 2004. Simple linear regression analysis based on annual mean data shows that the bottom salinity is significantly correlated with both the Susquehanna River discharge and the Gulf Stream (GS) index, which represents shelf and slope water salinity. This suggests that local forcings as well as external processes affect the variation of bottom salinity on interannual to decadal time scales. Empirical orthogonal function (EOF) analysis is used to extract patterns among 21 sampling stations along the bay. The first seven EOF modes explain approximately 85\% of total variance, and consequently they are combined to represent the variability of bottom salinity anomaly in the bay. The wavelet transform of the bottom salinity anomaly reveals significant areas centered at the periods of 2 and 7.5 years, which is consistent with the results from Fourier spectral analysis. The significant powers in the bottom salinity anomaly exhibits spectral correspondences to the wavelet power spectra of both the river discharge and the GS index, suggesting possible connections between them. Wavelet coherence is employed to determine whether relationship in power spectra between two time series is statistically significant. Our results clearly demonstrate that the interannual variability of the bottom salinity is forced by the freshwater discharge, and the quasi-decadal variability is associated with shelf-slope water condition through horizontal exchange. No evidence is found to indicate that there is influence of the El Niño Southern Oscillation (ENSO) on the variability of the river discharge, but the North Atlantic Oscillation (NAO) may be related to it at decadal or longer time scales.

4.1 Introduction

There have been increasing efforts to understand the physical responses of the ocean to large scale atmospheric forcings at interannual to decadal time scales. Previous studies have focused on the processes that control the variability of sea surface temperature (SST) and sea surface salinity (SSS) in the North Atlantic (e.g., Halliwell and Mayer, 1996; Robertson et al., 2000; Mignot and Frankignoul, 2003; Reverdin et al., 2007}. However, our understanding on the interannual variability of physical properties in coastal ocean is still at a rudimentary level. Local effects such as surface heat flux and freshwater discharge dominate the variability of temperature and salinity along the northeastern U. S. coastal areas, i.e., the Gulf of Maine and the Mid-Atlantic Bight (MAB) (Mountain and Manning, 1994; Mountain et al., 1996; Mountain, 2003; Taylor and Mountain, 2003). This may hold true for seasonal variations of temperature and salinity governed by local forcings associated with climate-induced changes. On interannual or longer time scales, nevertheless, temperature and salinity in coastal waters including estuaries can be largely influenced by processes other than local effects. The modeling work by (Crowley, 2005) showed that adjacent oceanic water significantly contributes to the heat and salt balances of Long Island Sound (LIS), New York. (Lee and Lwiza, 2005) found that the anomaly of temperature and salinity in LIS is driven by horizontal exchange processes through the eastern boundary. They also revealed that the salinity anomaly is significantly correlated with the Gulf Stream (GS) position. In other words, the variability of the salinity anomaly in LIS is closely connected to the shelf-slope water condition in the MAB due to exchange with adjacent ocean.

There have been a few studies that attempt to estimate the characteristics of long-term exchange between an estuary and its adjacent ocean in the MAB region using observations and modeling works (Austin, 2002; Wong and Valle-Levinson, 2002; Gay et al., 2004; Codiga and Aurin, 2007). Austin (2002) used a modeling approach to analyze the exchange rate between the Chesapeake Bay and the adjacent ocean during 1985-2000. Assuming that oceanic flux into the bay has a fixed value of salinity, the results of his model agreed with observations quite well for the most part. However, small but significant differences occurred between the models and observations, which seemed to vary on interannual or longer time scales. This led us to suspect the validity of

constant salinity in the adjacent ocean used as a boundary condition. Yet we have little knowledge about the influence of oceanic water on estuaries, and the variation of salinity due to external forcing is still uncertain. It is, therefore, crucial to examine the variability of coastal water properties associated with time scales involved and related to local and non-local forcings. This study partly extends the works of Austin (2002) and Lee and Lwiza (2005) by utilizing the wavelet analysis to elucidate the influence of river discharge and shelf-slope water on the variability of the bay salinity.

The goal of this study is to determine the processes involved in the long-term variability of salinity in the Chesapeake Bay. Temperature in shallow waters tends to contain greater variabilities than salinity because of active air-sea interactions such as latent and sensible heat fluxes. We used the monthly time series of salinity throughout the Chesapeake Bay where the U. S. Environmental Protection Agency (EPA) has been making extensive survey over 20 years. There are, however, no continuous long-term data in the adjacent shelf-slope region to match observations in the bay, and thus the GS index is employed to represent the condition of adjacent shelf-slope water (see Rossby et al., 2005, Figure 9). We explore the inter-relationship of bottom salinity anomaly with the Susquehanna River discharge and the GS index by determining major periodicities and connections between them. The paper is organized in the following manner: section 2 briefly describes the area of study. The details of data processing and wavelet analysis including continuous wavelet transform and coherence are given in section 3. The results of wavelet analysis including phase relationship and coherence between forcing variables are described in section 4. Other possible links influencing the variability of salinity anomaly in coastal waters is discussed in section 5, and results are summarized in section 6.

4.2 Study Area

The Chesapeake Bay is a partially mixed coastal plain estuary, and the largest in the U. S. It stretches for about 320 km from its seaward end at the Virginia Capes, Cape Charles and Cape Henry, to the mouth of the Susquehanna River at Havre de Grace,

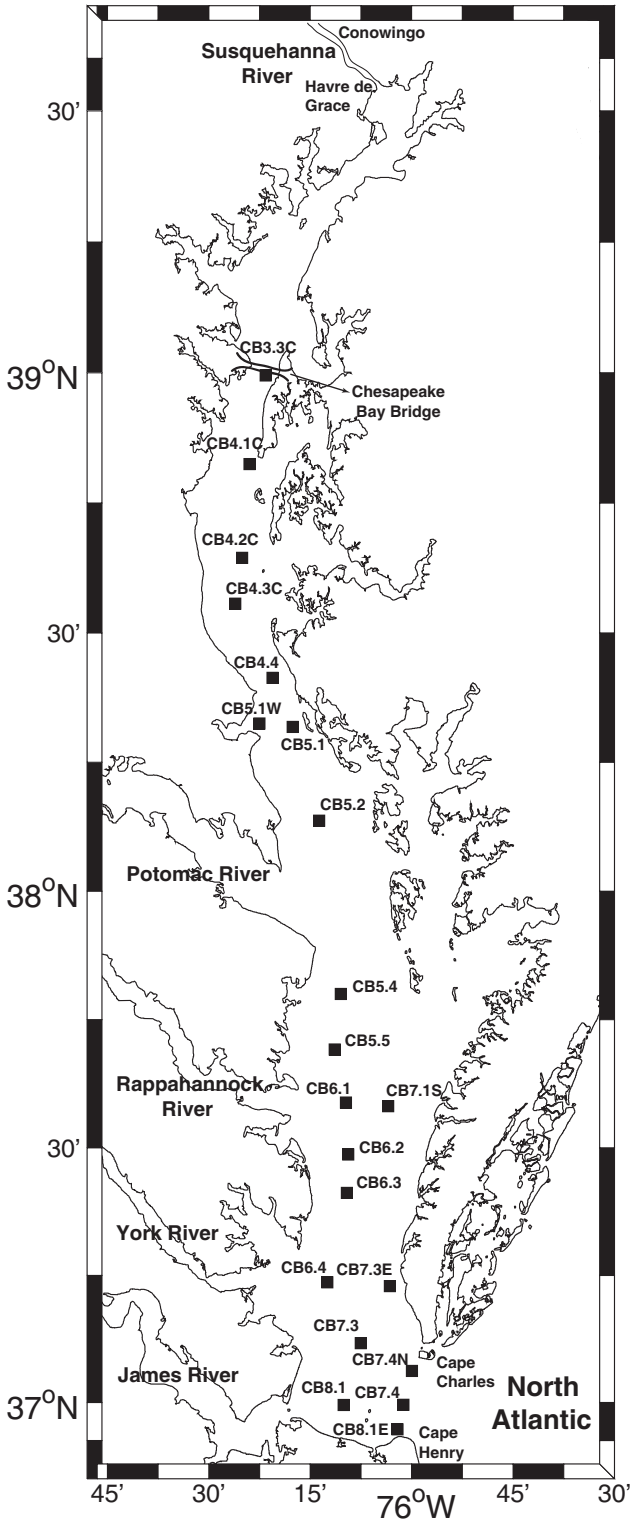

Figure 4-1. The Chesapeake Bay (Square markers indicate the locations of the Environmental Protection Agency water quality monitoring stations selected for this study

Maryland (Figure 4-1). The Chesapeake Bay system has a surface area of 6.5×10^3 km^2, a mean low water volume of 50 km^3, and a mean depth of 8.42 m (Schubel and Pritchard, 1986). There are several tributary systems in the Chesapeake Bay such as the Susquehanna, Potomac, Rappahannock, York, and James River. The mean annual river discharge to the bay is about 2570 m^3/s (Goodrich, 1988), and the Susquehanna River is the largest source of freshwater responsible for 45% of the total riverine input with an annual mean discharge of 1144 m^3/s. The Susquehanna River discharge peaks in March-April and is lowest in July-September. Exchange processes between the bay and the ocean are complicated since physical processes in the lower bay over sub-tidal time scales are influenced by a combination of atmospheric forcing, buoyancy forcing, and bathymetry (Wang and Elliott, 1978; Valle-Levinson and Lwiza, 1997; Wong and Valle-Levinson, 2002). The complex bathymetry of the lower bay is characterized by channels and shoals, namely, Chesapeake, Thimble Shoal, and Beach/North Channel. Oceanic water tends to enter the bay in the northern portion of the entrance and main channel, and bay water leaves through the southern portion (Valle-Levinson and Lwiza, 1997). The mean exchange rate is estimated to be approximately 8×10^3 m^3/s, which corresponds to the timescale of 90 days (Austin, 2002).

4.3 Data and Methods

4.3.1 Salinity anomaly

The EPA Chesapeake Bay Program has been monitoring water quality of the bay and its tributary estuaries since 1984, mostly on a monthly basis. Water quality data consist of temperature, salinity, chlorophyll *a*, oxygen, nutrients, and other geochemical constituents. All measurements are archived in the database available at URL http://www.chesapekaebay.net/data/index.htm. Although the data are available at 40 stations along the main stream of the bay between 1985 and 2004, there are only 21 stations where salinity is measured on a regular basis with gaps that are no longer than 3 consecutive months. Since the bottom layer of water column is more affected by oceanic

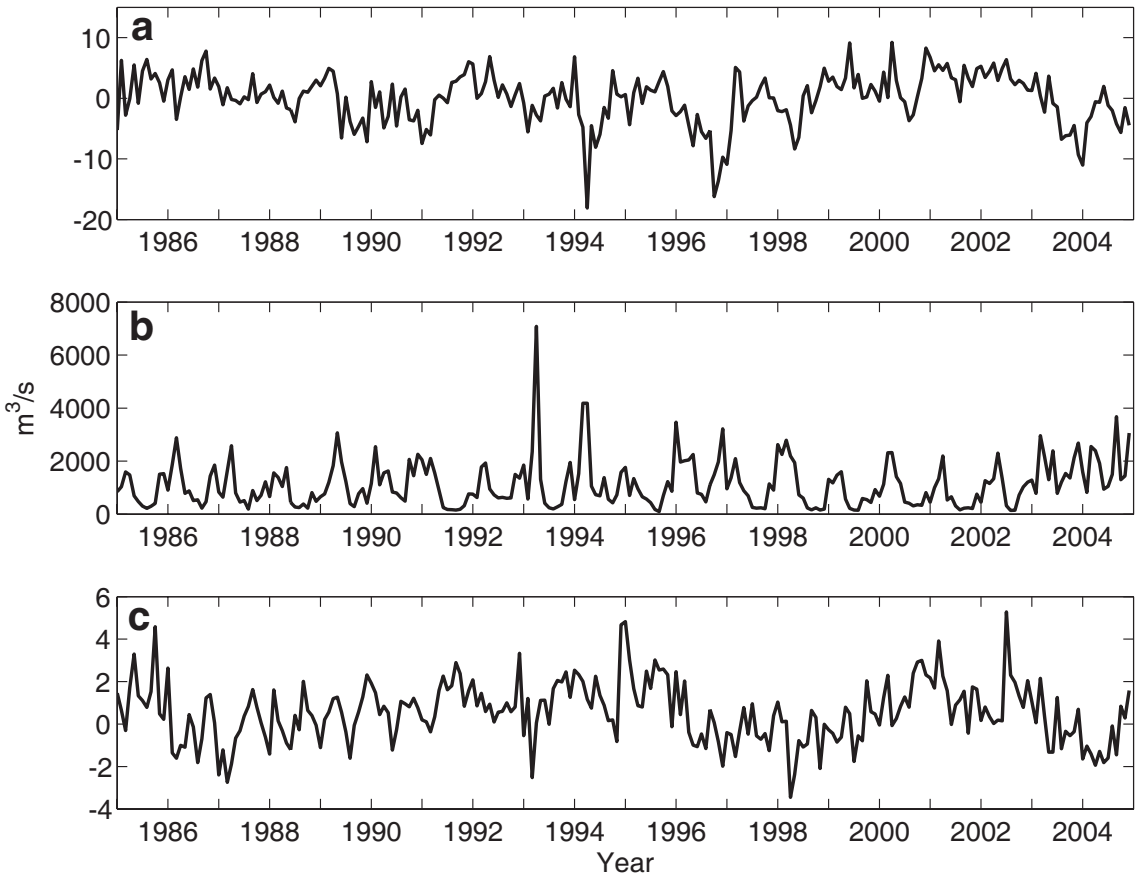

Figure 4-2. The monthly time series of (a) the bottom salinity anomaly (the principle component of combined EOF modes 1 to 7), (b) the Susquehanna River discharge, and (c) the Gulf Stream index. The principle component is constructed by combining the first seven modes in empirical orthogonal function analysis, and hereafter it is referred as the bottom salinity anomaly.

water, near-bottom values are collected to capture oceanic influence. Thus, this study is based on the bottom salinity data obtained at those 21 stations from the Chesapeake Bay Bridge to the mouth of the bay (Figure 4-1). The gaps less than 2 months are linearly interpolated, seasonal climatology is removed at each station, and then the bottom salinity anomaly is used for the analysis of this study. One way to examine the variability of bottom salinity anomaly through the bay would be to analyze all stations individually, which is very inefficient. Hence, we chose a more compact approach of using an empirical orthogonal function (EOF) method and extract principle components, which combines the information on the interannual variability for all 21 stations. The monthly anomaly data, which cover most of the bay area, are normalized prior the EOF analysis using a singular value decomposition method. The first EOF mode explains approximately 50% of total variance and the second (third) mode only accounts for about 13% (8%). Since the contribution of the first mode is relatively low, seven leading EOF modes are combined to explain 85% of the total variance, thus representing the variability of the bottom salinity anomaly reasonably well. For the rest of this study, unless otherwise stated, the analysis of the bottom salinity anomaly is based on the monthly time series (principle component) of the combined EOF modes from 1 to 7 as shown in Figure 4-2a.

4.3.2 Freshwater influx

The Susquehanna River discharge is considered as a good representation of the freshwater flow into the bay because it exhibits the largest influence on the Chesapeake Bay. The discharge from the Susquehanna River contains a broad range of spectrum due to the extensive area of the drainage basin (71,000 km^2), which covers parts of three states, i.e., Maryland, Pennsylvania, and New York. The discharge records (1968-2004) of the Susquehanna River at Conowingo, Maryland (station ID 01578310; Figure 4-1), were retrieved from the U. S. Geological Survey streamflow data archive. Figure 4-2b shows the monthly time series of the discharge rate between 1985 and 2004, but the anomaly of river discharge is analyzed for most of this study.

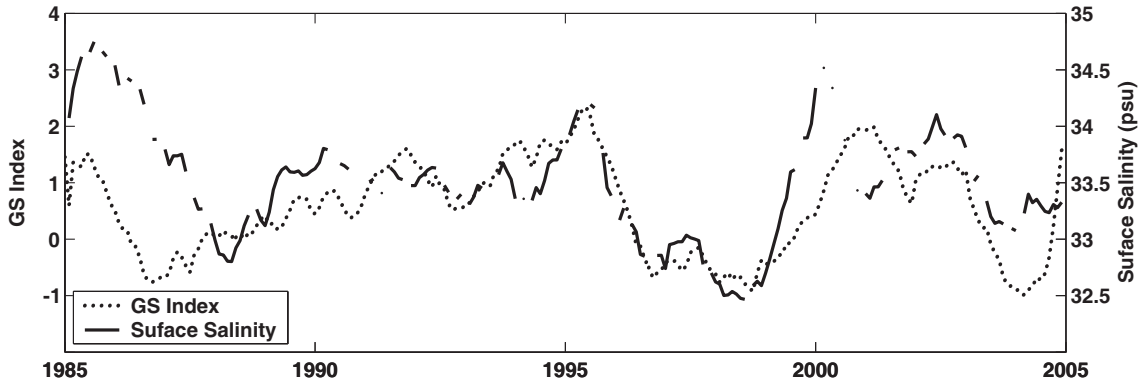

Figure 4-3. The monthly time series of the Gulf Stream (GS) index (dotted line) and mean surface salinity (solid line) across the continental shelf and Slope Sea (between 50 km and 250 km from Ambrose Light, New York) from the NOAA National Marine Fisheries Service ecosystem monitoring program on the Oleander. The data have been low-pass filtered with a 12-month moving average

4.3.3 The Gulf Stream index

Since the shelf-slope water in the MAB regions is the mixture of the Labrador Sea water and the GS water (Csanady and Hamilton, 1988), the shelf-slope water is relatively warm and saline (cold and fresh) when the GS is shifted farther north (south) from its mean position (Rossby and Benway, 2000). Thus, we used the GS index to examine the influence of shelf-slope water into the Chesapeake Bay, and the monthly GS index (the first EOF mode of the GS north wall position) was retrieved from Plymouth Marine Laboratory, U. K., available at URL http://www.pml.ac.uk/gulfstream/data.htm (Figure 4-2c). Note that the GS index is solely used as a proxy variable for shelf-slope water environment rather than trying to establish a direct link. Although surface salinity data are available further north in the MAB region from the National Oceanic and Atmospheric Administration (NOAA) National Marine Fisheries Service (NMFS) ecosystem monitoring program, the detailed analysis of the data is difficult because of large gaps in the monthly time series. However, the data record is long enough to provide evidence that the GS index can faithfully represent the variability of salinity in the shelf-slope region. In order to retain the effects of both the continental shelf and slope sea water, we used the monthly mean surface salinity measured between 50 km and 250 km from Ambrose Light, New York. Figure 4-3 demonstrates that the GS index is closely related to the surface salinity in the MAB region.

4.3.4 Wavelet

Fourier analysis has been widely used to examine periodicities in geophysical time series, and it is useful if underlying processes are stationary in time. However, most of geophysical data are nonstationary and their signals are often localized, which presents a difficulty for the Fourier analysis. The wavelet transform can be used to analyze the time series that contain nonstationary powers at many different frequencies (Daubechies, 1990), which is a more accurate and efficient method of time-frequency localization than the windowed Fourier transform (Kaiser, 1994). The application of wavelet transform can be found in numerous studies of geophysics including the El Niño Southern Oscillation

(ENSO) and the North Atlantic Oscillation (NAO) (Wang and Wang, 1996; Torrence and Webster, 1999; Jevrejeva et al., 2003), river discharges (Labat et al., 2005), SST (Mwale et al., 2004), sea level change (Jevrejeva et al., 2005), and variability in precipitation (Kayano and Andreoli, 2004). Kukulka and Jay (2003) also used it to analyze impacts of Columbia River on salmonid habitat.

There are two classes of wavelet transforms; the Continuous Wavelet Transform (CWT) and the Discrete Wavelet transform (DWT). The DWT is useful for noise reduction and data compression whereas the CWT is better for feature extraction (Grinsted et al., 2004). The CWT is only used here with a Morlet wavelet that is defined as

$$\psi_0(\eta) = \frac{1}{\pi^{1/4}} e^{i\omega_0\eta} e^{-\eta^2/2} \tag{4-1}$$

where ω_0 is non-dimensional frequency and η is non-dimensional time. This wavelet is a complex wave $\left(e^{i\omega_0\eta}\right)$ within a Gaussian envelope $\left(e^{-\eta^2/2}\right)$ which localizes the wavelet in time. The $\pi^{1/4}$ term is a normalization factor which ensures that the wavelet has unit energy (Addison, 2002). The wavelet is stretched in time (t) by varying its scales (s), so that $\eta = t/s$ whose resolution is adjusted by ω_0. For high values of ω_0 the scale resolution increases whereas time resolution decreases, and vice versa (Maraun and Kurths, 2004). The scale is generally different from the Fourier period $\left(\lambda = 4\pi s / \left(\omega_0 + \sqrt{2+\omega_0^2}\right)\right)$ for the Morlet wavelet; however, λ is approximately equal to s $\left(\lambda \approx 1.03s\right)$ when $\omega_0 = 6$ (Meyers et al., 1993). Since the Morlet wavelet provides a good balance between time and frequency localization (Grinsted et al., 2004), it is used with $\omega_0 = 6$ and a scale resolution is set up as 12 scales per octave in this study.

The CWT of time series $\left(x_n, n = 1, \ldots, N\right)$ with uniform time steps δt is defined as the convolution of x_n with the scaled and normalized wavelet,

$$W_n^X(s) = \sqrt{\frac{\delta t}{s}} \sum_{n'=1}^{N} x_{n'} \psi\left[(n' - n)\frac{\delta t}{s}\right] \tag{4-2}$$

In practice, the convolution is usually implemented using the fast Fourier transform (Torrence and Compo, 1998). Like the Fourier power spectrum, the wavelet power spectrum is defined as the absolute value squared of the wavelet transform $\left(\left|W_n^X(s)\right|^2\right)$, which gives variance at each scale and time.

Because of the finite length of data record, errors will occur at the beginning and end of the wavelet power. A number of methods have been developed to cope with the boundaries of signals. One solution adapted in this study is to pad the end of time series with sufficient zeroes before doing the wavelet transform. However, padding with zeroes introduces discontinuities at the end of time series, as one goes to larger scales, and decreases the amplitude near the edges (Torrence and Compo, 1998). The cone of influence (COI) is the region where the wavelet power caused by a discontinuity at the edge drops by a factor of e^{-2}. Hence, it is uncertain whether the decrease of power in the region of the COI is due to a true decrease in variance or an artifact of the zero padding.

The statistical significance of wavelet power can be assessed relative to the null hypotheses that a signal is generated by a stationary processes with a given background power spectrum (P_k). Many geophysical time series have distinctive red noise characteristics that can be modeled very well by a first order autoregressive (AR1) process. The Fourier power spectrum of an AR1 process lag-1 autocorrelation α (estimated from the observed time series, e.g., Allen and Smith, 1996) is given by

$$P_k = \frac{1-\alpha^2}{\left|1-\alpha e^{-2i\pi k}\right|^2} \tag{4-3}$$

where k is the Fourier frequency index (Grinsted et al., 2004).

Given two time series (x_n and y_n) with the wavelet transforms W_n^X and W_n^Y, where n is the time index and s is the scale, the cross-wavelet spectrum is defined as

$$W_n^{XY}(s) = W_n^X(s) W_n^{Y*}(s) \tag{4-4}$$

where the asterisk (*) indicates complex conjugate. Following (Torrence and Webster, 1999) and (Grinsted et al., 2004), the wavelet squared coherence is defined as the absolute value squared of the smoothed cross-wavelet spectrum normalized by the smoothed wavelet power spectra of two time series as follows,

$$R_n^2(s) = \frac{\left| S\left(s^{-1} W_n^{XY}(s)\right)\right|^2}{S\left(s^{-1}\left|W_n^X(s)\right|^2\right) \cdot S\left(s^{-1}\left|W_n^Y(s)\right|^2\right)} \tag{4-5}$$

where S is a smoothing operator. It is useful to think of the wavelet coherence as a localized correlation coefficient in a time frequency space. The smoothing operator S can be written as

$$S(W) = S_{scale}(S_{time}(W_n(s))) \tag{4-6}$$

where S_{scale} denotes smoothing along a wavelet scale axis and S_{time} denotes smoothing in time. The amount of smoothing is dependent on both the choice of wavelet and scale.

The phase difference in the wavelet coherence is also given by

$$\phi_n(s) = \tan^{-1}\left[\frac{\Im\left\{S(s^{-1} W_n^{XY}(s))\right\}}{\Re\left\{S(s^{-1} W_n^{XY}(s))\right\}}\right] \tag{4-7}$$

The smoothed real ($\Re$) and imaginary ($\Im$) parts should have already been calculated in (4-5). Both $R_n^2(s)$ and $\phi_n(s)$ are functions of time index (n) and the scale (s). More

detailed description of the wavelet methods can be found in Torrence and Compo (1998), Torrence and Webster (1999), and Grinsted et al. (2004). In this study the wavelet transforms and wavelet coherences are achieved using the MATLAB software package (available at URL http://www.pol.ac.uk/home/research/waveletcoherence) provided by Grinsted et al. (2004) based on the works of Torrence and Compo (1998) and Torrence and Webster (1999).

4.4 Results

The mean salinity of the Chesapeake Bay is a product of two competing processes, i.e., freshwater influx into the bay through rivers and exchange with the adjacent ocean (Austin, 2002). First, simple linear regression analysis is performed to examine the relationship of bottom salinity at station CB5.2 (see Figure 4-1) with the Susquehanna River discharge and the GS index from 1985 to 2004. The analysis is based on annual mean values because of the high variability of a monthly record in the GS index, which is caused by the GS meandering. Figure 4- 4 shows the significant relationship between the salinity and the river discharge with a correlation coefficient (r) of -0.71 ($p<0.01$) and between the salinity and the GS index with $r=0.60$ ($p<0.01$). The bottom salinity is expected to be higher (>20.4) during dry years (<1,250 m^3/s), but it was less than 19.2 in 1997 and 1998 (Figure 4-4a), which should be normally associated with a high discharge rate exceeding 1,750 m^3/s such as in 1996 and 2004 (wet years). Interestingly, these large deviations during the dry years of 1997 and 1998 are accompanied with the negative GS index (Figure 4-4b). The results above indicate that the variability of the bottom salinity in the middle bay is influenced by not only the river but also by the adjacent oceanic water. Thus, it should be no surprise that the combined effect of those two variables produces a stronger relationship with $r=0.80$ ($p<0.01$), based on multiple linear regression (not shown). Next we decided to examine the time scales for which the bottom salinity anomaly over the whole bay responds to the river discharge and the property of adjacent ocean. Using a fast Fourier transform method, power spectral analysis is performed to determine interannual or longer period signals. Figure 4-5a shows that there are two

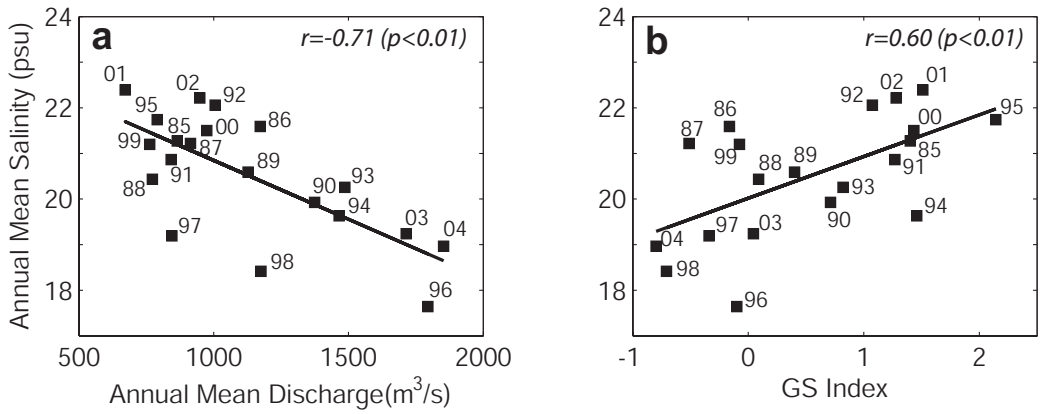

Figure 4-4. Linear regression analysis (a) between the bottom salinity at station CB5.2 and the Susquehanna River discharge and (b) between the bottom salinity and the Gulf Stream index. The analysis is based on annual mean data, and the correlation coefficient (r) is displayed with p-values

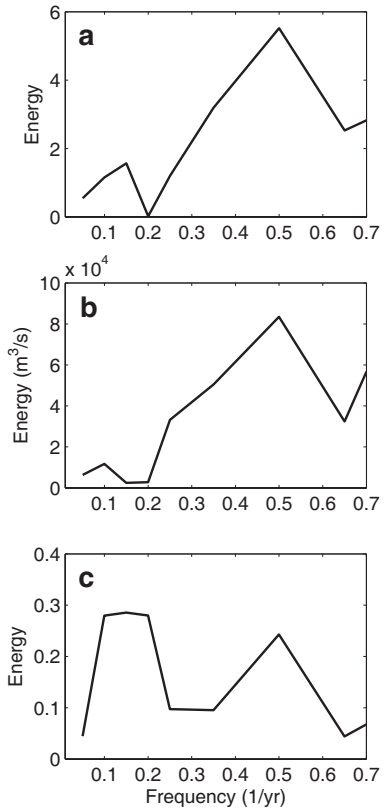

Figure 4-5. The power spectra for (a) the bottom salinity anomaly, (b) the Susquehanna River discharge anomaly, and (c) the Gulf Stream index during 1985-2004

major peaks centered at the periods of 2 and 6.7 years in the bottom salinity anomaly; one is interannual and another is quasi-decadal. The anomaly of the Susquehanna River discharge contains the periodicities of 2 and 10 years (Figure 4-5b) while the GS index exhibits the peaks at the periods of 2 and 6.7 years (Figure 4-5c). The spectral behavior of the bottom salinity anomaly is most likely related to the Susquehanna River discharge and/or the GS index at the interannual time scale (2 years). However, the quasi-decadal peak (6.7 years) in the bottom salinity anomaly seems to be associated with the broad range quasi-decadal peak (between 5 and 10 years) in the GS index rather than the decadal peak (10 years) in the river discharge anomaly.

Although the Fourier analysis is a useful tool to calculate the frequency contents of signals, it lacks in providing details on how spectral powers vary and how they are correlated between two time series with time. In order to isolate temporal variations and to correlate them with different processes, wavelet methods are employed using a Morlet wavelet. Figure 4- 6a shows the wavelet power spectrum of the bottom salinity anomaly, displayed in time frequency space. The largest significant sector (at the 5\% level) is observed at the quasi-decadal time scale for the interval from 6.5 to 9 years during the last 13 years of the 1985--2004 period, but it mostly lies in the region of cone-of-influence (COI). The edge effects become important in the COI region due to the discontinuity of data at the boundaries, but the significant power may be stronger if the data record is long enough, because of zero padding. There is another significant area at the interannual time scale (1.5-2.3 year band) from 1995 to 1998. Some elevated activities are also found at the periods of between 2.7 to 3.9 years but powers are not significant. Similar to the results of the Fourier spectral analysis, the wavelet power spectrum can be time-averaged and displayed with respect to its frequency, known as the global wavelet spectrum (Figure 4-6b). It shows interannual and quasi-decadal peaks (2, 3.3, and 7.5 years), with an additional one at the period of 14 years, which was not seen in the Fourier spectral analysis.

The wavelet transform is also applied to the freshwater discharge and the GS index in order to examine the similarities and differences of power spectra in connection with the bottom salinity anomaly. Although the time series of the Susquehanna River discharge and the GS index start in the late 1960s, the wavelet power spectra are

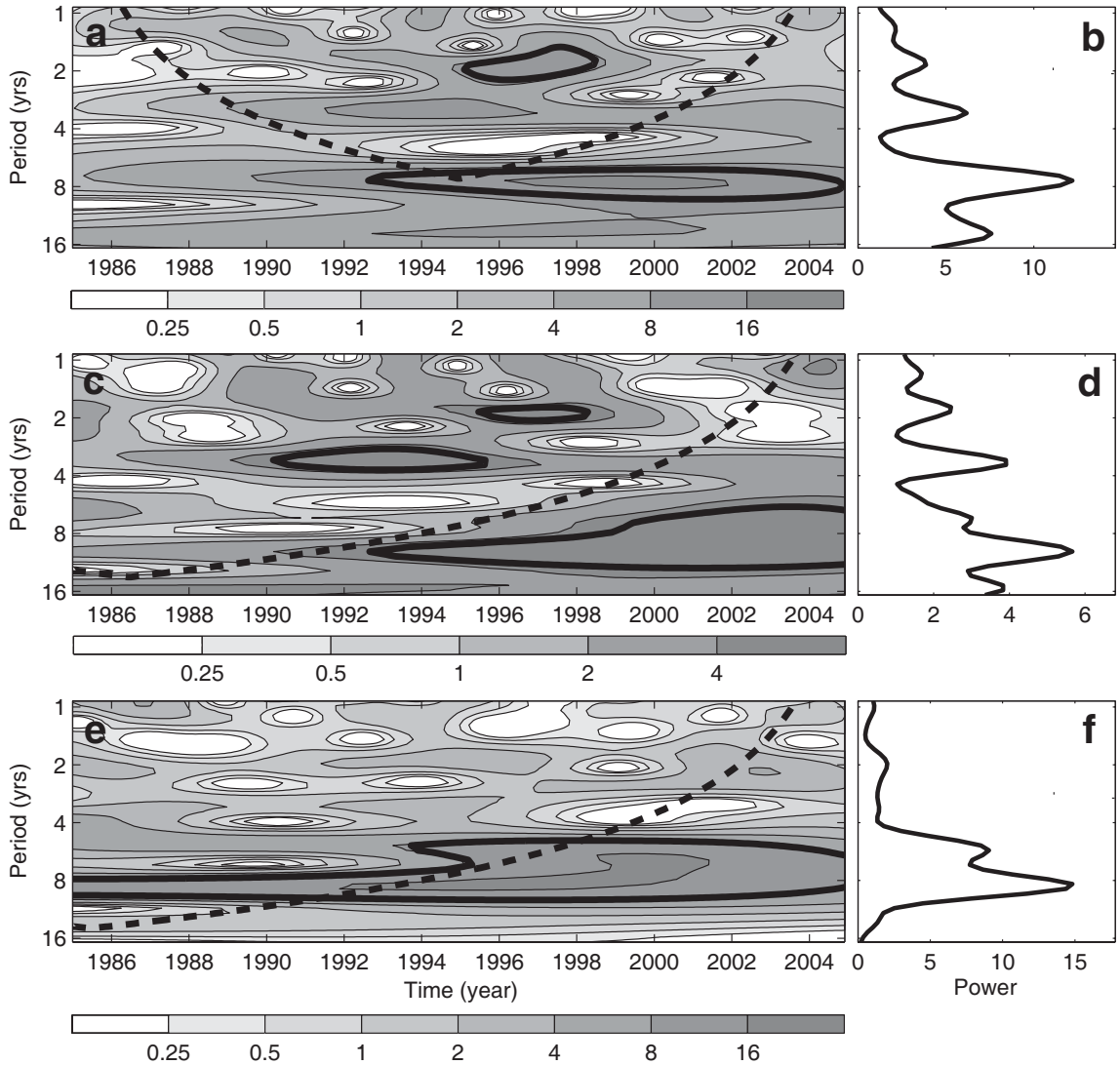

Figure 4-6. Left column: The wavelet power spectra of (a) the bottom salinity anomaly, (c) the Susquehanna River discharge anomaly, and (e) the Gulf Stream index. A thick black contour designates the 5% significant level against red noise. The dashed line indicates the cone of influence, and the color bar represents the variance for each panel. Right column: the global wavelet power spectra for (b) the bottom salinity anomaly, (d) the Susquehanna River discharge anomaly, and (f) the Gulf Stream index

displayed only for the last twenty years to match the length of available salinity data. Thus, lesser areas of COI exist in the Figure 4-6c and 6e compared to the wavelet power spectrum of the bottom salinity anomaly. Figure 4-6c shows the wavelet power spectrum of the Susquehanna River discharge anomaly from 1985 to 2004 and Figure 4-6d displays its global wavelet spectrum. The significant sectors and the peaks of the river discharge coincide with the high powers in the wavelet spectrum of the bottom salinity anomaly at the interannual time scales (2 and 3.3 years). This suggests that there may be a relationship between the interannual variability of the bottom salinity anomaly and the freshwater input. The largest significant sector lying in the area of COI starts at the period of 10 years in 1992 and gradually broadens to a 6-12 year band. Thus, the strongest power is observed at the decadal time scale (approximately 11 years) which is already found in the Fourier spectral analysis. Unlike the Susquehanna River discharge, the wavelet power spectrum of the GS index demonstrates only one major significant sector mainly at 7.5-9.5 year band from 1985 to 1994, which spreads to 5-10 year band thereafter (Figure 4-6e). It coincides with the largest significant area of the bottom salinity anomaly that is observed at the 6.5-9 year band. The global wavelet spectrum of the GS index (Figure 4-6f) is also similar to the broad bandwidth of the quasi-decadal peak from 5 to 10 years in the Fourier spectral analysis. These results suggest a possible interaction between the bay and the shelf-slope water at the quasi-decadal time scale.

To determine the relationship between two time series that are expected to be linked, it is useful to apply cross-wavelet transform and wavelet coherence between two variables. However, the cross-wavelet spectrum appears to be not suitable for the significance testing of interrelation between two processes because it often produces an artifact of significant powers (Maraun and Kurths, 2004). Instead, Maraun and Kurths (2004) suggest that the use of the wavelet coherence applying Monte Carlo simulation, which is adopted in this study. Figure 4-7a shows the squared wavelet coherence between the bottom salinity anomaly and the Susquehanna River discharge anomaly. Large areas stand out as being significant and the phase relationship is shown to be predominantly anti-phase in all those areas, i.e., negative correlation between two variables. The significant sectors are sporadically distributed at the periods of 1 to 3 years while the correlations are significant at the periods of 3 to 6.5 years throughout the data record.

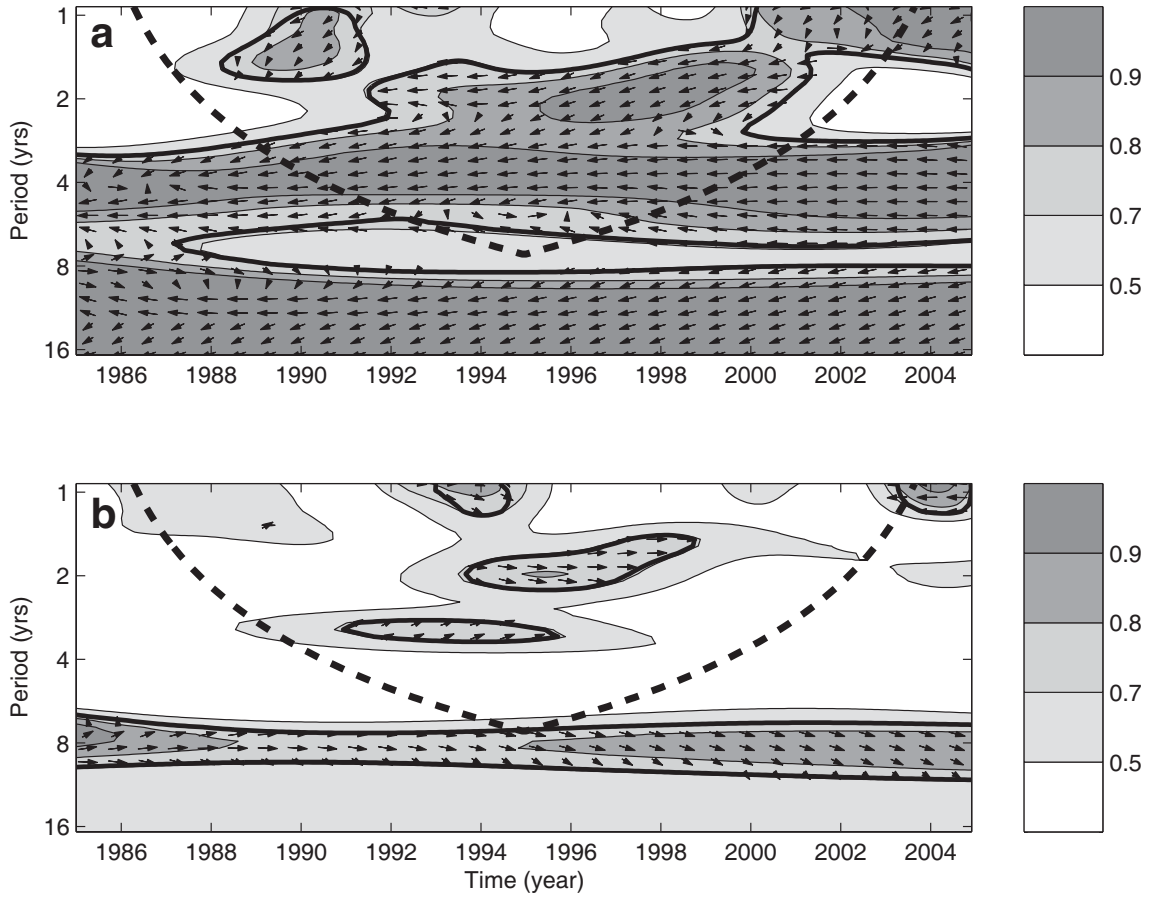

Figure 4-7. The wavelet coherence and phase (a) between the bottom salinity anomaly and the Susquehanna River discharge anomaly, and (b) between the bottom salinity anomaly and the Gulf Stream index. Contours are wavelet squared coherences 0.5, 0.7, 0.8, and 0.9. The 5% significance level from a Monte Carlo simulation (300 of surrogate data sets) is shown as a thick contour and the dashed line indicates the cone of influence. The vectors indicate the relative phase relationship between the first and the second time series (with in-phase pointing right, anti-phase pointing left, and the second time series leading the first by 90º pointing straight down

These results demonstrate that the interannual variability in the bottom salinity is driven by the river discharge. On the other hand, at 6.5-8.5 year band, most areas are found to be not significant or the in-phase relationship (positive correlation) is observed. This indicates that the quasi-decadal variability of the bottom salinity anomaly is not related to the river discharge. Instead, there may be a decadal or subdecadal (10-16 years) relationship between the salinity and the river discharge. Since this band is in the region of COI, we need another method to verify this result. The squared wavelet coherence between the bottom salinity anomaly and the GS index is shown in Figure 4-7b. The largest significant area of correlation is found at the 7--10 year band for the entire record and the phase relationship is predominantly in-phase, which indicates a positive correlation. This tends to suggest that the quasi-decadal variability in the bottom salinity anomaly is linked to the property of the shelf-slope water resulting from the ocean-bay exchange. However, being in COI region it also needs to be proved by another way. There are two minor but significant areas at the periods of 2 and 3 years between 1990 and 1998, which may stem from common frequencies at the interannual time scales.

In order to confirm the results of wavelet analysis, especially ones in the region of COI, we decide to band-pass filter data and examine them. The data (bottom salinity, river discharge and GS index) are separated at 8-10 year and 10-14 year bands, and then linear correlation between variables is computed. As shown in Figure 4-8, the bottom salinity is significantly correlated with GS index only at 8-10 year band with the correlation coefficient (r) of 0.41 ($p<0.05$). On the other hand, the bottom salinity is significantly correlated with the river discharge only at 10-14 year band with $r=-0.67$ ($p<0.05$). This corroborates the result of wavelet coherence; the quasi-decadal variability of bottom salinity is driven by the adjacent oceanic water. Moreover, Figure 4-8b reveals that the variability of the salinity anomaly longer than decadal cycle is associated with freshwater input, which may be linked to the large scale atmospheric forcings.

Vega et al. (1999) found that the salinity in the Chesapeake Bay correlates with the NAO and the SOI. Since those forcings are connected to the changes of precipitation patterns in North America (Dai et al., 1997), they may exhibit a direct relationship with variation of salinity in coastal waters. In order to examine the influence of the large scale atmospheric forcing in the variability of salinity in the Chesapeake Bay, the effects of the

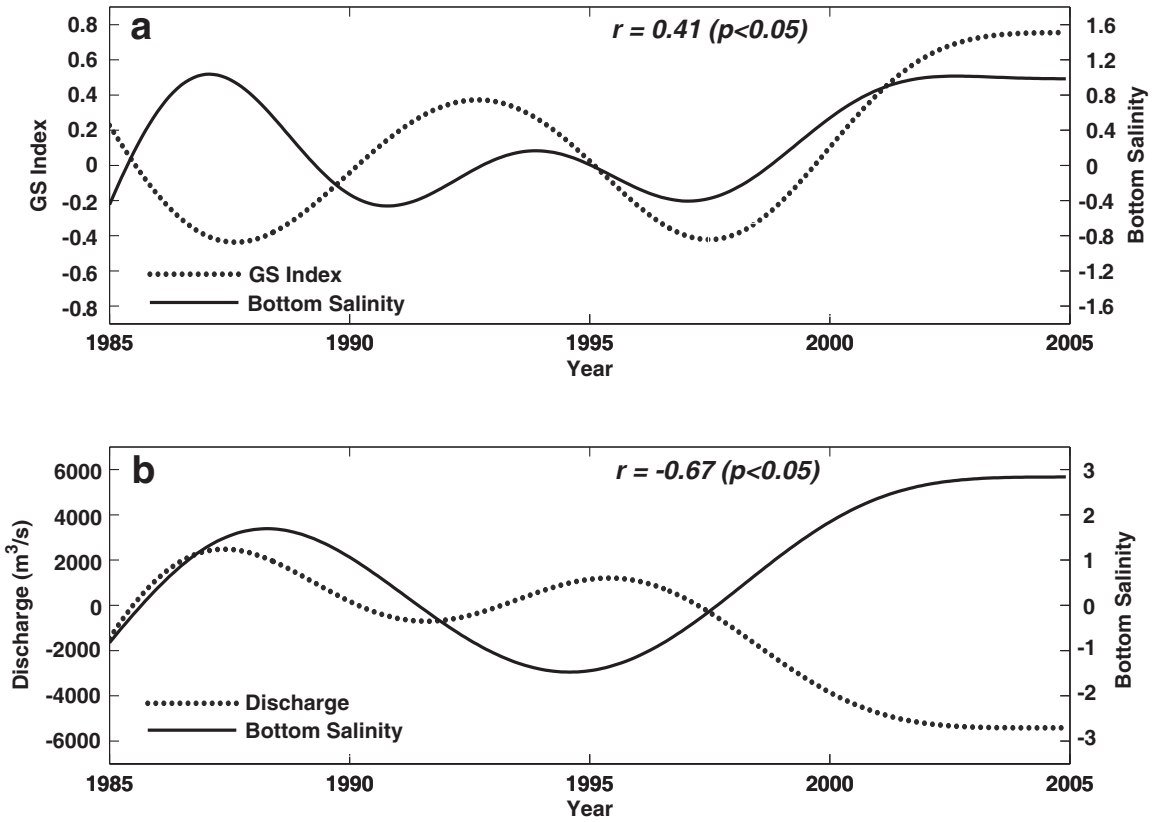

Figure 4-8. The relationship (a) between the bottom salinity anomaly and the Gulf Stream index (band-pass filtered at 8-10 year band), and (b) between the bottom salinity anomaly and the Susquehanna River discharge (band-pass filtered 10-14 year band). The correlation coefficient (r) are also indicated in each panel

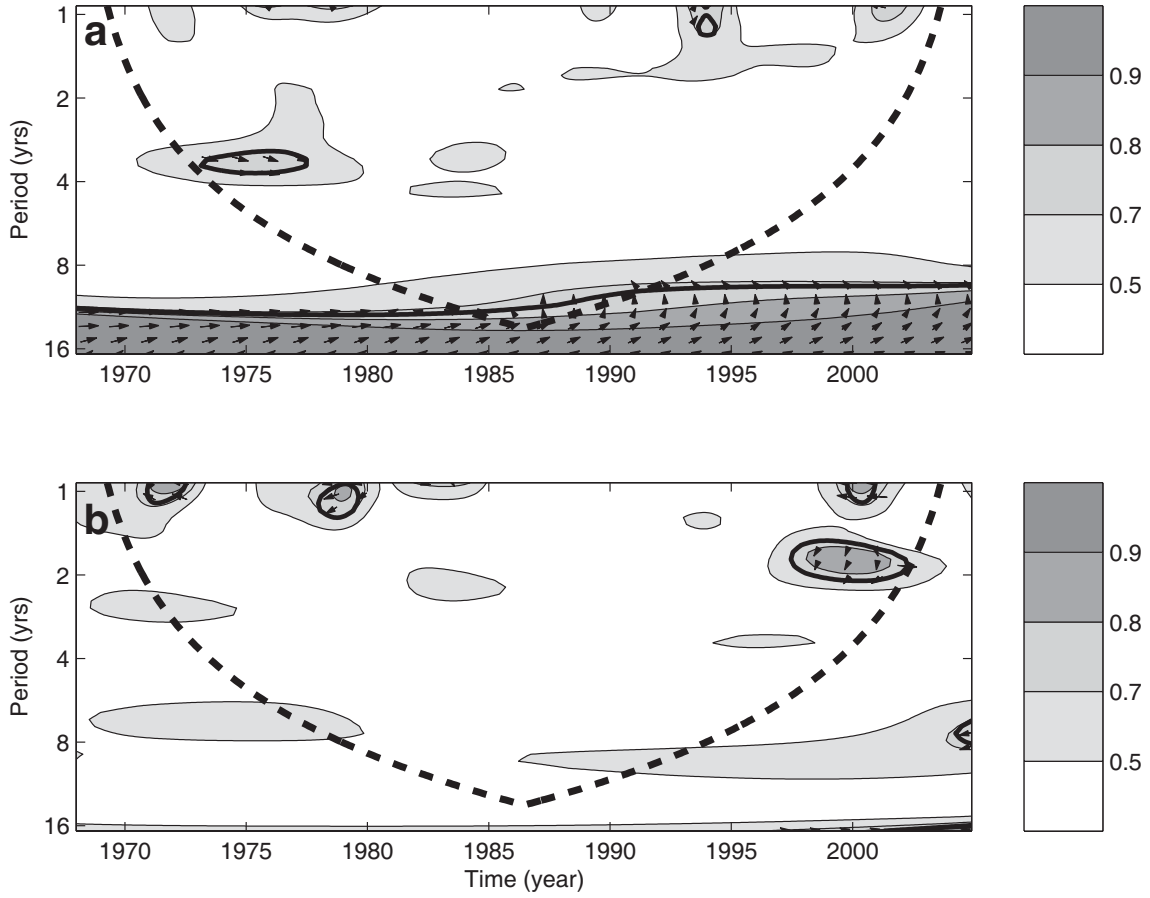

Figure 4-9. The wavelet coherence and phase (a) between the Susquehanna River discharge anomaly and the North Atlantic Oscillation, and (b) between the Susquehanna River discharge anomaly and the Southern Oscillation Index. Contours are wavelet squared coherences 0.5, 0.7, 0.8, and 0.9. The 5% significance level from a Monte Carlo simulation (300 of surrogate data sets) is shown as a thick contour and the dashed line indicates the cone of influence. The vectors indicate the relative phase relationship between the first and the second time series (with in-phase pointing right, anti-phase pointing left, and the second time series leading the first by 90º pointing straight down

NAO and the SOI are determined in the variability of the Susquehanna River discharge using the wavelet method. Figure 4-9a shows the wavelet coherence between the river discharge and the SOI during the period of 1968-2004, but no significant relationship is found on interannual to decadal time scales. On the other hand, the decadal variability of the river discharge appears to be related to the NAO (Figure 4-9b), which has been also observed in New England regions (Bradbury et al., 2002). Assuming that the interannual variability of salinity is related to the NAO, it is probably caused by the processes other than the variation of river discharge due to precipitation change. As a matter of fact, no direct relationship is found between the bottom salinity anomaly and the NAO except at the decadal time scale (not shown). This may account for the significant sector between the bottom salinity anomaly and the river discharge at the decadal (or subdecadal) time scale associated with the NAO.

4.5 Discussion

Gibson and Najjar (2000) reconstructed the variation of salinity in the Chesapeake Bay using the simple autoregressive statistical model based on the monthly mean salinity and the Susquehanna River flow. Since their study focused on the variability of salinity induced by the freshwater influx due to climate change, the correlations between the model and observations are shown to be weaker near the bottom and mouth of the bay. The model explains up to 93% of the variance in the surface salinity because of strong seasonality in the data. However, after removing the seasonal fluctuations, the model may not be able to reproduce the long-term variability of salinity that occurs on interannual to decadal time scales. When the wavelet transform is applied to the anomalies of their modeled data throughout the bay, the resulting power spectra resemble the power spectrum of the river discharge rather than that of the bottom salinity anomaly. For example, significant sectors are only observed at the interannual time scales up to four years, which is consistent with the results of this study indicating the influence of freshwater inflow. This is also evidence showing that long-term processes such as the

effects of adjacent oceanic water and ocean-bay exchange are excluded in the Gibson and Najjar (2000)'s model.

Several investigations that have been conducted in estuaries are based on the assumption that temperature and salinity in adjacent ocean are constant and/or that an oceanic flux is constant through a boundary. This may be true in cases where short-term processes are primarily involved. For instance, Austin (2002) examines how much water is exchanged between the bay and adjacent ocean. His study indicates that a considerable amount of water is exchanged through the open boundary with the oceanic flux of 8,000 m3/s into the bay. This may suggest the significant influence of adjacent oceanic water on the Chesapeake Bay since the mean annual river discharge to the bay is approximately 2,600 m3/s (Goodrich, 1988). The model showed good agreement with observations, however, there were significant discrepancies between the model and observations on an interannual time scale. This is most probably due to the assumption of constant oceanic salinity because the interannual variation of those discrepancies does not appear to be tied to the freshwater flux into the bay. Austin (2002) suggested two possible causes; one is due to the change of salinity outside the bay and another is due to the changes of exchange rate. Given the data at hand he could not ascertain the mechanisms involved.

This study has clearly shown that the interannual variability of the bottom salinity in the Chesapeake Bay is driven by the freshwater input. Although the Fourier power spectrum of the GS index exhibits the periodicities of 2 years (Figure 4-5c) and the wavelet coherence between the GS index and the bottom salinity anomaly shows the significant sectors at the 2-4 year band (Figure 4-7b), the influence of oceanic water may be overwhelmed by the local forcing at the interannual time scale. On the other hand, the quasi-decadal variability of the bottom salinity should be associated with non-local forcing because the river discharge does not contain a signal at the quasi-decadal band. By extending the connection between estuaries and adjacent shelf-slope waters, Figure 4-7b demonstrates that the quasi-decadal variability of bottom salinity in the Chesapeake Bay varies coherently with the property of adjacent ocean. Therefore, the adjacent oceanic waters through exchange processes play a significant role in the variability of the bottom salinity at the quasi-decadal time scales. Our results also suggest that NAO affects

salinity in the Chesapeake Bay in two different ways: shifting of the GS position (Taylor and Stephens, 1998) and changing precipitation pattern (Dai et al., 1997).

Although the GS index is used as a proxy for the shelf-slope water property, previous studies have shown that water properties in shelf-slope regions are associated with the GS position. For instance, when the GS position is shifted farther north, the shelf-slope salinity increases due to a lesser supply of the cold fresh Labrador Sea water into the region and thus decreasing its salinity (Schollaert et al., 2004). Thus, it is possible that the shifting of the GS position in the MAB region affects salinity in the Chesapeake Bay through exchange processes. This study has shown that the properties of shelf-slope waters vary at interannual and quasi-decadal time scales. However, it is the quasi-decadal variability that exerts most influence on the salinity variability of the bay. Our results also support Austin (2002)'s suggestion on the variation of oceanic salinity as the driving mechanism because his model underestimated the salinity in the early 1990s and overestimated it in the late 1990s. Since the GS was located in the northern positions (positive index) in the early 1990s and the southern positions (negative index) in the late 1990s, the adjacent ocean was relatively saline in the early 1990s and it was relatively fresh in the late 1990s (see Figure 4-3). This indicates that the salinity in the bay is more significantly affected by the adjacent ocean than previously thought.

Our results have shown that there are several processes involved which determine salinity in estuaries at various time scales. However, the influence due to the change of exchange rate between an estuary and adjacent ocean has not been examined because long-term ADCP data are not available near the mouth. In order to establish mechanistic links with the variability of salinity, future observational and modeling efforts need to include external processes such as the variation of adjacent ocean and large-scale climate variability. Also, there is a strong need to establish monitoring systems outside an estuary for the better understanding of responses of coastal ocean to the large-scale variability in ocean and atmosphere. Thus, future investigations can estimate how much the ocean-bay exchange varies temporally and determine how significantly the exchange contributes to the long-term balance of hydrographic properties in coastal waters as well as geochemical constituents in global cycles.

4.6. Summary

The linear regression analysis demonstrates the significant relationship of the bottom salinity anomaly with the Susquehanna River discharge and the GS index. This indicates that the salinity in the bay is associated with not only the local effects but also the external processes occurring in the adjacent shelf-slope region. The spectral analysis using the Fourier and wavelet methods reveal the two major periodicities of the bottom salinity anomaly at the interannual and quasi-decadal time scales. The wavelet analysis shows significant powers centered at the periods of 2 and 7.5 years in the bottom salinity anomaly. The wavelet squared coherence clearly shows that the interannual variability of salinity anomaly in the Chesapeake Bay is driven by the river discharge. On the quasi-decadal time scale the property of the adjacent ocean plays a significant role in the variability of the bottom salinity, indicating the importance of ocean-bay exchange processes.

Chapter 5
Numerical Simulation of Exchange Transport and Heat Budget in Long Island Sound

Abstract

Transport and heat balance in Long Island Sound (LIS) are investigated using a hydrodynamic ocean model which runs on a massively parallel Blue Gene/L super computer at Brookhaven National Laboratory, New York. The model is simulated with realistic forcing, i.e., tides, surface momentum and surface heat fluxes. Seasonal salinity and temperature variations are assimilated at 5 to 30-day time-scales. The model results are validated with tides, ADCP observations, and temperature measurements. In general, the simulated fields agree well with the observations. The magnitude of exchange transport decreases from east to west, with a range of 0.1×10^4 to 2.5×10^4 m^3/s, and it is order of 1.0×10^4 m^3/s in the central basin. The transport in the eastern sound shows the strong seasonality. It peaks in August (3.3×10^4 m^3/s) and becomes weaker (1.8×10^4 m^3/s) through the winter months. However, the strong seasonality of transport is not evident in the western sound. The role of horizontal advection is examined by separating the depth-integrated heat budget into its three contributions, i.e., storage ($\partial T/\partial t$), net surface heat flux (Q_{net}), and horizontal advection ($\boldsymbol{u}\cdot\nabla T$). It is found the net surface heat flux dominates the fall/winter heat balance, acting to cool the water column throughout the sound. In contrast, the horizontal advection plays a more significant role during spring/summer due to the heat loss over the shallow areas and the heat gain along the deep channel.

5.1 Introduction

Climate models have projected that global surface temperature will rise up to more than 4 ºC at the end of the 21st century (IPCC, 2007). However, it is very difficult to study the effects of temperature rise using observations in most cases. Thus, the logical approach is to use the effects of climate variability as a proxy to climate changes assuming the change in time-scale does matter much. Several studies have indicated the importance of temperature warming in ocean as an ecological regulator (e.g., Behrenfeld et al., 2006; Edwards and Richardson, 2004; Perry et al., 2005; Walther et al., 2002). There is amounting evidence showing a coastal warming trend (Nixon et al., 2004; Stachowicz et al., 2002). The response of estuaries to temperature rise results in severe hypoxic conditions (O'Shea and Brosnan, 2000; Wilson et al., 2008) and reduced primary production (Keller et al., 1999; Oviatt, 2004). Long Island Sound (LIS) is no exception, because it experienced mass mortality of American lobster (*Homarus americanus*) in 1999, which is most likely linked to hypoxic event as well as temperature increase. As the global temperature increases, it is expected that coastal embayments and estuaries in mid-latitudes like LIS will warm faster than the global average. Therefore, it is crucial to examine the temperature variability of the sound in relation to global warming for better understanding the connection between climate variability and environmental issues.

As the first step to examine the variability of the sound as a whole, Lee and Lwiza (2005) investigated the hydrographic data from 1991 to 2002 and emphasized the significant role of external forcing. Based on the relationship between net surface heat flux and temperature tendency, the study showed the importance of horizontal advection in the interannual variability of temperature, especially during summer. However, the standing issue has been to quantify how much water (heat and/or salt) are transported in and out of the estuary under the influence of adjacent ocean on long-term time-scales. Although Lee and Lwiza (2005) attempted to calculate the heat budget in LIS, the lack of velocity field observations undermined the efforts to examine the contribution of horizontal advection. However, soon after the study, two long-term projects were initiated to survey the current fields in LIS using direct velocity measurements from ferry mounted ADCP observations; 1) Bridgeport, CT from/to Port Jefferson, NY and 2) New London, CT from/to Orient Point, NY. By examining the velocity data collected from the two ferry services, Hao (2008) and Codiga and Aurin (2007) calculated the exchange

volume transport at the ferry transects. They showed that a significant amount of water is transported at the central sound ($1.0\sim1.2\times10^4$ m^3/s) and the eastern end ($1.8\sim3.0\times10^4$ m^3/s) with strong seasonality, respectively. The ADCP data from the two cross-sound ferry services are collected during operational hours (7 AM to 8.30 PM for Orient Point–New London ferry, and 6 AM to 10 PM for the Bridgeport–Port Jefferson ferry). They are restricted to one ferry transect each, and thus cannot resolve spatial patterns over the whole sound. Therefore, there is a need for developing a numerical modeling approach which will provide us the results to quantify the contribution of external forcing on pertinent spatial and temporal scales. Moreover, the development of hydrodynamic ocean model can be cooperated with biogeochemical models, which will allow us to investigate further environmental issues such as hypoxia.

There have been several modeling attempts around the LIS region from a simple box model to a 3-D hydrodynamic ocean models. Gay et al. (2004) calculated the exchange between LIS and adjacent ocean using an inverse method based on salinity data, but the exchange flow at the eastern end was found to be underestimated as compared to the observational study by Codiga and Aurin (2007). Valle-Levinson and Wilson (1998) examined the effects of rotation and vertical mixing on volume exchange during spring-neap tidal cycles over Mattituck Sill. Using simulations over a simplified sill, they showed that increased mixing during spring tides suppresses boundary current formation. In contrast, during neap tides, vertical mixing diminishes the reduced gravity, and thus boundary currents are strengthened. Crowley (2005) first applied the Regional Ocean Modeling System (ROMS) to LIS and examined the thermohaline circulation throughout the sound. This study showed that the intrusion of bottom water over the Mattituck Sill under conditions of weak vertical mixing during neap tide, which is consistent with the study of Valle-Levinson and Wilson (1998). The model results also showed that the strength of simultaneous eastward and westward transports vary seasonally, increasing with stratification. However, it was simulated only for spring and summer of 1998. Hao (2008) examined the momentum balance and residual flow in LIS based on the simulation developed by Crowley (2005). The longitudinal momentum balance is primarily between pressure gradient and advection and the dominant lateral balance is geostrophic in LIS. Hao (2008) also showed that inflow region concentrate over the

channel and surface outflow is intensified over the southern side of the channel. Based on the Princeton Ocean Model, Mau (2008) presented the comprehensive modeling study of the coastal buoyant outflow for an entire seasonal cycle and calculate the exchange transport between LIS and adjacent ocean. However, the study primarily focused on the Block Island Sound (BIS) region.

The previous model simulations successfully reproduced the complex tidal environment and exhibited very good skills in predicting the temperature and salinity fields around LIS. Using super computing power available, we are able to carry out a higher-resolution numerical simulation with a high level of realism for multiple years. As a case study, a three-dimensional ocean model is used to simulate flow and temperature fields for an entire year of 2005. ROMS is set up on a massively parallel supercomputer Blue Gene/L in Brookhaven National Laboratory (BNL), Upton, New York. The model is forced with tides, surface momentum, heat fluxes and assimilated with seasonal climatology. The model skills are assessed with the observations available around the MAB and LIS, and the model results are examined to quantify the volume transport and the contribution of horizontal advection to heat budget. Tidal elevation and current are evaluated around the MAB region including BIS focusing on horizontal and vertical structures of tidal ellipses. Then, we compare model results of current and temperature with two ferry-borne ADCP data sets and hydrographic properties. The objective of this study is 1) to assess the skill of the model to reproduce the temperature and flow fields, 2) to determine the three-dimensional exchange transport throughout the sound over the annual cycle and 3) to examine the role of horizontal advection in heat balance. The paper is organized in the following manner: section 2 briefly describes the area of study. The details of model configuration and data processing are described in section 3. Model results are verified with ADCP observations and monthly temperature measurements in section 4. The section also includes description of temporal and spatial structures of volume transport and the role of horizontal exchange and surface heat flux in heat budget. Discussion of the model results and suggestions for further study are presented in section 5, and results are summarized in section 6.

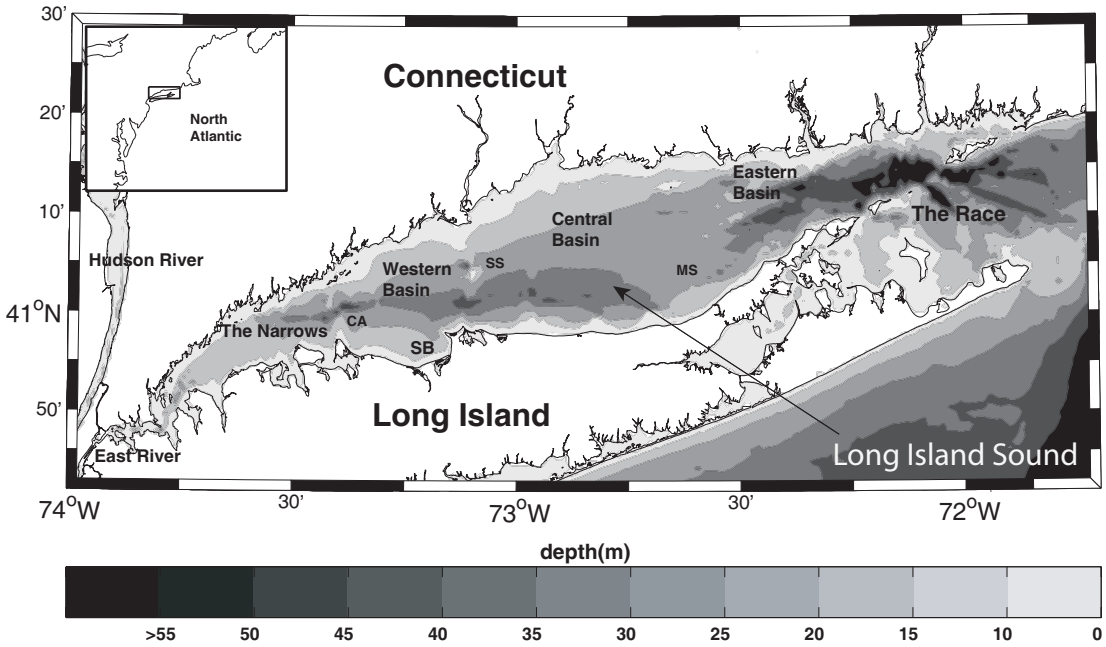

Figure 5-1. Long Island Sound and its bathymetry (SS, Stratford Shoal; CA, Cable and Anchor Reef; MS, Mattituck Sill; SB, Smithtown Bay).

5.2 Study Area

LIS is located in the northeast United States and bounded by the Connecticut and Long Island, New York (Figure 5-1). While the western end is connected to the Upper New York Bay (lower Hudson River) via the East River and the eastern end opens to the Blocks Island Sound through the Race communicating with the Atlantic Ocean. It is about 150 km long and 20 km wide (34 km at the widest point) with a mean depth of 21 m.. Major rivers including Thames, Housatonic, and Connecticut River are located along the Connecticut coast and comprise most of the freshwater discharge into the sound. The Connecticut River alone contributes 72% of the total freshwater input to the basin. The mean discharge into LIS is 560 m^3/s; the highest in April (1280 m^3/s) and the lowest in August (200 m^3/s). LIS is a glacial terminal moraine with complex bathymetry that is characterized by an asymmetrical V-shaped cross section with a deep channel on the southern side (Long Island coast) and a gradual slope on the northern side (Connecticut coast) as shown in Figure 5-1. Tides are characterized as a standing wave in the western basin and a progressive wave in the eastern basin (Hao, 2008), and tidal currents are strong in LIS, ranging from about 0.5 m/s in the Central Basin to 1 m/s at the eastern end (Vieira, 1990).

5.3 The Regional Ocean Model

The numerical simulation presented here is performed using the Regional Ocean Model System (ROMS), which is a free-surface, hydrostatic, terrain-following, primitive equations ocean model widely used by the scientific community for a diverse range of applications (e.g., Haidvogel et al., 2000;Di Lorenzo, 2003; Dinniman et al., 2003; Budgell, 2005; Warner et al., 2005; Wilkin, 2006). The model simulation was run on the massively parallel supercomputer IBM Blue Gene/L system at BNL.

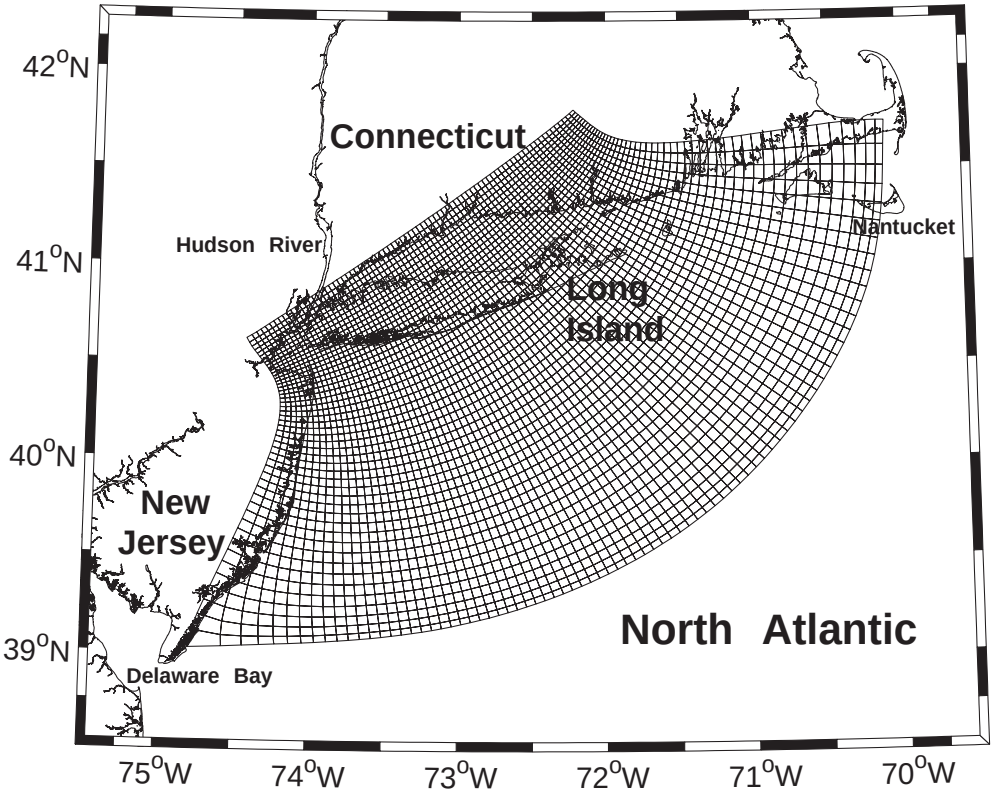

Figure 5-2. Model grid (240×400×16) (sub-sampled every 5 grid points)

5.3.1 Model configuration

The model domain extends from Delaware Bay to Nantucket Sound as shown in Figure 5-2. The model grid contains 250 by 400 cells with 16 evenly spaced sigma-levels in the vertical. The mean horizontal resolution is approximately 500 m in LIS. The model topography is based on the 30-second resolution bathymetry data and sub-sampled from the National Geophysical Data Center (NGDC) 3 arc-second Coastal Relief Model. The bathymetry data were interpolated onto the model grid and smoothed with a Shapiro filter until the r-factor (the change of slope between neighboring points) was reached to the maximum of 0.35. The minimum water depth is set at 5 m. The model was started from a state of rest with initial temperature and salinity fields. Open boundary conditions were applied to all tracers and baroclinic velocity using Orlanski-type radiation. The surface elevation and transport of five tidal constituents (M2, S2, N2, K2, and O1), obtained from an Advanced Circulation (ADCIRC) model tidal database, were prescribed along the open boundaries using Chapman and Flather condition. The East River was closed, and the model was forced with the net transport of water (–310 m^3/s with 26 psu) at the western end based on the study of Blumberg and Pritchard (1997). The vertical turbulence mixing used the Mellor and Yamada level-2.5 scheme, and the quadratic bottom drag coefficient was set to 0.004.

Three different simulations were performed for this study, viz., tidal validation, two-year spin-up with temperature and salinity nudging, and the third-year forced with surface heat fluxes and salinity assimilation. The results from the tidal and the third year simulations were only used for the analysis. Initially, the model was forced only by surface momentum fluxes (wind stress) and tides (elevation and velocity) along the open boundaries with constant temperature and salinity fields. The external and internal time steps were 2 seconds and 2 minutes, respectively. After the model was validated with tides, the parameters used in the tidal simulation were applied for the second simulation, which was run for two-repeat one-year (2005) cycles as a spin-up. The model temperature and salinity predictions were nudged to monthly climatology from a five-day time scale at the boundary points to decrease linearly to 30 days away from the boundary. The external and internal time steps were set to 1.5 seconds and 1.5 minutes, respectively.

Then, using the restart file from the second simulation, the model was simulated for an entire year of 2005 (third year) with wind and surface heat fluxes (shortwave, longwave, sensible, and latent), which were calculated by the bulk formulas of Fairall et al. (1996). Since the model surface forcing does not include the river discharge, the climatology of salinity field was nudged with same time scale used in the second simulation. The external and internal time steps were 1 second and 1 minute, respectively

5.3.2 Temperature and salinity climatology

Hydrographic data from 1950 to 2007 were obtained from the National Oceanographic Data Center (NODC) World Ocean Database. In order to remove extremes, the data falling into the 95% of confidence interval in each 1º× 1º geographical grid were considered as significant, and then monthly averaged for the MAB region with 0.5 degree resolution. After combining with from Connecticut Department of Environmental Protection (CTDEP) monitoring data sampled in 2005 (see Figure 5-3b), the monthly climatological fields of temperature and salinity at 16 sigma-levels were generated using Data-Interpolating Variational Analysis (DIVA) package (available at http://modb.oce.ulg.ac.be/projects/1/diva) with the correlation length scale of 2.0 degree. This method was used instead of the standard optimal interpolation because DIVA takes into account coastlines during interpolation (e.g., Troupin et al., 2008). Initial and boundary conditions were also generated based on monthly climatological fields.

5.3.3 Surface forcing

Hourly wind data (speed and direction) were obtained from buoys and C-MAN stations around the MAB region (Figure 5-3a). Wind speed at 10m was calculated at given wind speed and height following Large and Pond (1981), and then decomposed into x (east-west) and y (north-south) components after daily averaging. In order to

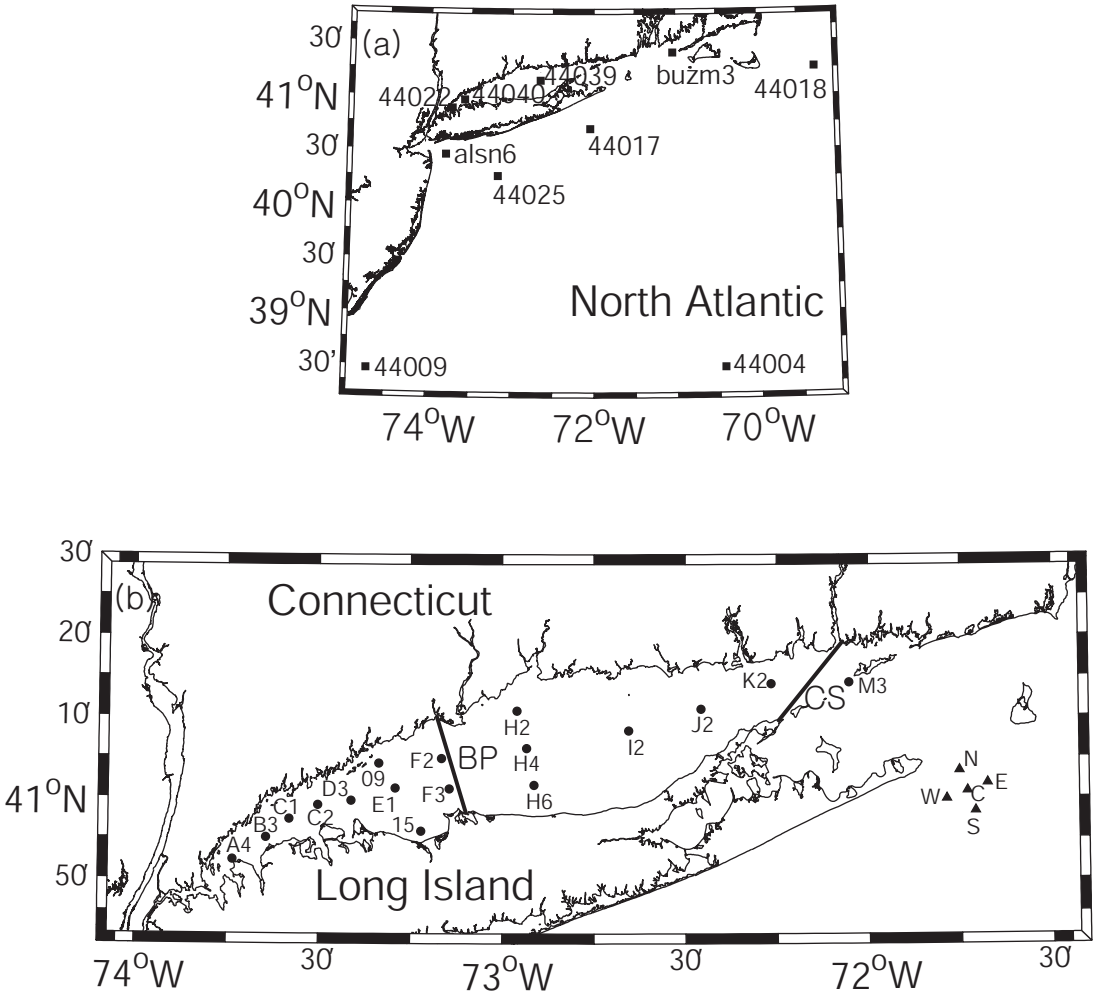

Figure 5-3. (a) Observational buoys and C-MAN stations around the Mid-Atlantic Bight including Long Island Sound. (b) Connecticut Department of Environmental Protection water quality monitoring stations are indicated as squares (17 major stations) with station names. ADCP mooring sites by Codiga and Rear (2004) are marked as triangles. Solid lines indicate ferry-based ADCP observations (BP, Bridgeport-Port Jefferson ferry service; CS, Cross Sound ferry service between Orient Point, NY, and New London, CT).

calculate surface heat flux terms, surface atmospheric variables were also retrieved from the buoys, namely, relative humidity, air temperature, and surface pressure, and then daily averaged. In addition, the three-hourly net shortwave radiation flux (difference between downward and upward shortwave radiation flux) and total cloud cover were retrieved from the National Centers for Environmental Prediction (NCEP) North American Regional Reanalysis (NARR). All variables were optimally interpolated with 0.1 degree resolution, and set up for ROMS to interpolate into curvilinear grid points.

5.4 Results

5.4.1 Model-data comparison

The model results for the tidal simulation agree well with Swanson (1976) and Moody et al. (1984) in the New York Bight (NYB). The phase of M2 tidal elevation is around 350 degree and the amplitude is nearly constant (~50 cm). The mean errors between the modeled and observed values are relatively small (<5 degree in phase and <4 cm in amplitude) among 19 stations (not shown). Figure 5-4 shows co-amplitude and co-phase lines of M2 tidal elevation in LIS. There is an amplitude minimum near Montauk Point and a maximum in the western end, whereas the maximum phase is located in the Peconic Bay. Although the phase of tidal elevation agrees well with observations, the amplitude is overestimated in the Western Basin and the Narrows by up to 15 cm. The error could be due to the disconnection between LIS and Upper New York Bay.

Table 5-1 lists the parameters of model and observed tidal ellipses in the NYB. The tidal currents exhibit more spatial variations in amplitude and phase than the tidal elevation. The modeled tidal current ellipses agree well with the observations except at sites LI2, P31 and CMICE (southern shore of Long Island) in phase and orientation. By excluding those three stations, the mean errors (the absolute differences between model and observation) over 16 stations are 1.8 cm/s in semi-major axis, 1.0 cm/s in semi-minor axis, 15 degree in orientation, and 14 degree in phase. The vertical structure of the model tidal ellipses are also compared with moored ACDP observations during fall/winter near

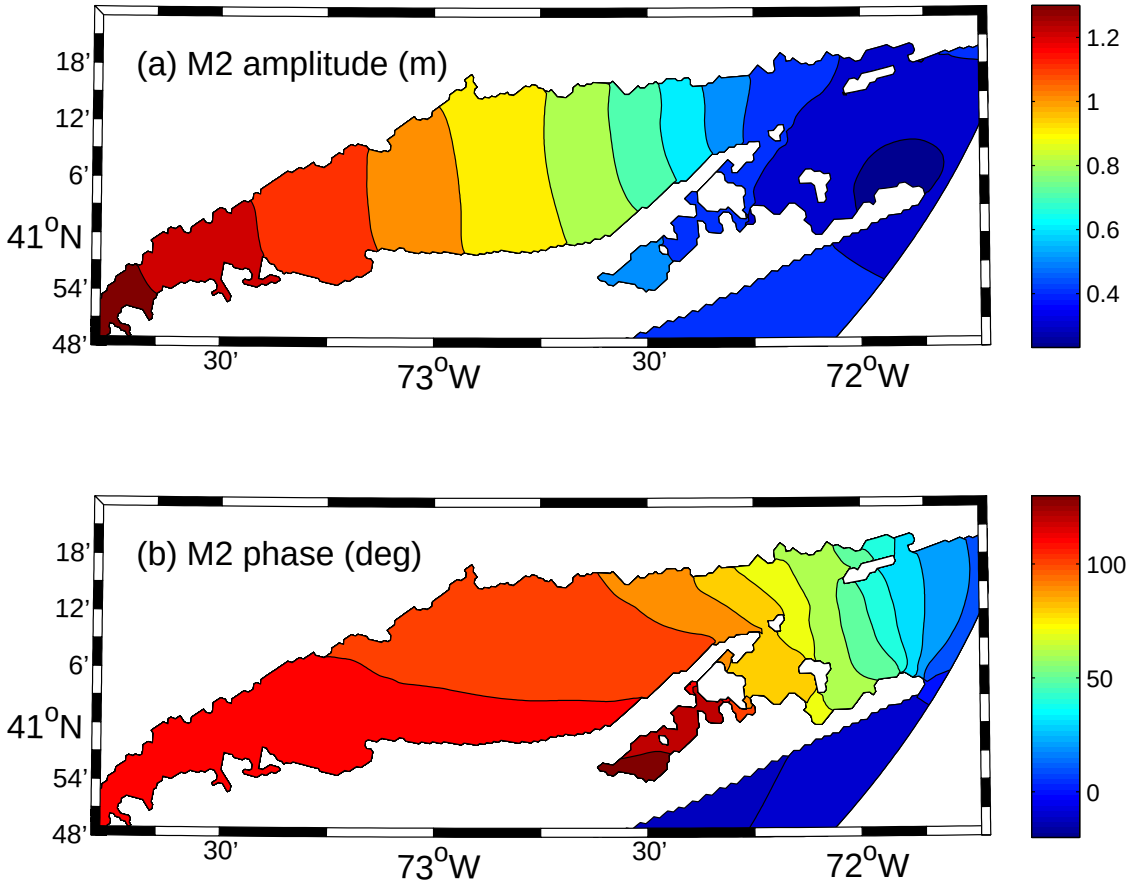

Figure 5-4. (a) amplitude and (b) phase of M2 tidal elevation in Long Island Sound.

Table 5-1. Tidal current ellipse parameters for observations (Moody et al., 1984) and model results.

Site	Observation				Model			
	semi-major (cm/s)	semi-minor (cm/s)	Phase (deg)	Orientation (degree)	semi-major (cm/s)	semi-minor (cm/s)	Phase (deg)	Orientation (degree)
NES743	5.1	-4.9	354	78	6.3	-5.1	43	43
NES742	8.7	-8.2	41	28	9.8	-8.0	42	46
NES762	6	-5.5	88	30	7.6	-6.3	41	40
NES741	9.4	-9	33	45	10.0	-8.8	5	90
P32	5	-3.3	230	147	7.4	-5.0	242	173
LI4	8.3	-5.3	253	134	7.7	-5.1	253	148
NES762W	8.6	-5.1	255	140	8.1	-4.8	252	146
LI3	8.5	-5.3	247	153	8.9	-5.7	246	165
LI2	8.7	-4.7	240	168	9.0	-4.5	59	3
P31	7.2	-1.6	223	179	9.8	-3.0	56	15
CMICE	9.6	-1.6	240	164	10.8	-1.5	64	17
ME	7.1	-2.9	235	124	12.4	-6.7	257	152
LTM	11.5	-3.9	286	146	11.7	-4.9	258	158
MESA7	16.8	-6.6	259	151	11.1	-3.8	264	148
FIRE ISLAND	6.7	-0.6	271	174	11.5	-1.7	263	175
28	12	-2.9	270	153	11.2	-2.9	262	161
15	12.6	-1.2	267	162	12.4	-1.7	270	164
49	12.1	-6.2	253	131	12.9	-7.0	273	136
LT6	6.2	1.1	270	141	8.5	-0.6	269	145

Block Island Sound (see Codiga and Rear, 2004), which are indicated as triangles in Figure 5-3b. Figure 5-5 shows that the model results and observations are generally in good agreement, but the largest discrepancy appears in semi-minor axis at the station N. The tidal ellipses rotate clockwise towards the bottom and amplitude decreases sharply at the bottom. However, due to absence of stratified condition in the model simulation, the orientation angle is relatively constant throughout the water column and the phase lag is less noticeable between surface and bottom.

After assessing the model skill with tides, the model was simulated with realistic surface forcing and salinity nudging after two-year spin-up time, and its results are used for the analysis in the rest of study. Figure 5-6 illustrates the structure of M2 longitudinal current amplitude and phase obtained from the ferry-borne ADCP observations (left column) between Bridgeport and Port Jefferson (see Figure 5-3b) and the model results (right column) during summer season. The comparison shows good agreement in the vertical and lateral structures. The tidal current is strong (~50 cm/s) on the main channel approximately at a depth of 10 m in both the model and observations, and the amplitude decreases with depth in similar fashion. In addition, the model indicates a strong tidal current on the northern flank at surface, which is not shown in the ADCP observations due to the shadow zone caused by side-lobe effects. The M2 phase diagram shows that the phase at the surface leads the bottom.

There are other ferry-based ADCP observations between Orient Point, New York and New London, Connecticut (see Figure 5-3b) near the Race, which have been described by Codiga and Aurin (2007). The processed data are accessible via their website (URL http://www.po.gso.uri.edu/~codiga/foster/main.htm). Their observations include the data collected during 2005, which allowed us to make direct comparison with the model results. Figure 5-7 illustrates M2 tidal ellipse parameters of the ADCP observations (left column) and the model output (right column), i.e., semi-major axis, semi-minor axis, phase and orientation. It is important to bear in mind that the first good ADCP bin is centered at 8 m in the ferry observations. Overall, the comparison between the model and observations shows excellent agreement in the vertical and lateral structures. The model slightly over-estimates the magnitudes of semi-major and semi-minor axis near surface layers, and the overestimation tends to penetrate into deeper

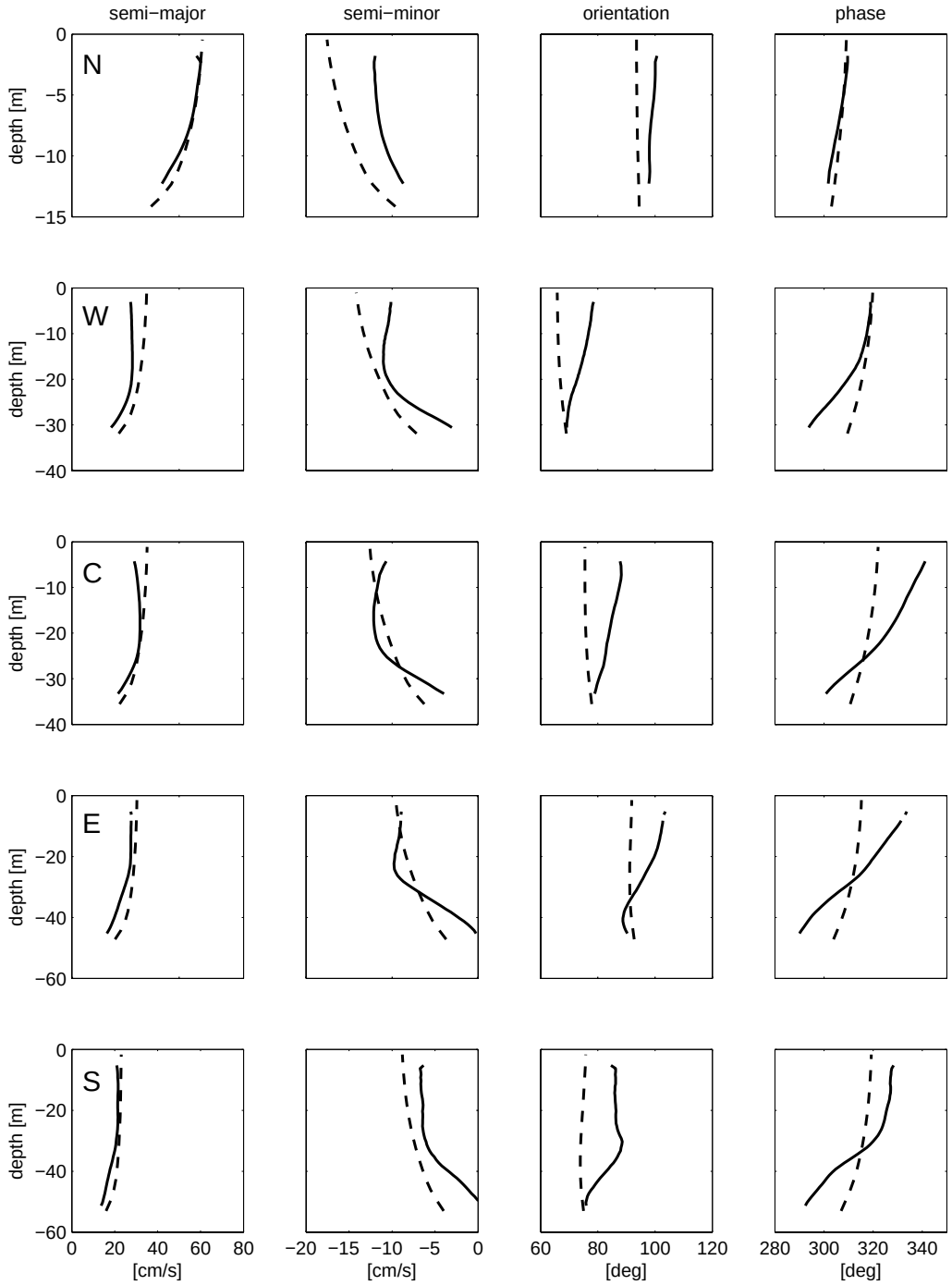

Figure 5-5. Vertical structure of M2 tidal ellipse parameters at the North(N), West(W), Central(C), East(E), and South(S) sites during fall/winter 2001 (Codiga and Rear, 2004) outside Block Island Sound. Model results are shown in dashed lines and observations in solid ones.

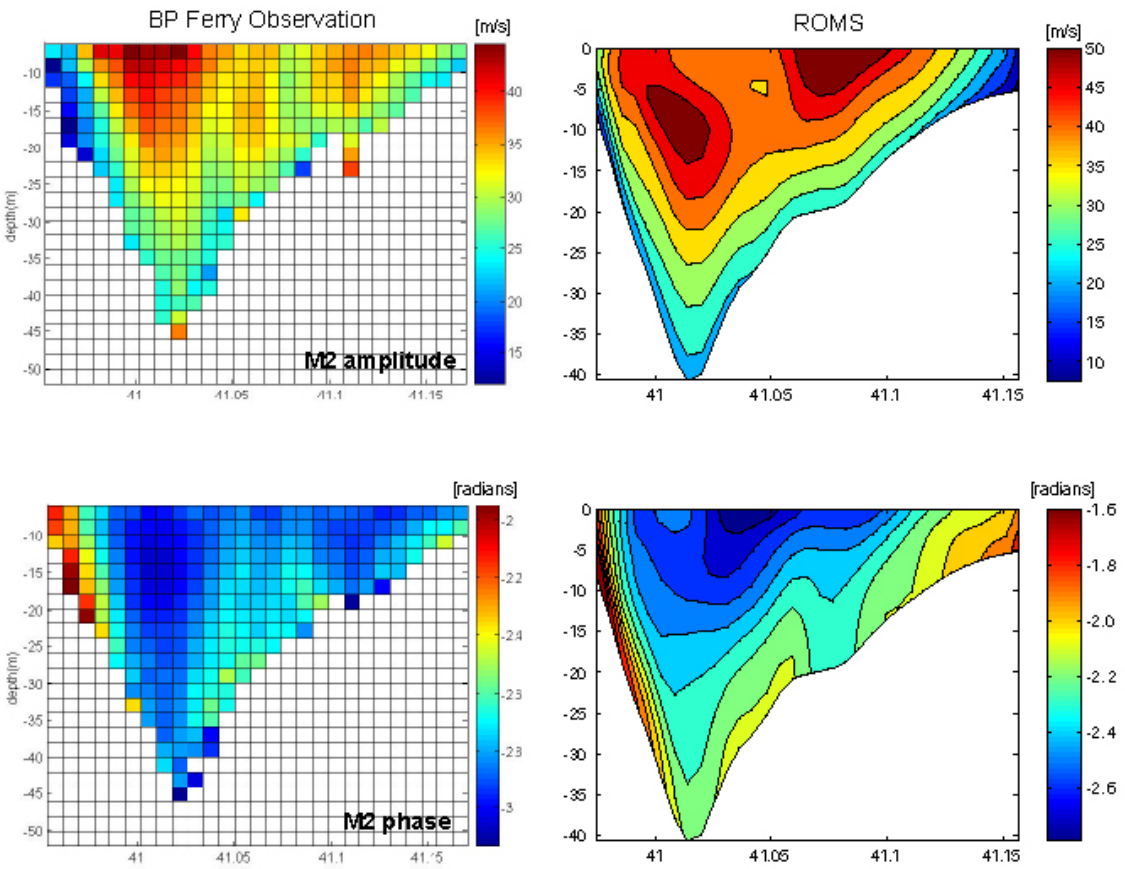

Figure 5-6. M2 amplitude and phase during summer. The ferry-based observations (7/19/03 to 8/13/03) between Port Jefferson, NY and Bridgeport, CT, (Hao, 2008) are displayed in the left column. The results from model simulation during summer are shown in the right column.

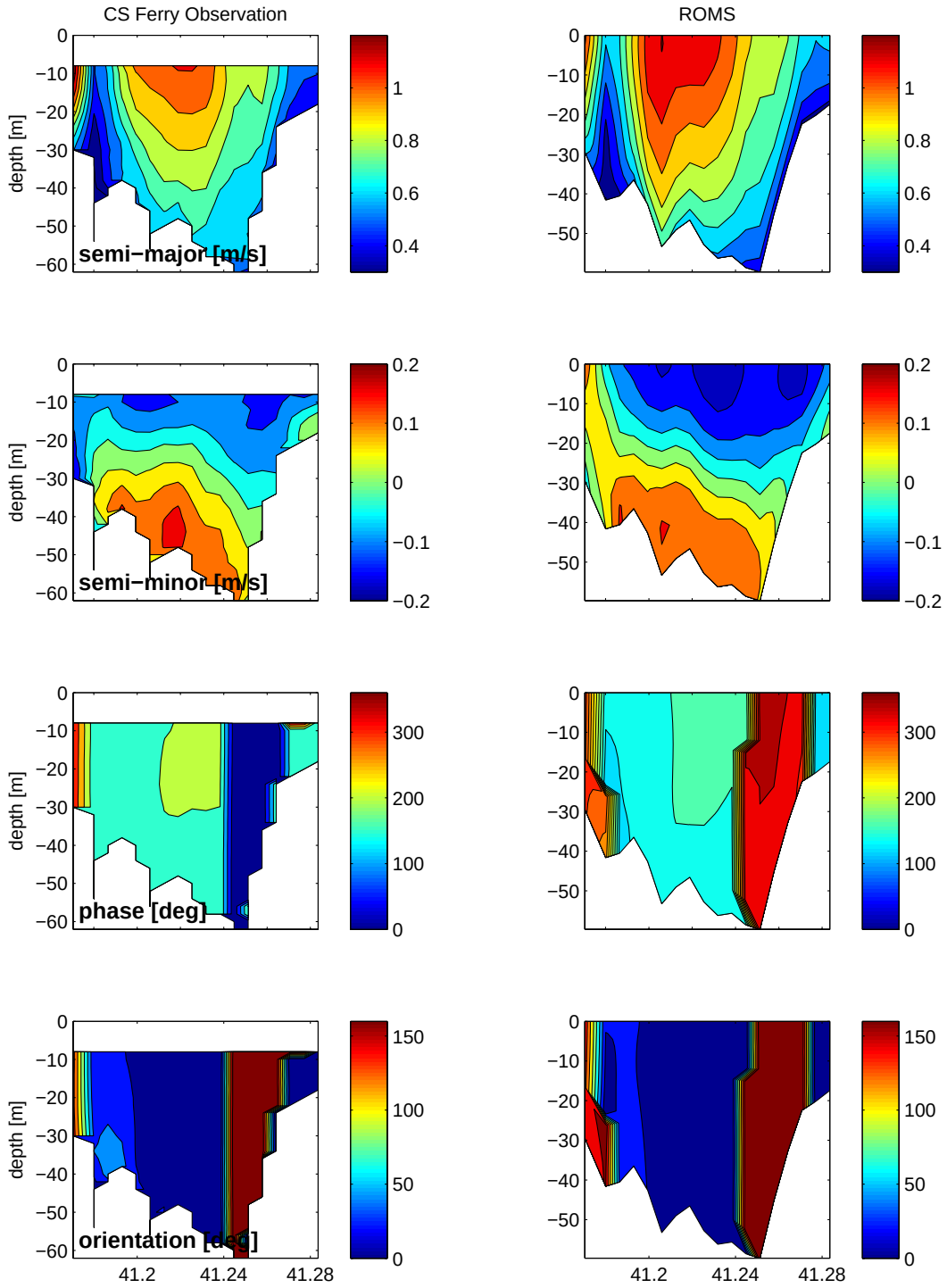

Figure 5-7. Comparison of M2 tidal ellipse parameters between ferry ADCP observation in 2005.

layers. The M2 phase diagram shows that the model phase slightly leads the observations on the northern side of the main channel by approximately 40º. Figure 5-8 provides a comparison of residual current structure obtained from the ADCP observations (left column) and the model simulation (right column). In general, the model agrees with the observations in volume transport and flow structure, which shows that an inflow concentrates over the deep channel and penetrates nearly to the surface, and a surface outflow is intensified over the southern side. There are also some few notable differences. For example, the inward transport (into-estuary) is 2.3×10^4 m^3/s in the observations, and 2.4×10^4 m^3/s in the model result. The difference could be due to the 8-m ADCP surface shadow zone. Compared to the observations, the model results indicate that outward (out-of-estuary) residual flows further extends from surface to a depth of ~30 m near Long Island showing a surface intensified outflow over the southern side of the channel. Inward (into-estuary) residual flow is relatively stronger over the channel and skewed towards the northern side of the channel, which is consistent with the previous modeling study by Hao (2008). With regards to the lateral flow, the model shows a strong positive (northeast) surface flow on the southern side of the channel and a negative (southwest) flow over the channel. Observations exhibit a weaker positive flow, and a negative flow more penetrate into the surface layer.

Without temperature nudging in the third simulation, the model was forced with surface heat fluxes and salinity variation is assimilated. The model results are compared with the monthly hydrographic data provided by CTDEP. The observed and modeled temperature in LIS are shown in scatter diagrams (Figure 5-9). Scattered points cluster around the slope = 1 diagonal line, indicating good agreement between the model and observations. RMSE (0.85 ºC near surface and 1.00 ºC near bottom) indicates that surface temperature is better fitted than the bottom temperature because summer temperature data tend to spread away from the line, i.e., the model underestimates bottom temperature during summer. The error of the surface temperature has a mean bias of 0.007 ºC with a standard deviation of 0.86 ºC while the error of bottom temperature is more biased with a mean bias of 0.53 ºC and a standard deviation of 0.85 ºC.

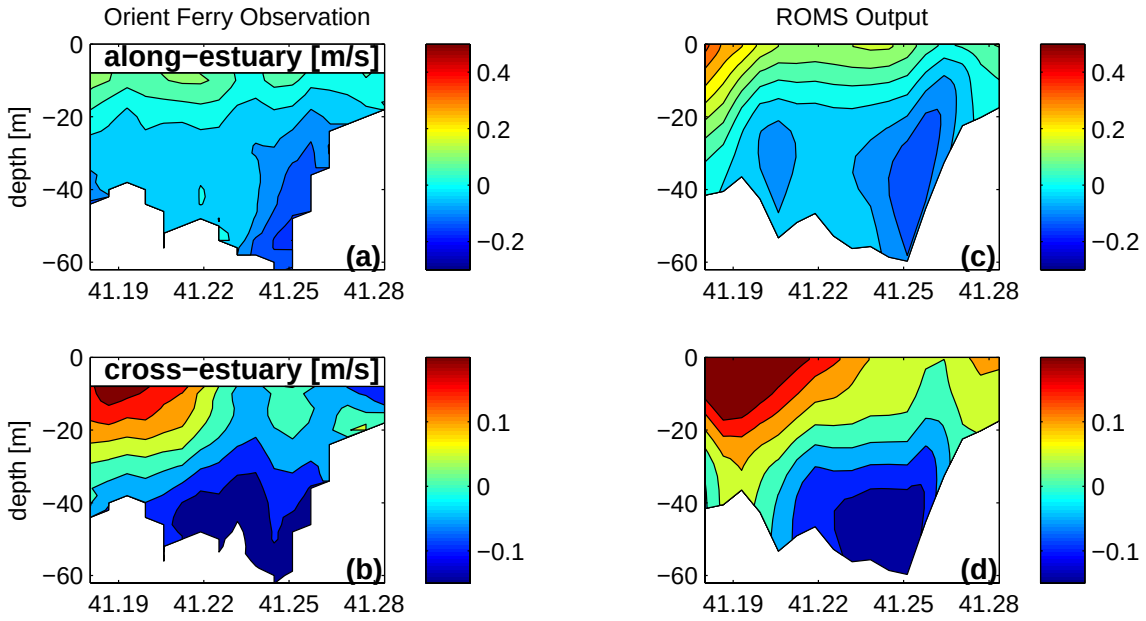

Figure 5-8. Left column: residual currents (m/s) from ferry ADCP observations at eastern Long Island Sound in 2005 (see also Codiga and Aurine, 2007). Right column: residual currents of along-estuary and cross-estuary components from model simulation of 2005.

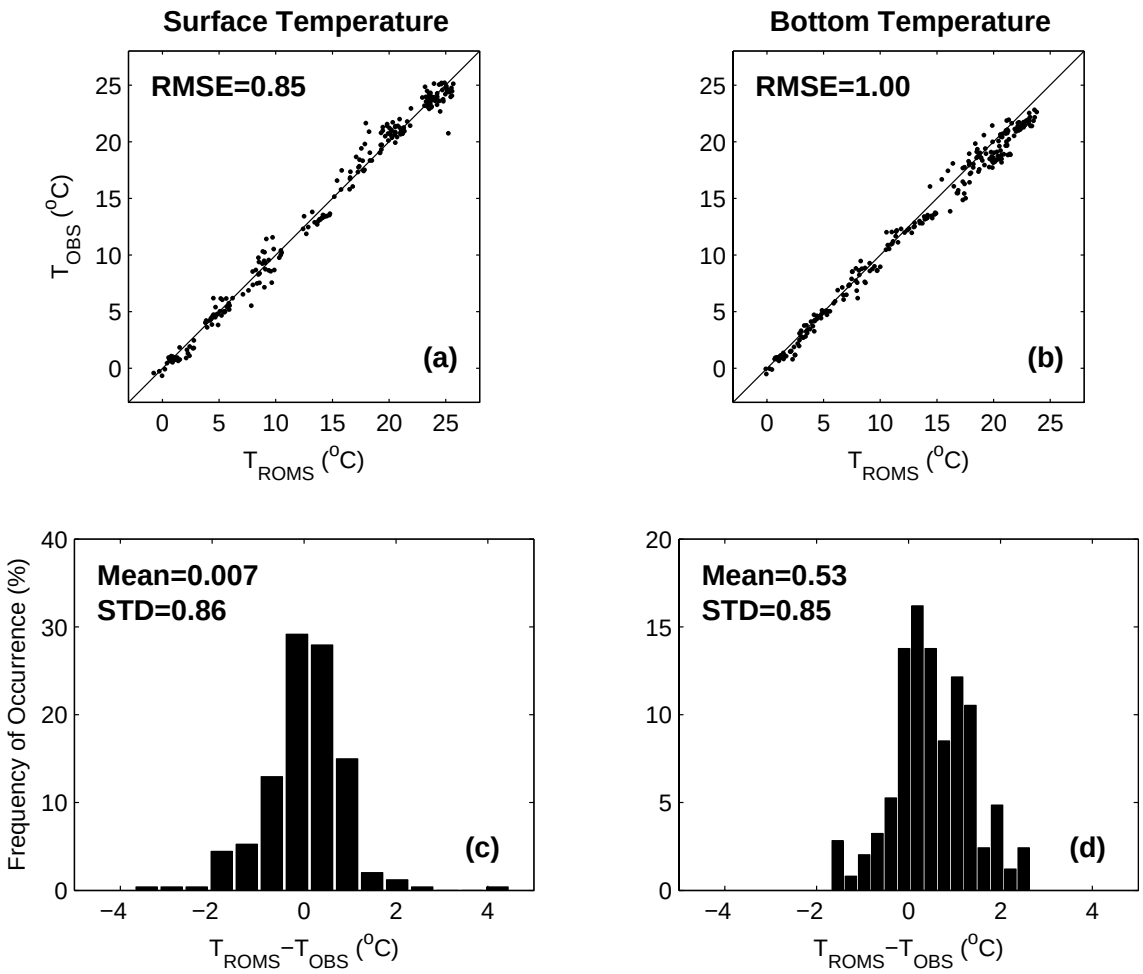

Figure 5-9. Scatter diagrams of observed versus modeled temperature at (a) surface and (b) bottom at sampling stations in the Connecticut Department of Environmental Protection monitoring program. Histograms of errors at (c) surface and (d) bottom between observation and model are also shown.

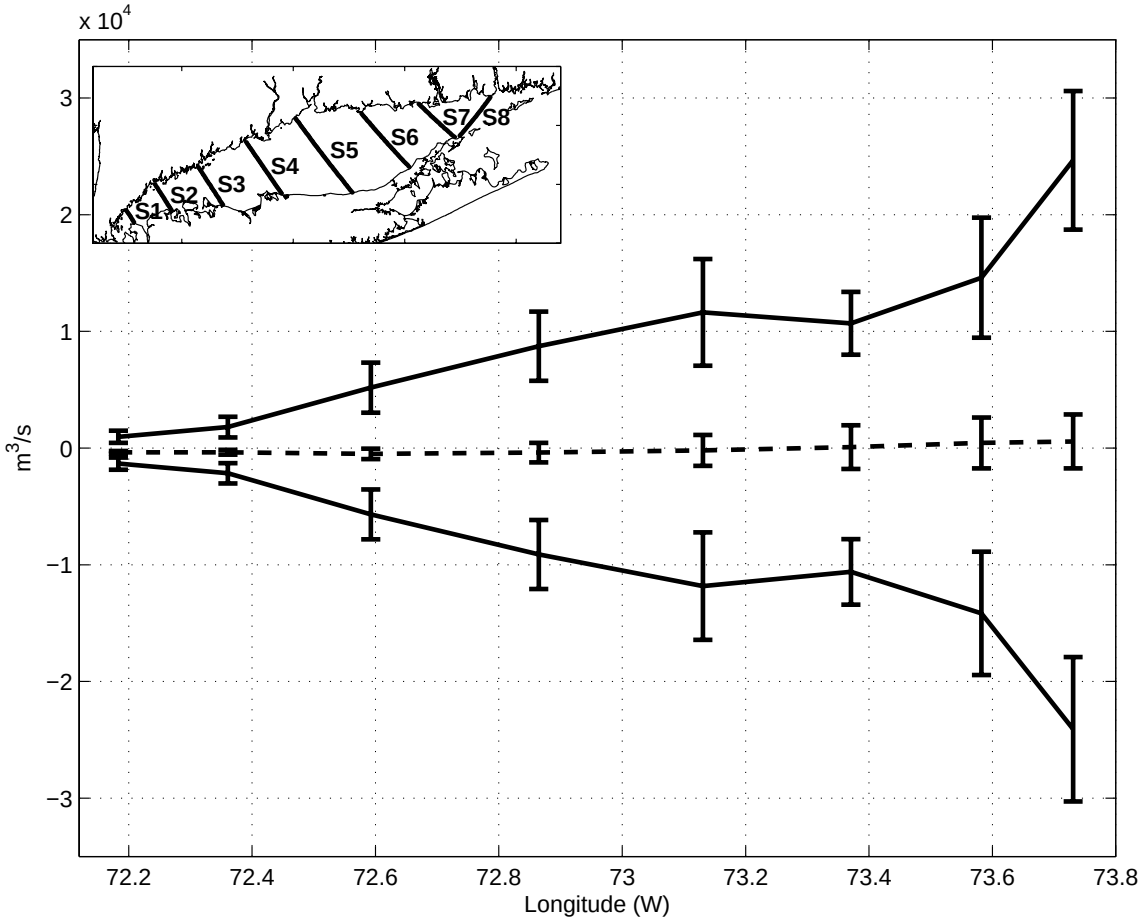

Figure 5-10. Means and standard deviations of exchanged (solid) and net volume transport (dashed) in Long Island Sound.

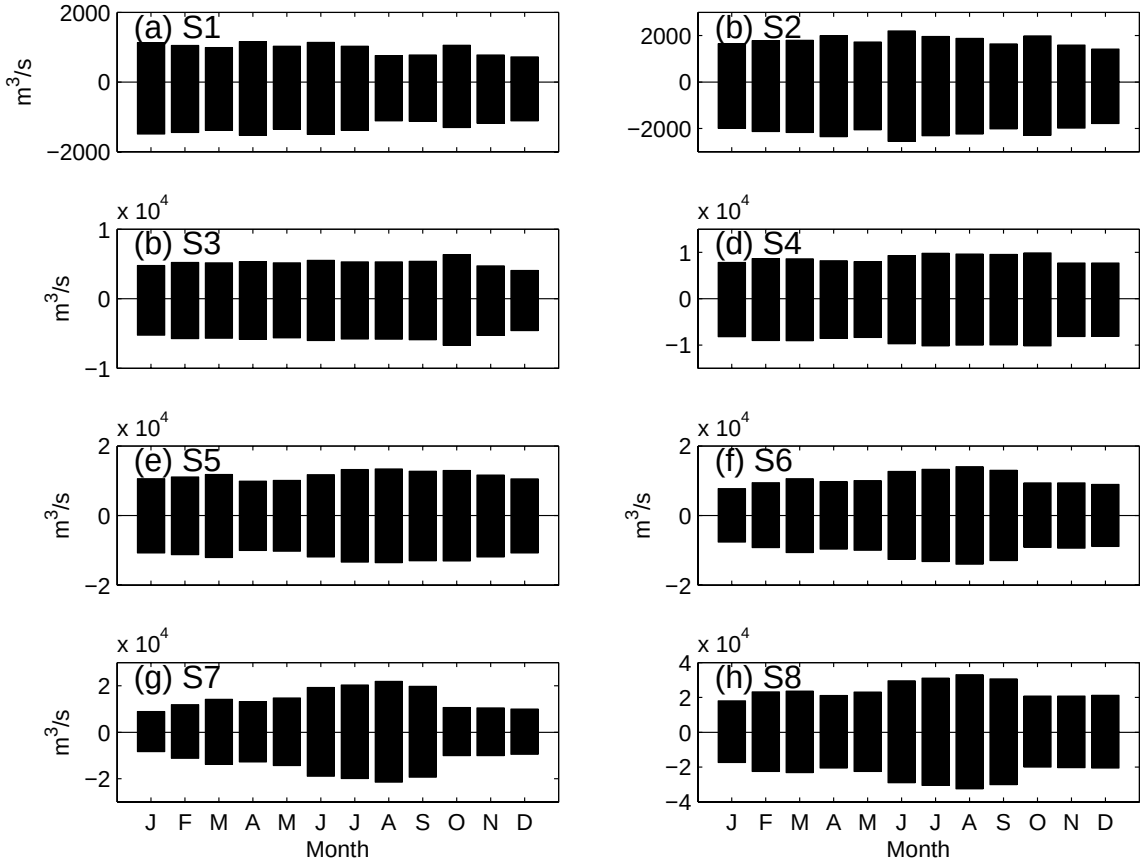

Figure 5-11. Monthly exchanged transport at each section shown in Figure 5-10. Positive values indicates inward (in-to-estuary) and negative values are outward (out-of-estuary) transport

5.4.2. Exchange transport

In order to examine how much of water is transported throughout the sound, the volume transport was calculated by multiplying the section-normal current velocity at each cell by the cell area. Figure 5-10 shows the mean and standard deviation of volume transport at 8 cross-sections in LIS including the sections near the BP and CS Ferry services. The residuals were also obtained by using a low-pass filter with the cutoff period of 34-hour. The magnitude of the exchanged transport indicates a general decrease from east to west, with a range of 0.1×10^4 to 2.5×10^4 m^3/s, and the magnitude in the central basin is in the order of 1.0×10^4 m^3/s. These numbers are generally in good agreement with the estimates of previous studies, i.e., 2.3×10^4 m^3/s (Codiga and Aurin, 2007), 1.8×10^4 m^3/s (Crowley, 2005), and 2.1×10^4 m^3/s (Mau, 2008) at the eastern end and $1.0\sim1.2\times10^4$ m^3/s (Hao, 2007) in the Central Basin. The dashed line with error bars indicates the means and standard deviations of the net transport at each section. The mean transport varies from one basin to another. The mean net transport is approximately between –400 and –500 m^3/s (westward) in the western sound. The direction of the net transport is reversed over the Mattituck Sill, and it becomes 570 m^3/s (eastward) at the eastern end.

Figure 5-11 shows monthly fluctuations of mean transport at the each section, indicating a stronger seasonal cycle in exchange transport towards the eastern end of the sound. The monthly transport in the Narrows (S1 and S2) and the Western Basin (S3) is approximately between 1000 and 5000 m^3/s, respectively, and the seasonal variation is less evident. The seasonal fluctuation tends to be more noticeable in the Central Basin (S4 and S5). It is stronger during summer and weaker during winter/spring with the magnitude of 1.0×10^4 m^3/s. The transport in the Eastern Basin (S6, S7, and S8) clearly indicates enhanced summer transport. It is substantially stronger (peak 3.3×10^4 m^3/s) during summer season centered on August, and weaker (minimum 1.8×10^4 m^3/s) through the winter months, which agrees well with the results from Codiga and Aurin (2007). However, the unexpected result is that the exchange transport is suppressed in April when the river discharge is the maximum.

5.4.3. Heat Budget

The role of horizontal advection in heat budget has never been quantified for the whole year throughout the sound. Here the heat balance is examined by separating the depth-integrated heat into its three components, i.e., storage ($\partial T / \partial t$), net surface heat flux (Q_{net}), and horizontal advection ($\boldsymbol{u} \cdot \nabla T$). The components are seasonally averaged for 2005. In general, heat budget terms indicate strong spatial and seasonal variation of heat balance in LIS. Figure 5-12 illustrates that the net surface heat flux term is significant in winter heat balance, acting to cool the water column sound-wide. Table 5-2 shows that longwave heat flux is the largest heat loss term during winter in the sound, followed by latent and sensible heat fluxes. In contrast, horizontal advection cools the water column only in the southern areas of the Central and Eastern Basin, and warms it in the rest of areas. The heat storage shows overall heat loss (~ –70 W/m^2) in most of areas except for some patchy areas along the Connecticut shore, which are affected by horizontal advection. This indicates that the surface heat fluxes dominate the heat balance during winter. In spring season, the net surface heat flux term becomes positive throughout the sound (Figure 5-13c). Shortwave heat flux is the strongest in a year and longwave heat flux is the only term acting as significant heat loss (Table 5-2). Thus, the net surface heat flux is fairly constant between 150 and 200 W/m^2 with the highest near the Mattituck Sill due to the spatial pattern of the shortwave heat flux (not shown). The heat storage shows a spatial pattern that follows the bathymetry of the sound since it is stronger along the main channel and becomes weaker in the shallower areas. This pattern suggests that the advection plays a significant role during spring season due to the heat gain along the deep channel and the heat loss over the shallow areas. This is similar to the surface flow pattern characterized by a concentrated seaward flow on the southern side of the basin and a broad inflow on the northern side of the basin (Hao, 2008). During summer, the net surface heat flux tends to be stronger in an eastward direction (Figure 5-14c) since the more heat loss due to longwave and latent heat fluxes is

Table 5-2. Sound-wide averaged seasonal surface heat fluxes (W/m^2)

	Shortwave	Longwave	Latent	Sensible
Winter	100	-67	-40	-28
Spring	225	-51	-3	6
Summer	219	-55	-36	-3
Fall	83	-82	-116	-53

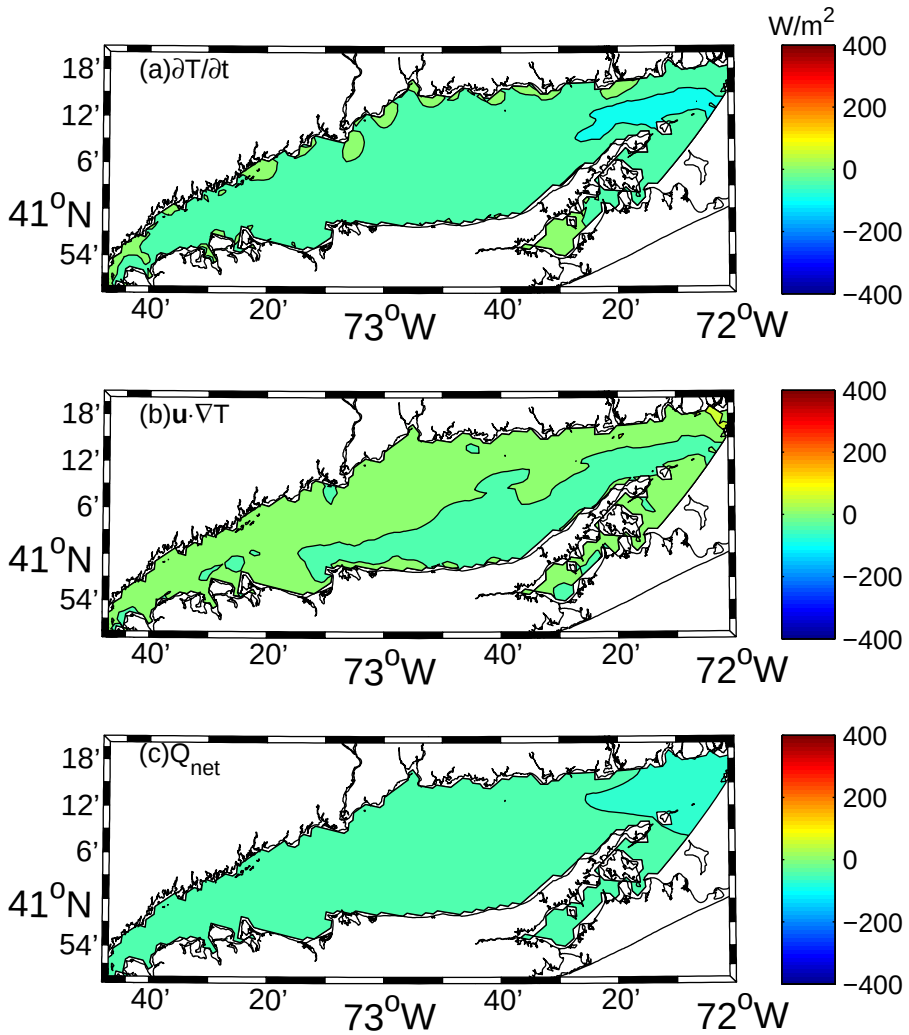

Figure 5-12. Winter seasonal average (January-March) of the three terms in the depth-integrated heat budget: (a) storage ($\partial T / \partial t$), (b) horizontal advection ($\boldsymbol{u} \cdot \nabla T$), and (c) net surface heat flux (Q_{net}).

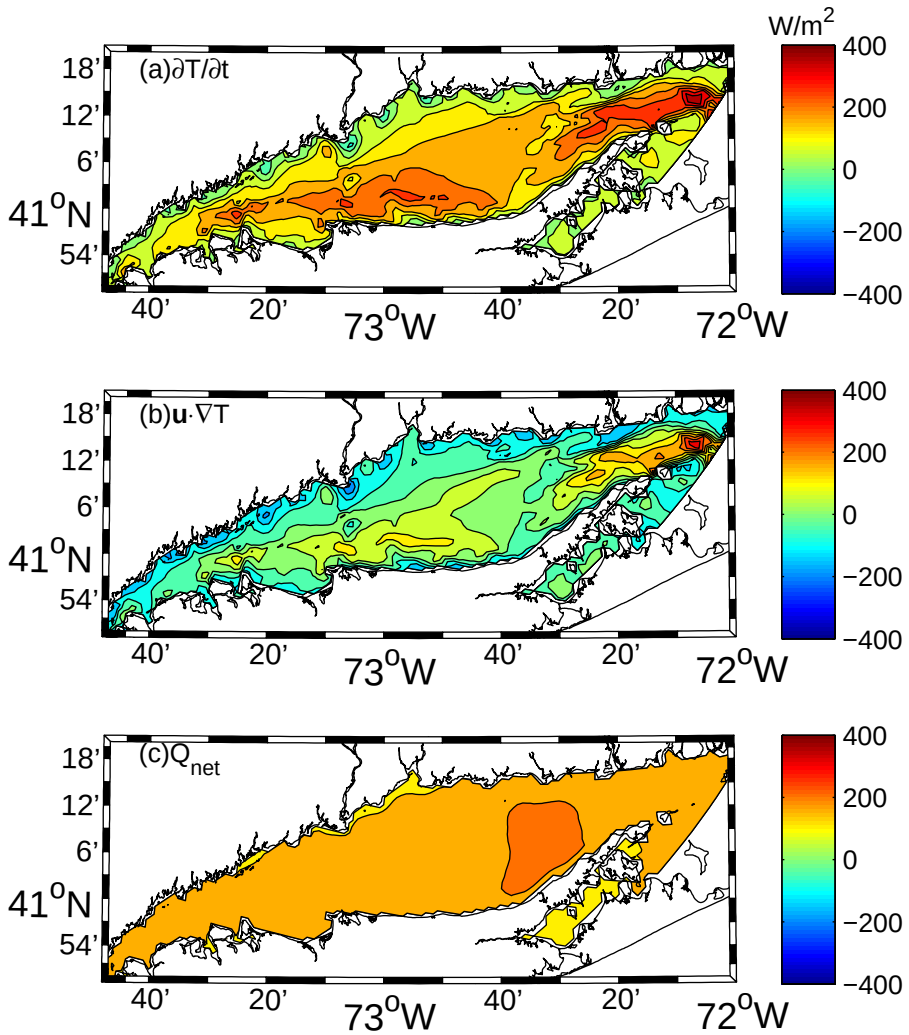

Figure 5-13. Spring seasonal average (April-June) of the three terms in the depth-integrated heat budget: (a) storage ($\partial T / \partial t$), (b) horizontal advection ($\boldsymbol{u} \cdot \nabla T$), and (c) net surface heat flux (Q_{net}).

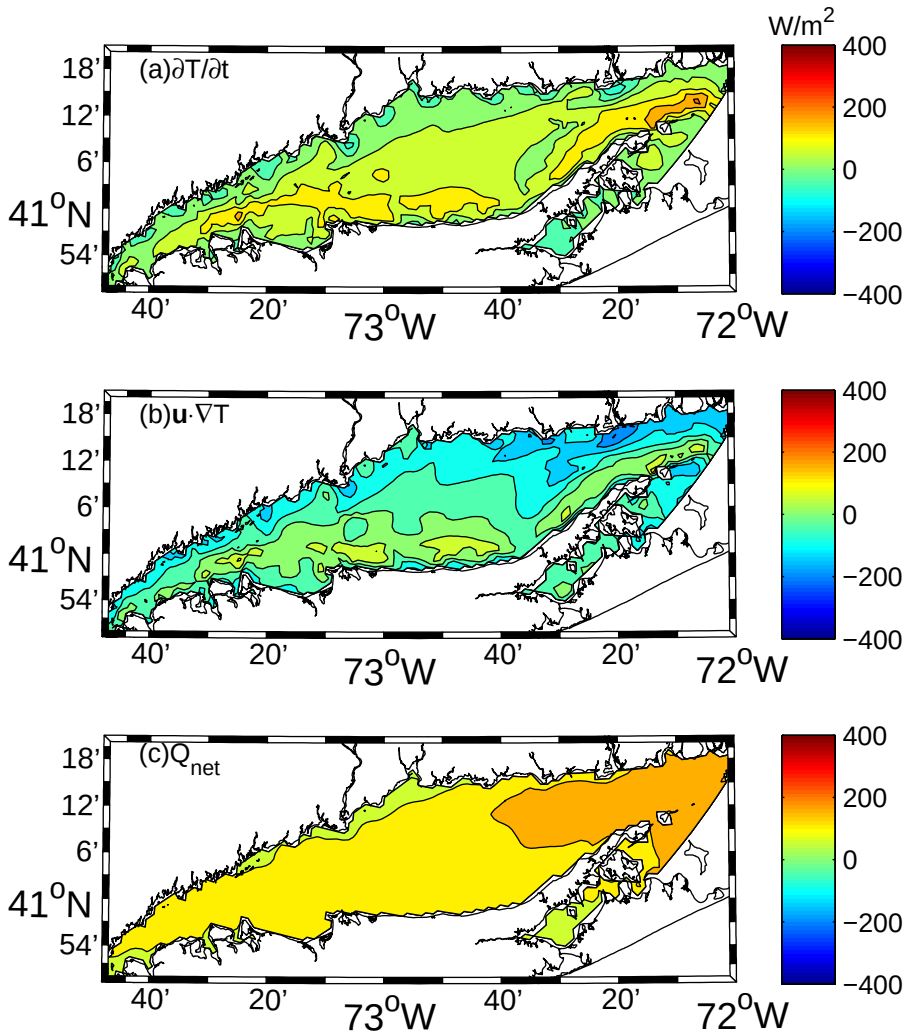

Figure 5-14. Summer seasonal average (July-September) of the three terms in the depth-integrated heat budget: (a) storage ($\partial T / \partial t$), (b) horizontal advection ($\boldsymbol{u} \cdot \nabla T$), and (c) net surface heat flux (Q_{net}).

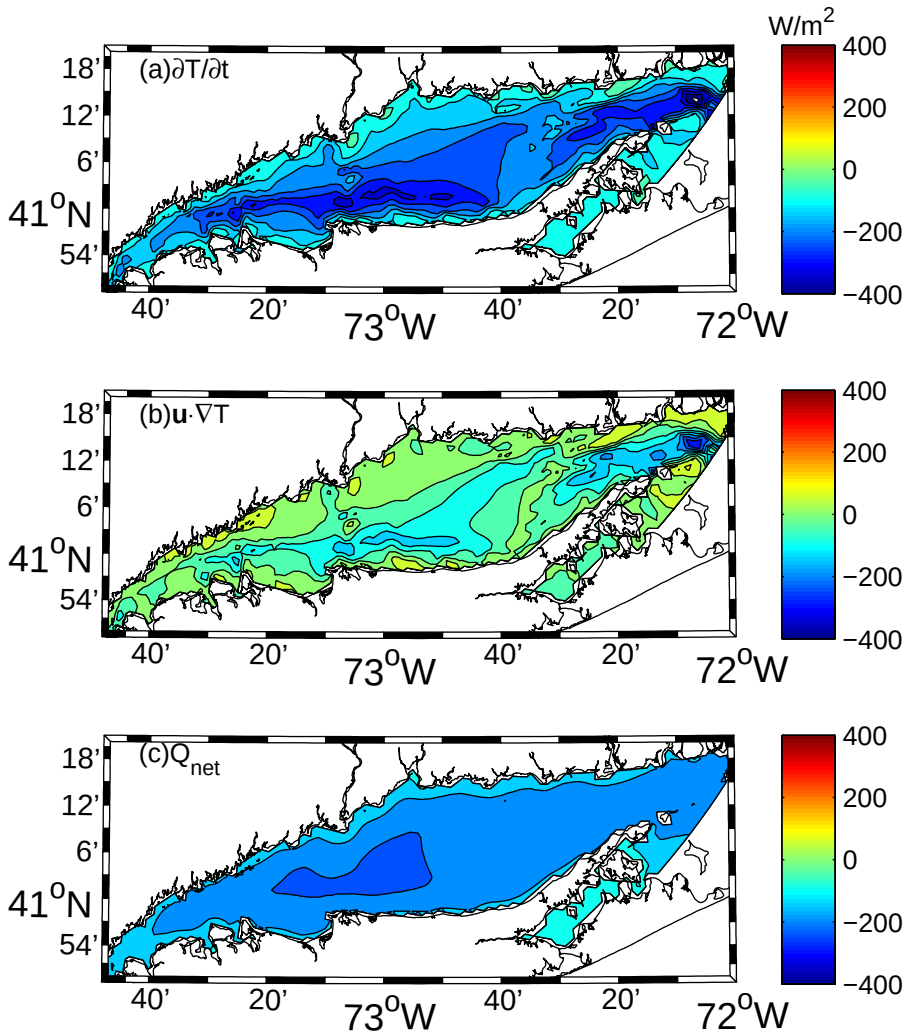

Figure 5-15. Fall seasonal average (October-December) of the three terms in the depth-integrated heat budget: (a) storage ($\partial T / \partial t$), (b) horizontal advection ($\boldsymbol{u} \cdot \nabla T$), and (c) net surface heat flux (Q_{net}).

found toward the western sound (not shown). It is interesting that the magnitude of surface heat flux is weaker than that in spring because latent heat flux becomes more significant in summer than in spring (Table 5-2). The horizontal advection also contributes more to heat loss than in spring and thus it continues to play a bigger role in heat budget during summer. Figure 5-15 shows that the sound loses the largest heat through the sea surface during fall and the strongest heat loss is located in the center of the Western and the Central Basin due to latent heat flux which is the strongest during fall (see Table 5-2). Unlike spring and summer season, the role of horizontal advection is reversed, i.e., the sound loses heat along the main channel and gains heat over the shallow area. The heat storage term demonstrates the role reversal between the net surface heat flux and the horizontal advection; stronger heat loss along the thalweg and weaker heat loss over the shallow areas. Overall, the net surface heat flux is significant over the sound during fall, but the horizontal advection plays a role in the Eastern Basin.

5.5 Discussion

Codiga and Aurin (2007) examined the transverse-vertical structure of velocity field at the eastern end of LIS based on two years of sampling (Novemeber 2002-January 2005). They obtained the annual mean volume transport of 22,700±5000 m^3/s. The model result (annual mean of 24,400±6000 m^3/s) shows excellent agreement with their ADCP observations. The seasonal variation of exchange transport is also stronger in summer season in both the observations and the model results. However, they found that the observations exhibit the maximum transport in May-June (30,000 m^3/s) and the minimum in November-December (18,000 m^3/s). The model transport is highest in August (33,000 m^3/s) and lowest in January (18,000 m^3/s), which contradicts the values of 4000~8000 m^3/s found by Gay et al. (2004). Although the model has shown the similar seasonal range as the observations, it slightly overestimated the maximum transport during summer. The discrepancy in magnitude could be caused by interannual variability and/or a shadow zone in shipboard ADCP measurements.

Crowley (2005) found that strong stratification due to surface heating and favorable wind condition in summer facilitates an intrusion of bottom water through BIS into the interior of LIS. Our study has also clearly shown that the exchange transports vary seasonally especially in the eastern sound, probably increasing with stratification. This variability of the seasonal transports can also have a direct effect on the residence time of the eastern basin, and it is expected that the residence time is shortened in summer than in other seasons. In contrast, the residence time varies little in the Narrows and Western Basin since the seasonality in the volume transport is not significant. In addition, the contribution of exchange between LIS and adjacent water is important in the seasonal heat budget since the sound is cooled down significantly by heat exchange with the adjacent water at an average rate of -8.2×10^{10} W (Crowley, 2005). Without this mechanism the average water temperate would increase by at least an additional 6 °C through the heating season (Crowley, 2005), which would likely have an impact on biogeochemical processes such as hypoxia. This implies that horizontal advection could play a role in the intrusion of oxygenated water from BIS as well as the decline of oxygen solubility in water column due to temperature increase. Previous studies indicated that various mechanisms control DO during summer in LIS, such as the density structure of the water column (Anderson and Taylor, 2001), horizontal transport of oxygen (Torgersen et al., 1997) and biological uptake (Welsh and Eller, 1991). In order to determine which process is dominant in DO dynamics, the current model simulation can be reconfigured by adding a nitrogen-based pelagic ecological model (Fennel et al., 2006) included in the ROMS package. For complicated biogeochemical processes in estuaries including sediment digenesis, ROMS can be coupled with the RCA water quality model which is an open-source code simulation system available at URL http://www.hydroqual.com/wr_rca.html.

This is the first modeling study to examine the sound-wide heat budget for whole annual cycle. Figure 5 of Lee and Lwiza (2005) shows that the net surface heat flux is stronger than the heat storage in spring/summer while they balance each other during fall/winter. It was suggested that the strong discrepancy between the net surface heat flux and the temperature tendency during spring/summer indicates the importance of horizontal advection in heat budget. The findings in this study have confirmed the

significant contribution of horizontal advection which cools the water column during spring/summer. The spatial patterns of heat flux due to horizontal advection coincide with the longitudinal mean current where the momentum balance is between pressure gradient and advection (Hao, 2008). Thus, the discrepancy is easily explained by the horizontal advection which was not included in the previous calculation. The previous modeling study by Crowley (2005) showed that the estuarine circulation makes relatively large contribution to the net heat transport during the stratified period and thus the exchange heat transport represents a loss of heat in LIS. In contrast, Figure 5-12 and 5-15 indicate that the net surface heat flux primarily controls the heat storage during fall/winter. However, further research is needed to simulate for longer periods of time in order to examine the interannual variability of temperature as well as salinity in LIS.

Since the water temperature is mainly affected by surface heat fluxes in fall/winter, the winter warming trend which has been reported (e.g., Stachowicz et al., 2002) is possibly connected to the regional climate change. The horizontal advection plays a minor role transporting the relatively warm water outside into the sound, and its contribution is relatively small. During spring/summer, the role of horizontal advection is reversed (heat loss) and becomes important in the variability of temperatures possibly associated with adjacent ocean. In general, the advection brings the shelf-slope water into the sound to warm or cool the water column. However, it is not certain how much the variability of adjacent ocean contributes to the interannual variability in LIS since there are two possible factors to consider; one is due to the change in properties outside the sound and another is due to the changes in exchange transport. Therefore, by running the model for 10 to 15 years, it will help to better understand the response of coastal ocean due to climate change on the surface heat flux, and the exchange transport into LIS. Freshwater discharge was not configured in this study, but further investigation will need to force the model without data assimilation. This will allow better examination of the effects caused by the interannual variability of river discharge. Earlier in this study we attempted to open the East River to connect the Upper Bay and LIS so that the influence of New York harbor could be examined. However, the simulation produced unrealistic results at the western sound. The residual flow at the western end was into the sound, which contradicts the volume fluxes (–240 to –400 m^3/s) into the East River found by

Blumberg and Pritchard (1997). This is probably due to low resolution around New York harbor and the East River areas. With only three spatial grid-points across the channel, frictional effects overwhelm the dynamics causing distortions in the flows. It still remains a challenge, but it can be done with higher resolution (e.g., 10 grid-points across the East River), albeit at a greater computational cost, or with nesting within the current simulation.

5.6 Summary

Numerical simulations of LIS in 2005 have been conducted using a ROMS model and driven by realistic atmospheric and tidal forcing. The model run is validated with a variety of observations around the sound. It reproduces tidal characteristics accurately as well as exhibits good skill in predicting the temperature field in LIS. The numerical simulation also has shown good agreement with the ADCP observations in the transverse-vertical structures of residual currents across the central sound and the eastern end. Tthe mean exchanged transport generally decreases from the eastern end (2.5×10^4 m^3/s) to the western sound (0.1×10^4 m^3/s), and the magnitudes in the central basin is order of 1.0×10^4 m^3/s. A strong seasonal change is evident in the Central and Eastern Basin. For example, the transport at the eastern end peaks (3.3×10^4 m^3/s) during summer season centered on August, and is weaker in the winter months (1.8×10^4 m^3/s). However, the monthly fluctuation of the mean transport in the Western Basin and the Narrows is less prominent. The depth-integrated heat budget terms (storage, horizontal advection, and net surface heat flux) reveal that the net surface heat flux plays an important role in during fall/winter whereas the horizontal advection significantly contribute to the heat budget in LIS during spring/summer. Further research is needed to investigate the interannual variability associated with climate change.

References

Addison, P. S., 2002. The Illustrated Wavelet Transform Handbook. The Institute of Physics, London.

Alexander, M.A., Timlin, M.S., Scott, J.D., 2001. Winter-to-winter recurrence of sea surface temperature, salinity and mixed layer depth anomalies. Progress in Oceanography 40, 41-61.

Allen, M. R., Smith, L. A., 1996. Monte Carlo SSA: Detecting irregular oscillations in the presence of colored noise. Journal of Climate 9, 3373-3404.

Aller, R.C., 1994. The sedimentary Mn cycle in Long Island Sound: Its role as intermediate oxidant and the influence of bioturbation, O_2, and C_{org} flux on diagenetic reaction balances. Journal of Marine Research 52, 259-295.

Aller, R.C., Cochran, J.K., 1976. $^{234}Th/^{238}U$ disequilibrium in near-shore sediment: Particle reworking and diagenetic time scales. Earth Planet Science Letters 29, 37-50.

Anderson, T.H., Taylor, G.T., 2001. Nutrient Pulses, Plankton Blooms, and Seasonal Hypoxia in Western Long Island Sound. Estuaries 24, 228-243.

Austin, J. A., 2002. Estimating the mean ocean-bay exchange rate of the Chesapeake Bay. Journal of Geophysical Research 110 (C11), 3192.

Bradbury, J. A., Dingman, S. L., Keim, B. D., 2002. New England drought and relation with large scale atmospheric circulation patterns. Journal of the American Water Resources Association 38 (5), 1287-1299.

Behrenfeld, M.J., O'Malley, R.T., Siegel, D.A., McClain, C.R., Sarmiento, J.L., Feldman, G.C., Milligan, A.J., Falkowski, P.G., Letelier, R.M., Boss, E.S., 2006. Climate-driven trends in contemporary ocean productivity. Nature 444, 752-755.

Berliand, M. E., Berliand, T. G., 1952. Measurement of the effective radiation of the earth with varying cloud amount (in Russian). Izv. Akad. Nauk SSSR Ser. Geofiz., no 1.

Blumberg, A.F., Pritchard, D.W., 1997. Estimates of the transport through the East River, New York. Journal of Geophysical Research 102, 5685-5703.

Breitburg, D.L., Adamack, A., Rose, K.A., Kolesar, S.E., Decker, M.B., Purcell, J.E., Keister, J.E., Cowan, Jr., J.H., 2003. The Pattern and Influence of Low Dissolved Oxygen in the Patuxent River, a Seasonally Hypoxic Estuary. Estuaries 26, 280-297.

Budgell, W.P., 2005: Numerical simulation of ice-ocean variability in the Barents Sea region. Ocean Dynamics, doi:10.1007/s10236-005-0008-3.

Bunker, A. F., 1976. Computation of surface energy flux and annual air-sea cycle of the North Atlantic Ocean. Monthly Weather Review 104, 1122-1140.

Buzzelli, C.P., Luettich, Jr., R.A., Powers, S.P., Peterson, C.H., McNinch, J.E., Pinckney, J.L., Paerl, H.W., 2002. Estimating the spatial extent of bottom-water hypoxia and habitat degradation in a shallow estuary. Marine Ecology Progress Series 230, 103-112.

Cameron, W.M., Pritchard, D.W., 1963. Estuaries. In: M.N. Hill, Editor, The Sea vol. 2, Wiley, New York, 306-324.

Chelton, D. B., 1983. Effects of sampling errors in statistical estimation. Deep-Sea Research 30, 1083-1101.

Churchill, J. H., 1985. Intrusion of outer shelf and slope water within the nearshore zone off Long Island, New York. Limnology and Oceanography 30 (5), 972-986.

Codiga, D. L., Aurin, D. A., 2007. Residual circulation in eastern Long Island Sound: Observed transverse-vertical structure and exchange transport. Continental Shelf Research 27, 103-116.

Codiga, D.L., Rear, L.V., 2004. Observed tidal currents outside Block Island Sound: Offshore decay and effects of estuarine outflow. Journal of Geophysical Research 109, C07S05, doi:10.1029/2003JC001804.

Cole, J.J., Caraco, N.F., Peierls, B., 1992. Can phytoplankton maintain a positive carbon balance in a turbid, freshwater tidal estuary? Limnology and Oceanography 37, 1608-1617.

Crowley, H.A., 2005. The seasonal evolution of thermohaline circulation in Long Island Sound. Ph.D. Thesis, Stony Brook University. Stony Brook, New York, USA.

Csanady, G. T., Hamilton, P., 1988. Circulation of slopewater. Continental Shelf Research 8, 565-624.

CTDEP, 2000. Information Regarding the Impacts of 1999 Lobster Mortalities in Long Island Sound. Connecticut Department of Environmental Protection (CTDEP), Hartford, Connecticut.

Czaja, A., Frankignoul, C., 2002. Observed Impact of Atlantic SST Anomalies on the North Atlantic Oscillation. Journal of Climate 15, 606-623.

Dai, A., Fung, I. Y., Del Genio, A. D., 1997. Surface observed global land precipitation variations during 1900-1988. Journal of Climate 10, 2943-2962.

Daubechies, I., 1990. The Wavelet Transform, Time-Frequency Localization and Signal Analysis. IEEE Transactions on Information Theory 36 (5), 961-1005.

Di Lorenzo, E., 2003: Seasonal dynamics of the surface circulation in the southern California Current System. Deep-Sea Research, Part II 50, 2371-2388.

Diaz, R.J., Rosenberg, R., 1995. Marine benthic hypoxia: A review of its ecological effects and the behavioural responses of benthic macrofauna. Oceanography and Marine Biology: an Annual Review 33, 245-303.

Dinniman, M. S., Klinck, J. M., Smith, W.O.,Jr., 2003: Cross shelf exchange in a model of the Ross Sea circulation and biogeochemistry. Deep-Sea Research, Part II 50, 3103-3120.

Dong, S., Kelly, K. A., 2003. Seasonal and interannual variations in geostrophic velocity in the Middle Atlantic Bight. Journal of Geophysical Research 108 (C6), 3172.

Dong, S., Kelly, K.A., 2004. Heat Budget in the Gulf Stream Region: The Importance of Heat Storage and Advection. Journal of Physical Oceanography 34, 1214-1231

Edwards, M, Richardson, A.J., 2004. Impact of climate change on marine pelagic phenology and trophic mismatch. Nature 430, 881-884.

Fennel, K., Wilkin, J., Levin, J., Moisan, J., O'Reilly, J., Haidvogel, D., 2006: Nitrogen cycling in the Middle Atlantic Bight: Results from a three-dimensional model and implications for the North Atlantic nitrogen budget. Global Biogeochemical Cycles, 20, GB3007, doi:10.1029/2005GB002456.

Gibson, J.R., Najjar, R. G., 2000. The response of Chesapeake Bay salinity to climate-induced change in streamflow. Limnology and Oceanography 45 (8), 1764-1772.

Goodrich, D. M., 1988. On meteorologically induced flushing in three US east coast estuaries. Estuarine, Coastal and Shelf Science 26, 111-121.

Grinsted, A., Moore, J. C., Jevrejeva, S., 2004. Application of the cross wavelet transform and wavelet coherence to geophysical time series. Nonlinear Processes in Geophysics 11, 561-566.

Emery, W. J., Thomson, R. E., 2001. Data Analysis Methods in Physical Oceanography (Second and Revised Edition). Elservier. Science B. V. Amsterdam, The Netherlands.

Fairall, C. W., Bradley, E. F., Rogers, D. P., Edson, J. B., Young, G. S., 1996. Bulk parameterization of air-sea fluxes for Tropical Ocean-Global Atmosphere Coupled-Ocean Atmosphere Response Experiment. Journal of Geophysical Research 101 (C2), 3747-3764.

Flagg, C. N., Houghton, R.W., Pietrafesa, L. J., 1994. Summertime thermocline salinity maximum intrusions in the Mid-Atlantic Bight. Deep-Sea Research II 41, 325-340.

Frankignoul, C., De Coëtlogon, G., Joyce, T. M., Dong, S., 2001. Gulf Stream Variability and Ocean-Atmospheric Interactions. Journal of Physical Oceanography 31, 3516-3529.

Fratantoni, P. S., Pickart, R. S., 2003. Variability of the shelf break jet in the Mid Atlantic Bight: Internally or externally forced? Journal of Geophysical Research 108 (C5), 3166.

Fung, I. Y., Harrison, D. E., Lacis, A. A., 1984. On the Variability of the Net Longwave Radiation at the Ocean Surface. Reviews of Geophysics and Space Physics 22(2), 177-193.

Gay, P.S., O'Donnell, J., Edwards, C.A., 2004. Exchange between Long Island Sound and adjacent waters. Journal of Geophysical Research 109, C06017.

Hagy, J.D., Boynton, W.R., Keefe, C.W., Wood, K.V., 2004. Hypoxia in Chesapeake Bay, 1950–2001: Long-term Change in Relation to Nutrient Loading and River Flow. Estuaries 27, 634-658.

Haidvogel, D.B., Arango, H.G., Hedstrom, K., Beckmann, A., Malanotte-Rizzoli, P., Shchepetkin, A.F., 2000: Model evaluation experiments in the North Atlantic Basin: Simulations in nonlinear terrain-following coordinates. Dynamics of Atmospheres and Oceans 32, 239-281.

Halliwell, G.R.,Jr., 1997. Decadal and Multidecadal North Atlantic SST anomalies Driven by Standing and Propagating Basin-Scale Atmospheric Anomalies. Journal of Climate 10, 2405-2411.

Halliwell, G.R., Jr., 1998. Simulation of North Atlantic Decadal/Multidecadal Winter SST anomalies Driven by Basin-Scale Atmospheric Circulation Anomalies. Journal of Physical Oceanography 28, 5-21.

Halliwell, G. R., Jr., Mayer, D. A., 1996. Frequency Response Properties of Forced Climate SST Anomaly Variability in the North Atlantic. Journal of Climate 9, 3575-3587.

Hao, Y., 2008. Tidal and Residual Circulation in Long Island Sound. Ph.D. thesis, School of Marine and Atmospheric Sciences, Stony Brook University, New York.

Hare, J. A., Cowen, R. K., 1996. Transport of larval and pelagic juvenile bluefish (Pomatomus saltatrix) from South Atlantic Bight spawning grounds to Middle Atlantic Bight nursery habitats. Limnology and Oceanography 41(6), 1264-1280.

Hearn, C.J., Robson, B.J., 2001. Inter-annual Variability of Bottom Hypoxia in Shallow Mediterranean Estuaries. Estuarine, Coastal and Shelf Science 52, 643-657.

HydroQual, Inc., 1995. Analysis of Factors Affecting Historical Dissolved Oxygen Trends in Western Long Island Sound. Job Number: NENG0040. Prepared for the Management Committee of the Long Island Sound Estuary Study, Stamford, Connecticut, and the New England Interstate Water Pollution Control Commission. Mahwah, New Jersey, USA.

IPCC, 2007. Climate Change 2007: The Physical Science Basis. Contribution of Working Group I to the Fourth Assessment Report of the Intergovernmental Panel on Climate Change.

Jensen, L.M., Sand-Jensen, K., Marcher, S., Hansen, M., 1990. Plankton community respiration along a nutrient gradient in a shallow Danish estuary. Marine Ecology Progress Series 61, 75-85.

Jevrejeva, S., Moore, J.C., Grinsted, A., 2003. Influence of the Arctic Oscillation and El Niño-Southern Oscillation (ENSO) on ice conditions in the Baltic Sea: The wavelet approach. Journal of Geophysical Research 108 (D21), 4677.

Jevrejeva, S., Moore, J.C., Woodworth, P. L., Grinsted, A., 2005. Influence of large-scale atmospheric circulation on European sea level: results based on the wavelet transform method. Tellus 57A, 183-193.

Justić, D., Rabalais, N.N., Turner, R.E., 1996. Effects of climate change on hypoxia in coastal waters: A doubled CO_2 scenario for the northern Gulf of Mexico. Limnology and Oceanography 41, 992-1003.

Kaiser, G., 1994. A Friendly Guide to Wavelets. Birkhäuser, Boston.

Kayano, M. T., Andreoli, R. V., 2004. Decadal variability of northern northeast Brazil rainfall and its relation to tropical sea surface temperature and global sea level pressure anomalies. Journal of Geophysical Research 109, C11011.

Kaputa, N.P., Olsen, C., 2000. Long Island Sound Ambient Water Quality Monitoring Program: Summer Hypoxia Monitoring Survey 1991–1998 Data Review, Connecticut Department of Environmental Protection, Bureau of Water Management. Hartford, Connecticut, USA.

Kaski, S., Kangas, J., Kohonen, T., 1998. Bibliography of self-organizing map (SOM) papers: 1981– 1997. Neural Computing Surveys 1, 102–350.

Keller, A.A., Oviatt, C.A., Walker, H.A., Hawk, J.D., 1999. Predicted impacts of elevated temperature on the magnitude of the winter-spring phytoplankton bloom in temperate coastal waters: A mesocosm study. Limnology and Oceanography 44, 344–356.

Keller, A.A., Taylor, C., Oviatt, C., Dorrington, T., Holcomb, G., Reed, L., 2001. Phytoplankton production patterns in Massachusetts Bay and the absence of the 1998 winter-spring bloom. Marine Biology 138, 1051–1062.

Kemp, W.M., Sampou, P.A., Garber, J.G., Tuttle, J., Boyton, W.R., 1992. Seasonal depletion of oxygen from bottom waters of Chesapeake Bay: roles of benthic and planktonic respiration and physical exchange processes. Marine Ecology Progress Series 85, 137-152.

Kemp, W.M., Boynton, W.R., Adolf, J.E., Boesch, D.F., Boicourt, W.C., Brush, G., Cornwell, J.C., Fisher, T.R., Glibert, P.M., Hagy, J.D., Harding, L.W., Houde, E.D., Kimmel, D.G., Miller, W.D., Newell, R.I.E., Roman, M.R., Smith, E.M., Stevenson, J.C., 2005. Eutrophication of Chesapeake Bay: historical trends and ecological interactions. Marine Ecology Progress Series 303, 1-29.

Kohonen, T., 2001. Self-Organizing Maps, 3rd edition. Springer-Verlag, New York, 501 pp.

Kukulka, T., Jay, D. A., 2003. Impacts of Columbia River discharge on salmonid habitat: 1. A nonstationary fluvial tide model. Journal of Geophysical Research 108 (C9), 3293.

Kuo, A.Y., Neilson, B.J., 1987. Hypoxia and Salinity in Virginia Estuaries. Estuaries 10, 277-283.

Kushnir, Y., 1994. Interdecadal variations in North Atlantic sea surface temperature and associated atmospheric conditions. Journal of Climate 7, 141–157.

Labat, D., Ronchail, I., Guyot, J. L., 2005. Recent advances in wavelet analyses: Part 2 - Amazon, Parana, Orinoco and Congo discharges time scale variability. Journal of Hydrology 314 (1-4), 289-31.

Large, W. G., 1996. An Observational and Numerical Investigation of the Climatological Heat and Salt Balances at OWS Papa. Journal of Climate 9, 1856-1876.

Lee, Y.J., Lwiza, K.M.M., 2005. Interannual variability of temperature and salinity in shallow water: Long Island Sound, New York. Journal of Geophysical Research 110, C09022.

Lee, Y.J., Lwiza, K.M.M., 2008. Factors driving bottom salinity varability in the Chesapeake Bay. Continental Shelf Research 28, 1352-1362.

Lentz, S. J., 2003. A climatology of salty intrusions over the continental shelf from Georges Bank to Cape Hatteras. Journal of Geophysical Research 108 (C10), 3326.

Lentz, S. J., Beardsley, R. C., Irish, J. D., Manning, J., Smith, P. C., Weller, R. A., 2003. Temperature and salt balances on Georges Bank February–August 1995. Journal of Geophysical Research 108(C11), 8006.

Liu, Y., Weisberg, R.H., 2005. Patterns of ocean current variability on the West Florida Shelf using the self-organizing map. Journal of Geophysical Research 110, C06003.

National Research Council, 2000. Clean Coastal Waters: Understanding and Reducing the Effects of Nutrient Pollution. National Academy Press, Washington, D. C., 405 pp.

Nixon, S.W., Granger, S., Buckley, B.A., Lamont, M., Rowell, B., 2004. A one hundred and seventeen year coastal water temperature record from Woods Hole, Massachusetts. Estuaries, 27(3), 397-404.

Nixon, S.W., Granger, S.L., Nowicki, B.L., 1995. An assessment of the annual mass balance of carbon, nitrogen, and phosphorus in Narragansett Bay. Biogeochemistry 31, 15-61.

Mau, J.C., Wang, D.P., Ullman, D.S., Codiga, D.L., 2008. Model of the Long Island Sound outflow: Comparison with year-long HF radar and Doppler current observations. Continental Shelf Research 18, 1791-1799.

Maraun, D., Kurths, J., 2004. Cross wavelet analysis: significance testing and pitfalls. Nonlinear Processes in Geophysics 11, 505-514.

Meyers, S. D., Kelly, B. G., O'Brien, J. J., 1993. An introduction to wavelet analysis in oceanography and meteorology: With application to the dispersion of Yanai waves. Monthly Weather Review 121, 2858-2866.

Mignot, J., Frankignoul, C., 2003. On the interannual variability of surface salinity in the Atlantic. Climate Dynamics 20, 555-565.

Moody, J.A., Butman, B., Beardsley, R.C., Brown, W.S., Daifuku, P., Irish, J.D., Mayer, D.A., Mofield, H.O., Petrie, B., Ramp, S., Smith, P., Wright, W.R., 1984. Atlas of tidal elevation and current observations on the northeast American continental shelf and Slope. US Geological Survey Bulletin 1611, 122pp.

Mountain, D. G., 2003. Variability in the properties of Shelf Water in the Middle Atlantic Bight, 1977-1999. Journal of Geophysical Research 108 (C1), 3014.

Mountain, D. G., Manning, J. P., 1994. Seasonal and interannual bariability in the properties of the surface waters of the Gulf of Maine. Continental Shelf Research 14 (13), 1555-1581.

Mountain, D. G., Strout, G. A., Beardsley, R. C., 1996. Surface heat flux in the Gulf of Maine. Deep Sea Research 43, 1533–1546.

Mwale, D, Gan, T. Y., Shen, S. S. P., 2004. A new analysis of variability and predictability of seasonal rainfall of central southern Africa for 1950--94. International Journal of Climatology 24 (12), 1509-1530.

Oja, M., Kaski, S., Kohonen, T., 2002. Bibliography of self-organizing map (SOM) papers: 1998– 2001 addendum. Neural Computing Surveys 3, 1–156.

O'Shea, M.L., Brosnan, T.M., 2000. Trends in Indicators of Eutrophication in Western Long Island Sound and the Hudson-Raritan Estuary. Estuaries 23, 877-901.

Oviatt, C.A., 2004. The Changing Ecology of Temperate Coastal Waters During a Warming Trend. Estuaries 27(6), 895-904.

Oviatt, C.A., Keller, A., Reed, L., 2002. Annual primary production in Narragansett Bay with no bay-wide winter-spring phytoplankton bloom. Estuarine, Coastal and Shelf Science 54, 1013–1026.

Parker, C.A., O'Reilly, J.E., 1991. Oxygen depletion in Long Island Sound: A historical perspective. Estuaries 14, 248-264.

Payne, R. E. 1972. Albedo of the Sea Surface. Journal of the Atmospheric Sciences 29, 959-970.

Perry, A.L., Low, P.J., Ellis, J.R., Reynolds, J.D., 2005. Climate change and distribution shifts in marine fishes. Science 308, 1912-1915.

Rabalais, N.N., Turner, R.E., Wiseman, Jr., W.J., 2002. Gulf of Mexico hypoxia, aka "The dead zone". Annual Review of Ecological and Systematics 33, 235-263.

Redalje, D., Lohrenz, G., S. E., Verity, P. G., Flagg, C. N., 2002. Phytoplankton dynamics within a discrete water mass off Cape Hatteras, North Carolina: the Lagrangian experiment. Deep-Sea Research II 49 (20), 4511–4531.

Reverdin, G, Kestenare, E., Frankignoul, C., Delcroix, T., 2007. Surface salinity in the Atlantic Ocean (30 degrees S--50 degrees N). Progress in Oceanography 73 (3--4), 311-340.

Reyment, R.A., Joreskog, K.G., 1996. Applied factor analysis in the natural sciences. Cambridge University Press, Cambridge, 371 pp.

Richardson, A.J., Risien, C., Shillington, F.A., 2003. Using self-organizing maps to identify patterns in satellite imagery. Progress in Oceanography 59, 223– 239.

Riley, G.A., 1952. Hydrography of the Long Island and Block Island Sounds. Bulletin of the Bingham Oceanographic Collection 13, 5-39.

Risien, C.M., Reason, C.J.C., Shillington, F.A., Chelton, D.B., 2004. Variability in satellite winds over the Benguela upwelling system during 1999 – 2000. Journal of Geophysical Research 109, C03010.

Ritter, C., Montagna, P.A., 1999. Seasonal hypoxia and models of benthic response in a Texas bay. Estuaries 22, 7-20.

Robertson, A. W., Mechoso, C. R., Kim, Y.-J., 2000. The influences of Atlantic Sea Surface Temperature Anomalies on the North Atlantic Oscillation. Journal of Climate 13, 122-138.

Roemmich, D., McGowan, J., 1995. Climatic warming and the decline of zooplankton in the Californian Current. Science 267, 1324-1326.

Rossby, T., 1999. On gyre interactions. Deep-Sea Research II 46, 139-164.

Rossby, T., Benway, R. L., 2000. Slow Variation in mean path of the Gulf Stream east of Cape Hatteras. Geophysical Research Letter 27 (1), 117-120.

Rossby, T., Flagg, C. N., Donohue, K., 2005. Interannual variations in upper-ocean transport by the Gulf Stream and adjacent waters between New Jersey and Bermuda. Journal of Marine Research 63, 203-226.

Rossby, T., Gottlieb, E., 1998. The Oleander Project: Monitoring the Variability of the Gulf Stream and Adjacent Waters between New Jersey and Bermuda. Bulletin of the American Metrological Society 79(1), 5-18.

Schollaert, S. E., Rossby, T., Yoder, J. A., 2004. Gulf Stream cross-frontal exchange: possible mechanisms to explain interannual variations in phytoplankton chlorophyll in the Slope Sea during the SeaWiFS years. Deep-Sea Research II 51,173-188.

Schubel, J. R., Pritchard, D. W., 1986. Responses of Upper Chesapeake Bay to Variation in Discharge of the Susquehanna River. Estuaries 9 (4A), 236-249.

Shiah, F.-K., Ducklow, H.W., 1994a. Temperature regulation of heterotrophic bacterioplankton abundance, production, and specific growth rate in Chesapeake Bay. Limnology and Oceanography 39, 1243-1258.

Shiah, F.-K., Ducklow, H.W., 1994b. Temperature and substrate regulation of bacterial abundance, production and specific growth rate in Chesapeake Bay, USA. Marine Ecology Progress Series 103, 297-308.

Sprague, L.A., Langland, M.J., Yochum, S.E., Edwards, R.E., Blomquist, J.D., Phillips, S.W., Shenk, G.W., Preston, S.D., 2000. Factors affecting nutrient trends in major rivers of the Chesapeake Bay watershed. Water Resources Investigations Report 00–4218, United States Geological Survey. Richmond, Virginia, USA.

Stachowicz, J.J., Terwin, J.R., Whitlatch, R.B., Osman, R.W., 2002. Linking climate change and biological invasions: Ocean warming facilitates nonindigenous species invasions. Proceedings of the National Academy of Sciences of the United States of America 99(24), 15497-15500.

Staroscik, A.M., Smith, D.C., 2004. Seasonal patterns in bacterioplankton abundance and production in Narragansett Bay, Rhode Island, USA. Aquatic Microbial Ecology 35, 275-282.

Swanson, R.L., 1976. Tides. MESA, 4; New York Sea Grant Institute, 44 pp.

Swanson, R.L., Parker, C.A., 1988. Physical environmental factors contributing to recurring hypoxia in New York Bight. Transactions of the American Fisheries Society 117, 37-47.

Taylor, M. H., Mountain, D. G., 2003. The role of local wintertime atmospheric heat flux in determining springtime temperature variability in the northern Middle Atlantic Bight during 1965-1973. Continental Shelf Research 23, 377-386.

Taylor, A. H., Stephens, J. A., 1998. The North Atlantic Oscillation and the latitude of the Gulf Stream. Tellus 50A, 134–142.

Taylor, A. H., Jordan, M. B., Stephens, J. A., 1998. Gulf Stream shifts following ENSO events. Nature 393, 638.

Thomas, E., Gapotchenko, T., Varekamp, J. C., Mecray, E. L., Buchholtz ten Brink, M. R., 2000. Benthic foraminifera and environmental changes in Long Island Sound, Journal of Coastal Research 16, 641-655.

Torgersen, T., Deangelo, E., O'Donnell, J., 1997. Calculations of horizontal mixing rates using ^{222}Rn and the controls on hypoxia in western Long Island Sound, 1991. Estuaries 20, 328–345.

Torrence, C., Compo, G. P., 1998. A Practical Guide to Wavelet Analysis. Bulletin of the American Meteorological Society 79 (1), 61-78.

Torrence, C., Webster, P. J., 1999. Interdecadal Changes in the ENSO-Monsoon System. Journal of Climate 12, 2679-2690.

Troupin, C., Beckers, J.-M., Ouberdous, M., Sirjacobs, D., 2008. Diva User's Guide. GeoHydrodynamics and Environment Research, MARE, University of Liège, Liège, Belgium.

Umoh, J. U., Thompson, K. R., 1994. Surface heat flux, horizontal advection, and the seasonal evolution of water temperature on the Scotian Shelf. Journal of Geophysical Research 99 (C10), 20403-20416.

U. S. Environmental Protection Agency. 1998. Long Island Sound Study: Phase III Actions of Hypoxia Management. Report No. EPA 902-R-98-002, United States Environmental Protection Agency. Stamford, Connecticut, USA.

Valle-Levinson, A., Lwiza, K. M. M., 1997. Bathymetric influences on the lower Chesapeake Bay hydrography. Journal of Marine System 12, 221-236.

Valle-Levinson, A., Wilson, R.E., 1998. Rotation and vertical mixing effects on volume exchange in eastern Long Island Sound. Estuarine Costal and Shelf Science 46, 573-585

Vega, A. J., Rohli, R. V., Sui, C. H., 1999. Climatic Relationship to Chesapeake Bay Salinity during Southern Oscillation Extremes. Physical Geography 20 (6), 468-490.

Verbrugge, N., Reverdin, G, 2003. Contribution of Horizontal Advection to the Interannual Variability of Sea Surface Temperature in the North Atlantic. Journal of Physical Oceanography 33, 964-978.

Vesanto, J., Himberg, J., Alhoniemi, E., Parhankangas, J., 2000. Self-Organizing Map (SOM) Toolbox for Matlab 5. In Technical Report A57, Helsinki University of Technology. Helsinki, Finland.

Vieira, M.E.C., 1990. Observations of Currents, Temperature and Salinity in Long Island Sound, 1988. A Data Report. Special Data Report #6, Marine Sciences Research Center, State University of New York. Stony Brook, New York, USA.

Vieira, M.E.C., 2000. The long-term residual circulation in Long Island Sound. Estuaries 23, 199-207.

Welsh, B.L., Eller, F.C., 1991. Mechanisms Controlling Summertime Oxygen Depletion in Western Long Island Sound. Estuaries 14, 265-278.

Walther, G.R., Post, E., Convey, P., Menze, A., Parmesan, C., Beebee, T.J.C., Fromentin, J.M., Hoegh-Guldberg, O., Bairlein, F., 2002. Ecological responses to recent climate change. Nature 416, 389-395, doi:10.1038/416389a.

Wang, D.-P., Elliott, A. J., 1978. Non-Tidal Variability in the Chesapeake Bay and Potomac River: Evidence for Non-Local Forcing. Journal of Physical Oceanography 8, 225-232.

Wang, B., Wang, Y., 1996. Temporal Structure of the Southern Oscillation as Revealed by Waveform and Wavelet Analysis. Journal of Climate 9, 1586-1598.

Warner, J.C., W.R. Geyer, and J.A. Lerczak, 2005: Numerical modeling of an estuary: a comprehensive skill assessment, Journal of Geophysical Research 110, C05001, doi:10.1029/2004JC002691.

Watanabe, M., Kimoto, M., 2000. On the persistence of decadal SST anomalies in the North Atlantic. Journal of Climate 13, 3017-3028.

Weiss, R., 1970. The solubility of nitrogen, oxygen and argon in water and seawater. Deep Sea Research 17, 721-735.

Wilkin, J., 2005. The Summertime Heat Budget and Circulation of Southeast New England Shelf Waters. Journal of Physical Oceanography 36, 1997-2011.

Wong, K.-C., Valle-Levinson, A., 2002. On the relative importance of the remote and local wind effects on the subtidal exchange at the entrance to the Chesapeake Bay. Journal of Marine Research 60, 477-498.